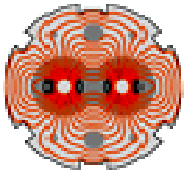

LHC Project Note 296
27 May 2002
Claire.Fynbo@cern.ch
Graham.Stevenson@cern.ch

Radiation Environment in the Dispersion Suppressor regions of IR1 and IR5 of the LHC

Author(s) / EST-LEA: Claire A. Fynbo, TIS: Graham R. Stevenson

Keywords: annual doses, particle fluence, radiation, point loss, dispersion suppressor, IP1, IP5, quench diodes, Pt3, Pt7

Summary:

This report presents the expected annual dose and high energy particle fluences due to point losses and beam-gas interactions in the dispersion suppressor regions (covering the magnet string Q8-Q11 and the dipoles) downstream of the high luminosity interaction points IP1 and IP5. Results show that some areas in the dispersion suppressors will be found with doses comparable to the arc annual levels (*i.e.* several Gy / y to several tens Gy / y), although positioning of the more radiation sensitive equipment will be important due to the non-uniformity of the dose distribution. Hot-spot regions with doses per year > 100 Gy are observed in the vicinity of MB9A, MB9B, the empty cryostat and Q11. Details of dose to the quench diodes are also provided. An indication of the minimum dose value required for the radiation hardness of equipment to be placed in the dispersion suppressors of IR1 and IR5 is given.

In addition, discussion will be extended to the expected dose in the dispersion suppressor regions of Points 3 & 7 in the light of predicted proton loss distributions for these sections of the LHC ring. In comparison to the expected dose in DS1 and DS5, the maximum annual dose in DS3 and DS7 is expected to be much lower.

To enable investigation of possible electronics problems due to Single Event Effects, details of the expected particle fluences in the LHC tunnel of the dispersion suppressors are presented in the form of fluence : dose ratio maps. These are given for a range of particle energy cuts (100 keV - 100 MeV). It is found that the radiation environment (R=fluence / dose) is the same for both DS1 and DS5 regions. Typically,in the vicinity of a dipole / quadrupole (excluding Q11), we expect a ratio of $\sim 5 \times 10^{10}$cm^{-2}Gy^{-1} for neutrons $>$ 100 keV, which falls to $\sim 2 \times 10^{9}$cm^{-2}Gy^{-1} for hadrons > 100 MeV. This gives values for the expected neutron fluences > 100 keV of $\sim 1 \times 10^{13}$cm^{-2} in DS1 and $\sim 1.5 \times 10^{13}$cm^{-2} in DS5, and hadrons > 100 MeV of $\sim 4 \times 10^{11}$cm^{-2} and $\sim 6 \times 10^{11}$cm^{-2}in DS1 and DS5 respectively, at a position close to the cryostat alongside dipole MB9B. Similarly, for a position under dipole MB9B, we expect values of: $\sim 2.5 \times 10^{12}$cm^{-2} in DS1 and $\sim 4 \times 10^{12}$cm^{-2} in DS5 for neutron fluences > 100 keV, and $\sim 1 \times 10^{11}$cm^{-2} in DS1 and $\sim 1.6 \times 10^{11}$cm^{-2} in DS5 for hadron fluences > 100 MeV.

1. Introduction

Doses in the Dispersion Suppressor (DS) regions of IR1 and IR5 arise from two main sources: point losses downstream of the high luminosity Interaction Points IP1 and IP5, and the secondary particle cascades originating from inelastic interactions of protons with the residual gas molecules in the beam pipes (beam-gas interactions). Of these the largest dose contribution is from point losses, thus they are the dominant factor for induced radioactivity and radiation damage in the dispersion suppressor and adjacent arc cells. The aim of this report is to use predicted beam-loss distributions in the dispersion suppressors to provide an estimate of the expected annual dose in and around the magnets Q8-Q11.

The resulting products of the colliding 7 TeV proton beams in the high luminosity interaction points of LHC are basically of three kinds: i) protons are emmitted with a low momentum and a large emission angle with respect to the beam, of which most will be captured by the TAS and TAN absorbers situated in the straight sections downstream of the interaction points, ii) protons are emitted with relatively small momentum transfers (inelastic diffractive losses), and iii) protons are scattered elastically, resulting in small momentum and angular deviations, staying within the acceptance of the ring. It is the second class of losses - the inelastic diffractive losses - which can induce significant proton loss in the DS regions. Specifically it is the protons which have a relative momentum offset δ_p lying in the range $\delta_{p,min}(0.01) < \delta_p < \delta_{p,max}(0.25)$ which are candidates to be lost downstream of the TAN and up to the first adjacent arc cell beyond which the LHC optics is periodic. For protons lost further downstream in the arc sections, *i.e.* those with a momentum offset $\delta_p < 0.01$, these will be candidates to be intercepted by the momentum cleaning system in IR3 [Ajg00]. Thus, to obtain an accurate estimate of the dose due to point losses in the dispersion suppressors downstream of the interaction points IP1 and IP5, reliable values of the inelastic diffractive loss distributions in these regions are required.

In addition to the dose arising from these point losses, there will be an extra contribution due to interactions of the protons with the residual gas in the beam pipes. The rate of these collisions will be the same as that in the LHC standard arc sections, *i.e.* for the 'Design Machine' beam-gas interactions will occur at a rate of $1.65 \times 10^{11}\mathrm{m}^{-1}\mathrm{y}^{-1}(1.05 \times 10^{4}\mathrm{m}^{-1}\mathrm{s}^{-1})$ [Pot95a], [Pot95b]. Full dose maps for the dispersion suppressor regions containing estimation of the total annual dose due to point losses and beam-gas interactions are given in Appendix A of this report.

Since materials are susceptible to the integrated radiation dose, high doses pose a threat to the electronics and machine components to be placed in the tunnel. This leads to the need for reliable electronics which are sufficiently radiation hard to be able to survive the LHC running conditions. However, high doses will not be the only problem facing the reliability of the proposed electronics. Dose is a quantity describing the amount of energy absorbed by a material. Deposition of energy leads to heating which is not necessarily a problem. A greater threat to the electronics will be the large numbers of high energy neutrons and hadrons that will also be present in the vicinity of the machine. The phenomenon of Single Event Upset (SEU), *i.e* a sudden large deposition of energy in a sensitive part of an electronic component due to the interaction of these particles with the electronics, is in itself a non-destructive effect, but one which potentially concerns every memory element temporarily storing a logic state - it can lead to data corruption and possibly even loss of control functions due to memory upsets. Thus information on the expected particle fluences of high energy neutrons and hadrons in the LHC tunnel is required. This will be helpful in determining whether electronics to be placed in the vicinity of the dispersion suppressors will suffer problems; if the tolerance of the equipment is known through previous testing. To this end, Appendix B shows the distribution of neutron and hadron fluences, for different energy cuts, in the tunnel surrounding the dispersion suppressors.

The remainder of this report is structured as follows. In Section 2 a presentation of the proton losses in the DS regions of IR1 and IR5, as calculated in [Bai00], will be given, followed in Section 3 by a description of the FLUKA simulation of the DS region. Section 4 will discuss the results of the predicted dose in the DS regions with extension made in Section 5 to discuss the expected dose in DS 3 & 7, in light of the predicted proton loss distributions in these regions. Section 6 will present the Fluence:Dose ratios in the tunnel and Section 7 will provide a summary of the radiation environment in the dispersion suppressors of the LHC

and give an indication of the required radiation resistance of equipment to be installed here.

2. Proton losses in the dispersion suppressors of IR1 and IR5

Studies of the proton losses expected in the regions downstream of the high luminosity collision points IP1 and IP5 are now available under the LHC optics version 6.2 [Ajg00], [Bai99],[Bai00]. Previous loss studies have shown the need to include two horizontal collimators in the straight sections upstream of D2 and Q5 in order to prevent quenches of the downstream magnets; the first to protect the chain of magnets D2-Q4 and the second upstream of Q5 to significantly reduce the losses in the DS regions. In the following, the proton loss distributions used here will always be for the scenario in which these collimators are present.

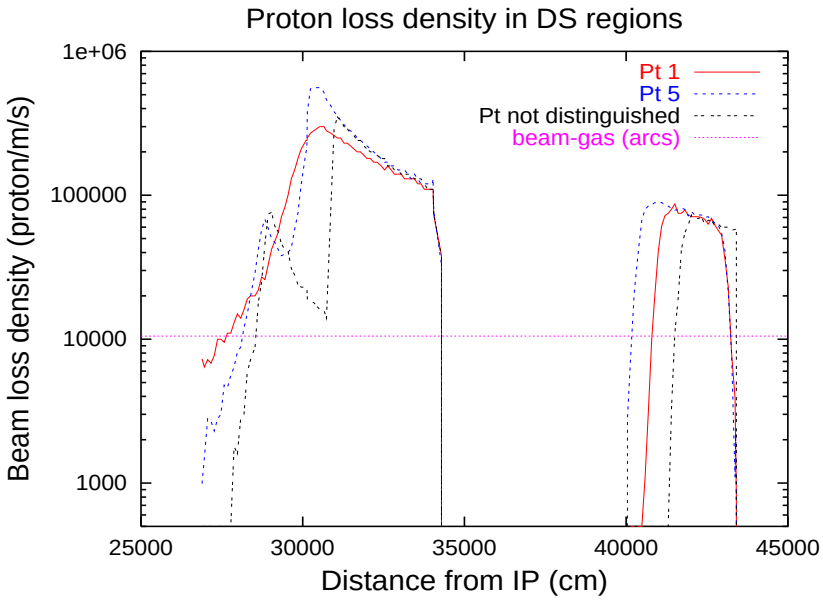

Figure 1: Proton loss density downstream of the High Luminosity points IP1 & IP5. The first major set of losses occurs in the dipoles MB8A/B whilst the second set occur in the region of MB11A/B. Loss values are taken from [Bai00] for the case with collimators present upstream of the DS region. Shown for comparison (pink dotted line) is the proton loss density in the arc sections of the LHC due to beam-gas interactions (1.05×10^4 m^{-1}s^{-1}) [Pot95b]

The proton loss distributions as presented in [Bai00] include the effects of beam-beam crossings, such that the losses in the two regions IR1 and IR5 are dependent on the orientation of the crossing plane, *i.e.* a crossing angle of 0.3 mrad in the vertical plane of IP1 and the same in the horizontal plane of IP5 is included in the beam-loss simulations. This leads to differences in the trajectories of the off-momentum protons in the two regions, thus to different beam-loss distributions for DS sections 1 and 5. The beam-loss density as a function of distance from the IP for the two dispersion suppressor regions IR1 & IR5 is shown in Figure 1 for a rate of 3.5×10^8 inelastic interactions per second in the IP. Values are taken from Table 3 of [Bai00]. The loss density for zero crossing angle is also shown [Bai99] (labelled "Pt not distinguished"), and the corresponding doses also presented in Section 4. In this case no distinction is made between the interaction points 1 and 5. The case of '0' crossing has been included here since future work on the collision scheme used in calculating the loss distributions will include a better matching of the dispersion function at the ends of the straight sections. In this case the loss distribution in the dispersion suppressors will be closer to the result of [Bai99] than [Bai00], *i.e.* the loss densities of '0' crossing are not obsolete. The three cases give a total proton loss in the DS of: 1.1×10^7 protons/s for IR1, 1.3×10^7 protons/s for IR5 [Bai00] and correspondingly 8.5×10^6 protons/s for the result of [Bai99]. Thus, the results calculated here for the vertical and horizontal crossing scenarios will present the more pessimistic case for the doses to be found in the DS regions of IR1 and IR5 than those of '0' crossing.

For comparison the rate of beam-gas interactions is shown as the horizontal line in Figure 1. In localized regions of the dispersion suppressors it can clearly be seen that proton loss rates are more than an order of magnitude higher than in the standard arc sections. It is these regions of maximum loss rate which will determine the maximimum doses that equipment placed in the DS regions will have to survive. In these regions the extra dose to be added due to beam-gas interactions is essentially negligible, whereas in other sections of the DS, where there are essentially no point losses, the extra dose due to beam-gas interactions at a given point will be comparable to (or even greater than) the contribution at that point arising from point losses upstream.

Note, the proton loss distributions presented here are based on the LHC optics version 6.2. These losses are dependent on the optics of the straight sections of the interaction region. The following dose distributions remain valid as long as there are no major changes to the inner region optic layouts of IR1 or IR5.

3. FLUKA simulation of the LHC dispersion suppressor regions IR1 & IR5

In the following the hadronic cascade simulations were performed using the Monte-Carlo particle shower code FLUKA[Fas01a], [Fas01b], using as full and accurate description of the DS main dipole (MB) and quadrupole (MQ, MQTL, MQM, MQML) magnets as possible.

3.1 The geometry

The full FLUKA geometry for the LHC DS region downstream of IP1 and IP5, consisting of eight main bending dipole magnets (MBA / MBB), four quadrupoles, and their correcting magnets, is shown in Figure 2. The geometry is setup according to LHC design optics 6.2 (which for the dispersion suppressor regions remains valid for the optics version 6.3[1]). The geometry explicitly models the left DS region covering the magnet strings C11L1-C8L1 and C11L5-C8L5. The corresponding geometries for the right hand DS regions are not exact mirror images about the interaction point as the geometry is not symmetric. To obtain the geometry setup for the right DS regions one needs to flip the FLUKA geometry about the interaction point and invert the magnets - such that the outgoing proton beam from the IP will impinge on the BPM end of the quadrupoles and the decapole corrector magnets in the dipoles. However, the longitudinal dose distribution presented here for the left DS regions will be equally valid for the right hand side DS regions as a function of distance from the IP, keeping in mind the inversion of the magnet elements.

3.2 FLUKA simulation

Point losses arising from the high luminosity experiments occur in the beam-pipe in which the protons are outgoing from the interaction point. For both IP1 & IP5 that is the outermost beam-pipe closest to the tunnel wall for both left and right DS sections. Dose arising from beam-gas interactions will contribute equally in both rings. Thus higher doses will be expected to be found towards the outside of the LHC ring in the DS sections.

Annual dose due to point losses:

To obtain the dose estimate in the LHC dispersion suppressors due to point losses, 7 TeV proton beams were sent down the outside beam pipe in the outgoing direction from the IP and interaction of the protons forced every 2 metres along the entire length of the $\sim$171 m DS section. For each longitudinal position of

[1]The largest difference in optics v6.3 for the dispersion suppressor magnets here would be in the MQM which increases by 22mm, the standard MQ increases in length by 4mm [Ost01] - these differences will not significantly alter the results presented here for optics v6.2

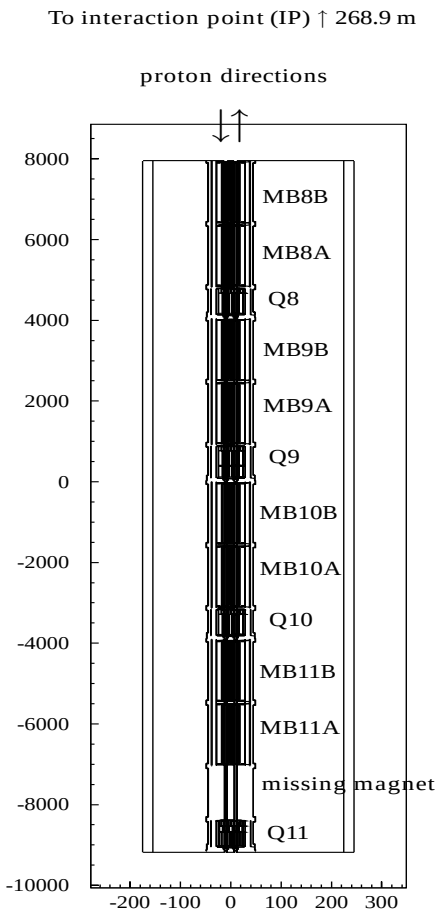

Figure 2: FLUKA simulation of the left DS geometry for IR1 & IR5, specifically for C11L1-C8L1 and C11L5-C8L5 under LHC optics version 6.2. All dimensions are in (cm). Longitudinal dimensions relate to the FLUKA coordinate system which is centred by the quadrupole Q9. The Interaction Point IP1 or IP5 lies ∼268 m from MB8B. The directions of the 7 TeV proton beams are indicated by the single arrows.

the proton interaction point a separate simulation run is required. Energy depostion was scored in various sized meshes covering the entire geometry: $2 \times 2 \times 50\,\mathrm{cm}^3$ mesh bins were used in the central regions to cover the beam-pipe and coil sections; bins of size $5 \times 5 \times 50\,\mathrm{cm}^3$ were used to cover the magnet yokes and cryostat regions and bins of size $20 \times 20 \times 50\,\mathrm{cm}^3$ were used to score dose in the air of the tunnel, tunnel walls and floor. Details of the dose at a specific longitudinal position in the DS section are known to 50 cm (longitudinal dimension of scoring bin). The final energy deposition in each mesh bin is the total of all contributions arising from each of the interaction point runs. This is a valid method for obtaining the total dose since contributions arising upstream of the interaction point are orders of magnitude lower than the dose deposited downstream under the development of the hadronic and electromagnetic cascades - there is essentially no backscattering. Due to the local nature of the proton point losses, each run in which the protons are forced to interact at a given longitudinal position from the IP has to be weighted accordingly to the loss density (as given in Figure 1) at that distance from the IP before summation. For a given interaction point, the resulting particle cascades contribute to the dose at all points downstream of the interaction point. The significance of its contribution to the total energy deposition at a position far downstream of the loss point will be determined by its weighting, *i.e.* losses in the magnets where the maximum loss density occurs (MB8, Q8), will contribute a significant energy deposition in the end regions of the dispersion suppressors (missing magnet and Q11) in addition to the energy deposition resulting from losses closer to these magnets.

The total energy deposition (GeV) weighted by the loss density is then converted to Dose (1 Gy=1 J/Kg) to give the annual dose per year in each scoring bin. Due to the large proportion of neutrons produced by

interactions within the magnet material surrounding the beam pipes, dose estimations are sensitive to the type of material used to score energy deposition [Huh96], *i.e.* dose scored in a hydrogenous material such as polythene can be as much as twice the dose scored in an inorganic material such as aluminium or air. Thus, this simulation uses the correct material for each magnet component wherever possible to provide the most accurate dose estimation for the different sections in the magnets.

Total annual dose:

To calculate the extra dose contribution in the dispersion suppressor region due to beam-gas interactions, the above simulation runs were weighted by the appropriate proton loss rate for collisions with the residual gas in the beam-lines. In addition, simulation runs were performed for the second beam-pipe, since beam-gas interactions occur uniformly distributed in both beam-lines. Thus in total, 173 simulation runs were made covering the entire length of the DS geometry. The total dose due to beam-gas interactions was obtained by summing the contributions for each beam-line weighted by the proton loss rate for beam-gas interactions: this rate will be similar to that in the standard arc sections, thus the value was taken to be $1.65 \times 10^{11}\,\mathrm{m}^{-1}\mathrm{s}^{-1}$ for two beam-lines [Pot95b]. The total annual dose in the DS regions is then given by the sum of the contribution due to point losses and the contribution due to beam-gas interactions. The dose maps showing the total annual dose are presented in Appendices A1 - A6. These should be used to determine the required radiation resistance of materials and electronics to be placed in the dispersion suppressors. However, to obtain a feeling for the importance of the individual contributions, Figures (3a) and (3b) show the contribution to the annual dose from point losses in the DS regions of Pt1 and Pt5 respectively, whilst Figure (4) shows the contribution due to beam-gas interactions. Figure (4) is plotted to the same scale as Figure (3) for ease of comparison.

Figure (3) clearly shows that point losses dominate the contribution to the total dose in localised regions of the DS, corresponding to the positions (just downstream) of the largest proton loss rates - this is for the region downstream of Q8 / MB9 and again for the missing magnet and Q11. In regions where proton point loss rates are very low, (*i.e.* between $\sim$350m - 400 m from the IP), there is still a contribution to the total dose which arises from the point loss interactions upstream of this region. This contribution is a few gray / y which is similar to that of beam-gas interaction doses. The additional dose due to beam-gas interactions is given in Figure (4). This shows a relatively uniform dose contribution over the entire DS section of $\sim$1-2 Gy / y close to the tunnel wall rising to $\sim$5 Gy / y close to the magnets. Higher doses of a few tens Gy / y are observed in the regions of the inter-magnet gaps. Thus the beam-gas dose distribution in the tunnel of the DS section is very similar to that found in the tunnel of the standard arc sections. However, the missing magnet section shows higher doses ($\sim$100 Gy / y) due to the reduction in shielding material surrounding the beam-lines. This clearly shows the importance of shielding by the magnets of the LHC machine.

Note, in this simulation, since interactions are only considered in the length of the geometry shown, contributions to the dose at the end of the FLUKA DS section arising from interactions upstream of MB8B are not taken into consideration. Thus, doses in the first half of the magnet MB8B are not complete and should be ignored - reliable doses can be taken to start from approximately the middle of the outer dipole MB8B.

Particle fluences:

Since the average particle fluence in a volume is equal to the total length travelled by the particles inside that volume divided by the volume (*i.e.* $\phi = tracklength/V$), in addition to scoring energy deposition in each of the mesh bins, the tracklength of neutrons, protons and charged pions was also scored. Summation of all contributions in each scoring bin from each of the simulation runs is required to obtain the total tracklength in a given scoring region and appropriate weighting made by the proton loss rate due to point losses and beam-gas interaction rates as described above. Analysis of the particle fluence data was made for various energy cuts including, neutrons $>$ 100 keV which are responsible for bulk damage in Si, and hadrons $>$ 20 MeV & 100 MeV which are responsible for SEUs.

To define the radiation environment in the DS regions we take the ratio of Fluence:Dose in each scoring bin giving units of: number of particles $\mathrm{cm}^{-2}\mathrm{Gy}^{-1}$. This data is shown in Appendix B. Using the dose maps

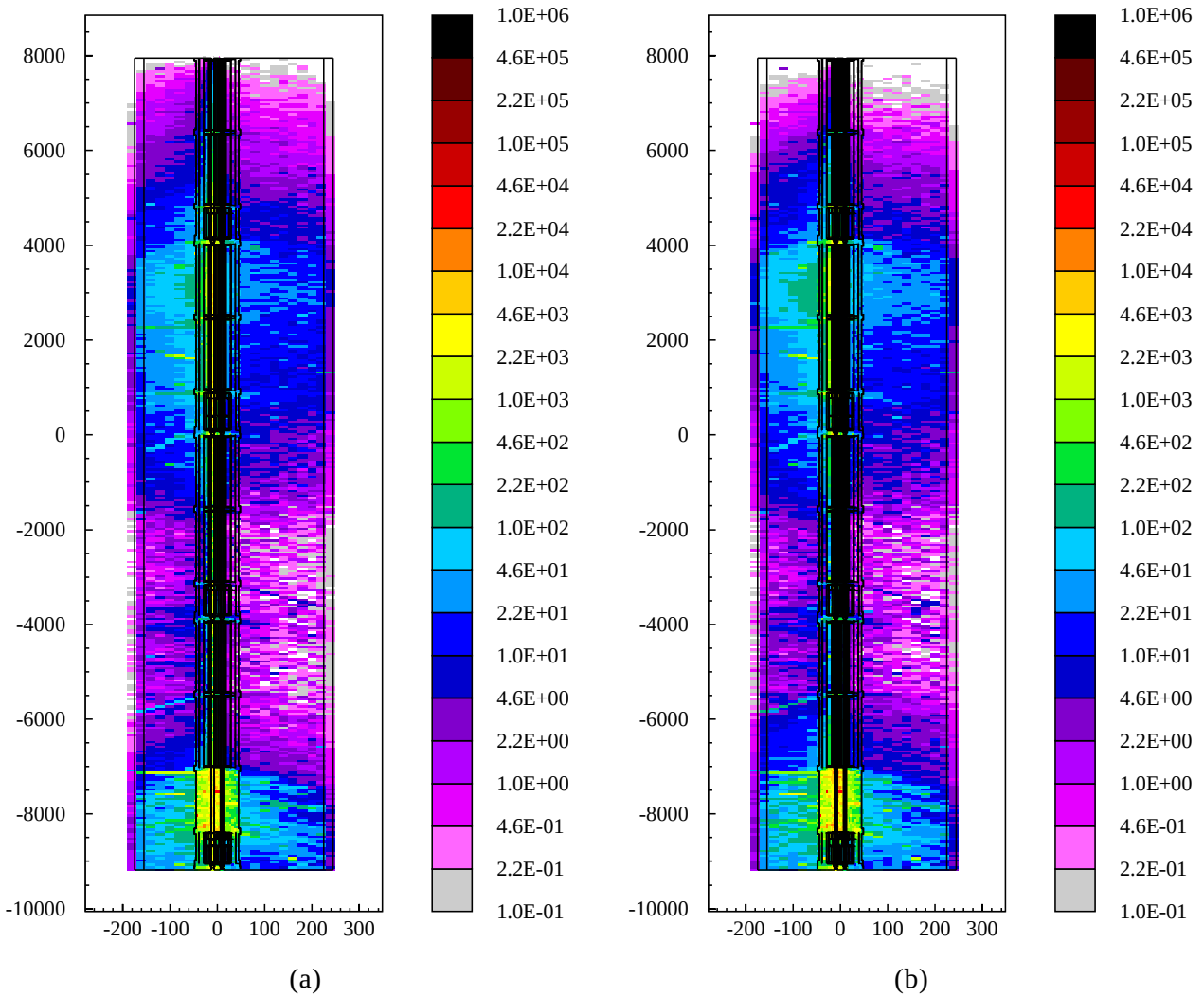

Figure 3: Contribution to annual dose (Gy / y) in dispersion suppressor regions due to point losses for a) DS1 (proton loss weighting given by red solid line in Figure (1)) and b) DS5 (proton loss weighting given by blue dashed line in Figure (1)).

of Appendix A, absolute values for the particle fluence can easily be obtained.

3.2.1. Extra detail of the quenchdiode regions

In order to determine whether expensive, high radiation tolerant quench diodes will be required in the dispersion suppressors of the LHC, the intricate design of the magnet diodes has been reproduced in as much detail as possible for both dipole and quadrupole diodes. This is to estimate as accurately as possible the dose distribution within the volume of the diode housing region and to individual components *e.g* the silicon wafers. A previous study of dose to the quench diodes due to beam-gas interactions in the LHC arcs has provided preliminary estimates of the total dose to the volume within the diode housing. This gives a figure of 180 Gy for 10 years averaged over the whole diode region for two rings and shows an order of magnitude gradient in the radial dimension across the diode [Ste97]. In this simulation the various components of the diode have been included separately with their respective material composition. The explicit geometry is shown in Figure (5a) for the quadrupole diode Q11 (note: in the dispersion suppressors of IR1 and IR5, only Q11 contains a quench diode), and Figure (5b) for the dipole diodes. All simulated

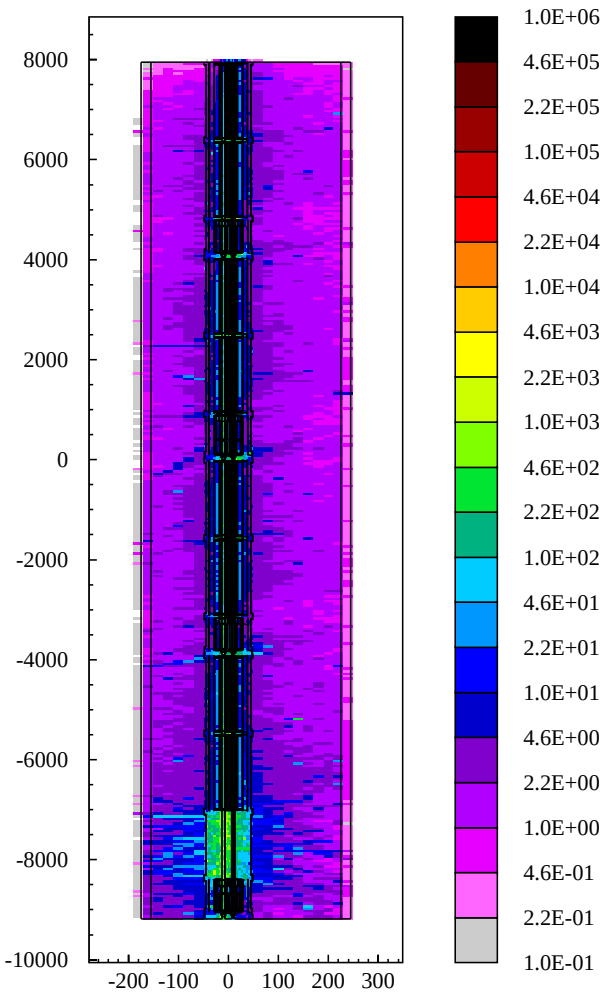

Figure 4: Contribution to annual dose (Gy/y) in dispersion suppressor regions due to beam-gas interactions. This is for a proton loss rate of 1.65×10^{11} m^{-1}s^{-1}. Plotted to same scale as dose for point losses.

dipole magnets of the DS region include a diode of the form Figure (5b). In the real magnet diodes the sensitive component consists of a set of very thin individual silicon wafers. This has been simulated by considering all the wafers as one component of thickness 0.9 cm situated between blocks of copper (see Figure (5)).

To obtain a detailed distribution of the dose in this region, fine scoring meshes of size $1 \times 1 \times 2\,\mathrm{cm}^3$ were placed over each magnet diode as well as scoring energy deposition in each volume region. The total dose in each mesh bin and geometry region is obtained using exactly the same method as above for the entire DS geometry scoring.

4. Doses in the Dispersion Suppressor regions IR1 and IR5

Results of the total annual dose (point loss + beam-gas interactions) in the DS regions of IR1 and IR5 can be found in Appendices A1 - A6 of this report.

The following discussion will concentrate primarily on the case of differing proton losses in Points 1 & 5, since this will provide the most pessimitic scenario for the doses in the DS regions. The case when no distinction is made between collisions in IP1 or IP5 is included in Appendix A.1. This case will be discussed

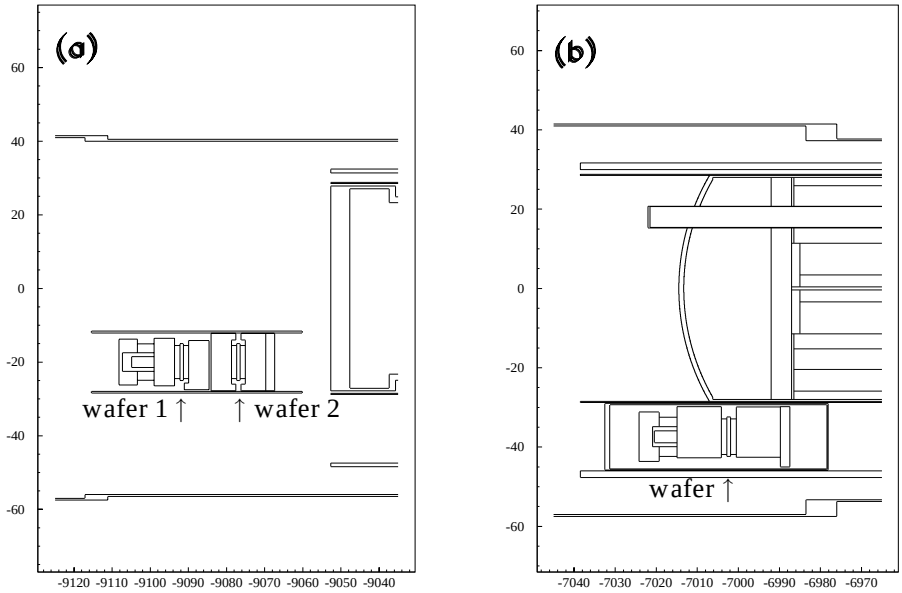

Figure 5: FLUKA simulation of the a) quadrupole and b) dipole diodes in the dispersion suppressors. Each dipole in the DS lattice includes a diode of the form (b). In the DS regions IR1 and IR5, the only quadrupole to have a quench diode is Q11. In the simulation the individual thin Si wafers of the diode have been placed together to form one Si wafer of thickness 0.9 cm (2 wafers in the case of the quadrupole diode). These are indicated by the arrows above.

briefly in Section 4.1.4 since these values are not necessarily obsolete [Bai00].

Note on the scale keys of dose maps:
In the following appendices, all dose maps are given to the same scale. For plots with horizontal keys, due to space restrictions and clarity of reading it is not possible to give all division labels on the plot. The exact value of a given colour code can be obtained from the vertical keys of other plots in which the labelling is given for all divisions.

4.1. Doses in and around the DS magnets

The expected annual doses in the LHC tunnel surrounding the magnet string are given in Appendix A.1. Figures 12 - 14 show the doses radially out from the magnet string to the tunnel wall for the points 1, 5 and for the case when no distinction is made between the two points (pt0) respectively. The doses expected above and below the magnet string are shown in Figures 16 - 18. Specific details for each cut are given with the relevant figure. The dose maps show similar distributions for the three cases due to the similarity of the point loss distributions used in the weighting of the energy deposition runs. Point 5 tends to show larger extended regions of higher dose than Point 1 due to it having the higher loss density of the two.

4.1.1. Doses alongside the dispersion suppressor magnets

Plots of the dose alongside the magnet string at the height of the beam-axis are found in Figures 12 & 16 and Figures 13 & 17 for DS1 and DS5 respectively. Here the localised nature of the point loss distributions can clearly be seen. “Hot-spots” occur in the vicinity of the dipole magnets MB9A and MB9B, reaching annual doses in excess of $\sim 200\,\mathrm{Gy/y}$ alongside the magnets and $100\,\mathrm{Gy/y}$ at the outer tunnel wall, for both Points

1 and 5. This "hotest" region extends the full length of MB9B for Point 5, whilst being much smaller for Point 1. Alongside MB9B for both Points 1 & 5 typical doses are easily 100 Gy / y. Alongside dipoles MB9A doses are a few tens of gray reaching as high as ~ 100 Gy / y (however with the indication that in the central regions one could see a few areas reaching values of ~ 1000 Gy / y). This higher dose region extends as far downstream as the quadrupole Q9 where one can still find doses up to ~ 100 Gy / y close to the magnet cryostat falling to a few tens of gray at the outer tunnel wall. These "hot-spots" are due to the fact that the maximum of the proton loss density for both regions occurs upstream of the dipoles MB9, hence the resulting maximum dose deposition is some metres downstream of the maximum loss point in MB8A / Q8. Other significant "hot" regions are found in the vicinity of the missing magnet and the quadrupole Q11. These are due to the second set of large proton losses occuring in this vicinity (see Figure 1) as well as the contributions to the dose from the region of maximum proton loss upstream near Q8. Doses alongside Q11 are a few tens to 100 Gy / y, reaching several hundreds of gray per year close to the magnet cryostat. In the magnet regions where there are essentially no point losses (MB10A, Q10 and MB11B) the total dose arising from upstream point loss contributions plus beam-gas interactions is comparable to those found in the LHC standard arc sections. Due to the fact the dominant proton losses in the DS regions arise from point losses, there is no uniform dose distribution along the magnet string. This makes it difficult to determine a "typical" dose alongside a dipole, quadrupole or gap region. To give an indication of the radial dose distribution in the LHC tunnel, cross-sectional cuts can be found in Appendix A.3 for the regions of higher dose by MB9M and Q11 for DS1 and DS5. All other positions in the tunnel of the dispersion suppressors will see lower doses than these.

By far the hottest region in the dispersion suppressors of Points 1 and 5 is the section containing the missing magnet. Here doses within the cryostat are thousands of gray per year, falling to hundreds of gray per year at the outer tunnel wall (with possible spots reaching a few thousands of gray per year in the space between the cryostat and the outer tunnel wall). This is an obvious candidate for a position that could cause problems with equipment / electronics if they have to be placed close to this spot. One possibility for reducing the dose in this region would be to fill the cryostat region with extra material.

Proton point losses in the DS occur in the beam-pipe closest to the outer tunnel wall, hence we observe the maximum dose towards the outside of the ring. On the opposite side of the magnet string, (inside the ring), the dose from point losses can be up to an order of magnitude lower. Doses do however still reach a few tens of gray per year opposite MB9B at the position of the tunnel wall and a few hundreds of gray per year in the vicinity of the missing magnet and Q11. To give an overview of the DS region a summary of the longitudinal dose distribution at the cryostat surface and at the tunnel wall for each magnet is given in Figure (6) for IR1 and Figure (7) for IR5.

4.1.2. Doses under the dispersion suppressor magnets

Maps showing the dose due to point losses under the magnet string in the DS regions of Points 1 and 5 can be seen in Figures (16) and (17) respectively. These are averaged over a 60 cm slice about the central point between the beam-pipes (40 cm slice in the central region) as shown in Figure (11). In general, the doses under the magnet string are not so high as those directly alongside the outside of the magnet string at the level of the beam-axis. For both DS regions, doses will be less than ~ 100 Gy / y, except under Q11 and the empty cryostat region. Here doses can reach ~ 1000 Gy / y. To give a summary of the expected dose under the DS magnet string, the longitudinal dose distribution averaged over a height of 30 cm lying between the cryostat and the floor surface (of the doses presented in Figures (16) and (17)), are shown in Figures (8a) and (8b) respectively for Points 1 and 5.

4.1.3. Doses in the tunnel floor of the dispersion suppressors

In the vicinity of the regions of highest proton loss we note that higher doses will also be observed in the concrete floor of the tunnel. Maps showing the dose distribution in the tunnel floor can be found in

Appendix A.2. For DS1, in the vicinity of MB9B doses of the order $\sim 50\,\mathrm{Gy/y}$ are seen, with higher doses of $\sim 100\,\mathrm{Gy/y}$ observed for the same position in DS5. Higher doses are seen in the vicinity of the missing magnet and Q11, reaching values possibly as high as $\sim 1000\,\mathrm{Gy/y}$ in both DS regions. This could be of concern for any radiation sensitive equipment that will be placed on the tunnel floor.

4.1.4. Dose in dispersion suppressors for case with no distinction made between IR1 and IR5

Results for the case where no distinction is made between Points 1 and 5 (Appendix A.1: Figures 14 & 18) show similar distributions to those discussed above, although hot-spot regions tend to have lower dose maxima and are less extended than those when the two Points are considered separately. Due to further work to be performed regarding the absolute loss distributions in the dispersion suppressors, these results are not obsolete [Bai00] and are included here for completeness.

4.2. Maximum dose in the inner regions of the dispersion suppressors

Maximum doses are observed radially outwards in the beam-axis plane. Due to the large dose gradient about the beam-axis (*i.e.* doses above/below the beam-axis are much lower than along the beam-axis), to obtain an estimate of the maximum doses to components that will be situated around the beam-axis, Figures (23) and (26) in Appendix A.4 show the annual dose averaged over a 4 cm slice[2] about the beam-axis for the inner regions of the magnets for the length of the dispersion suppressor regions of Points 1 and 5 respectively. The dose distribution along the beam-pipes in the DS is not constant due to the non-uniform longitudinal proton loss distribution. The maximum dose reaches a value of at least $10^5\mathrm{Gy/y}$ along the outer beam-pipe of both MB9 dipole magnets. Typical doses along the beam pipes in other sections of the dispersion suppressors are of the order 10^3-$10^4\,\mathrm{Gy/y}$, which are similar to the levels found along the beam-pipes in the standard arc sections.

4.2.1. Dose along beam-pipe in MB9 section - on beam-axis

The maximum dose occurs a few metres downstream of the maximum proton loss points, thus maximum doses are observed along the beam-pipe of the dipole magnets MB9A and MB9B. The maximum dose averaged over 4 cm about the beam-axis for the inner regions of magnets MB9A/B is shown in Appendix A.4 (Figures 24 and 27) and a selection of cross-sectional cuts through the outer beam pipe of these magnets in Figures 25 and 28. In the inner magnet coils, maximum doses are observed in the plane of the beam-axis and to the side in which the dipole magnetic field is biasing the particles (towards the inside of the ring). Doses as high as $\sim 2.2 \times 10^5\,\mathrm{Gy/y}$ are found in the beam-screens/pipes and inner coils of DS1 and maxima approximately a factor 2 higher in DS5 ($\sim 5 \times 10^5\,\mathrm{Gy/y}$). There is at least an order of magnitude difference in the annual dose between the top:middle and bottom:middle of the coils. For components which will be installed between magnets and close to the beam-pipes, these should be able to withstand annual doses of $\sim 10^5\,\mathrm{Gy/y}$ to ensure survival at all positions in the dispersion suppressors.

[2] This is for the same cut as shown in Figure (11), but the shaded region covers a slice of 4 cm about the axis for the inner magnet regions, not 20 cm.

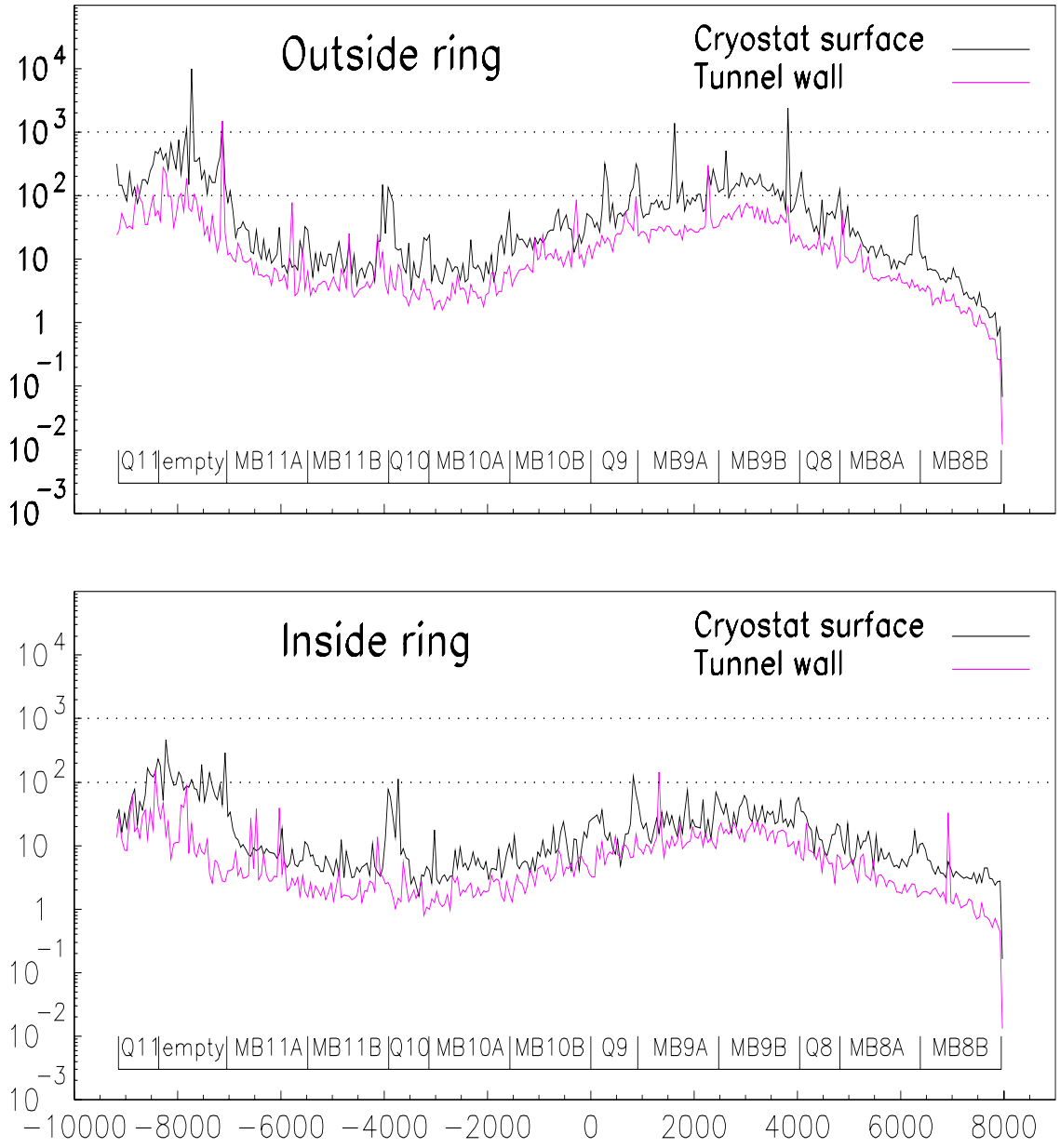

Figure 6: Doses alongside the magnets of the dispersion suppressors of PT1 for a radial position at the surface of the cryostat (black line) and at the tunnel wall (pink line). The upper plot shows the longitudinal dose distribution at the height of the beam-axis averaged over a 20 cm slice (see Fig. 11) outside of the LHC ring. The lower plot shows the longitudinal distribution for the same radial positions but for the inside of the LHC ring. To guide the eye, the horizontal dotted lines indicate the 100 Gy/y mark and the 1000 Gy/y mark. The schematic under the plot indicates the position of the individual magnets, delimited by their virtual interconnection planes.

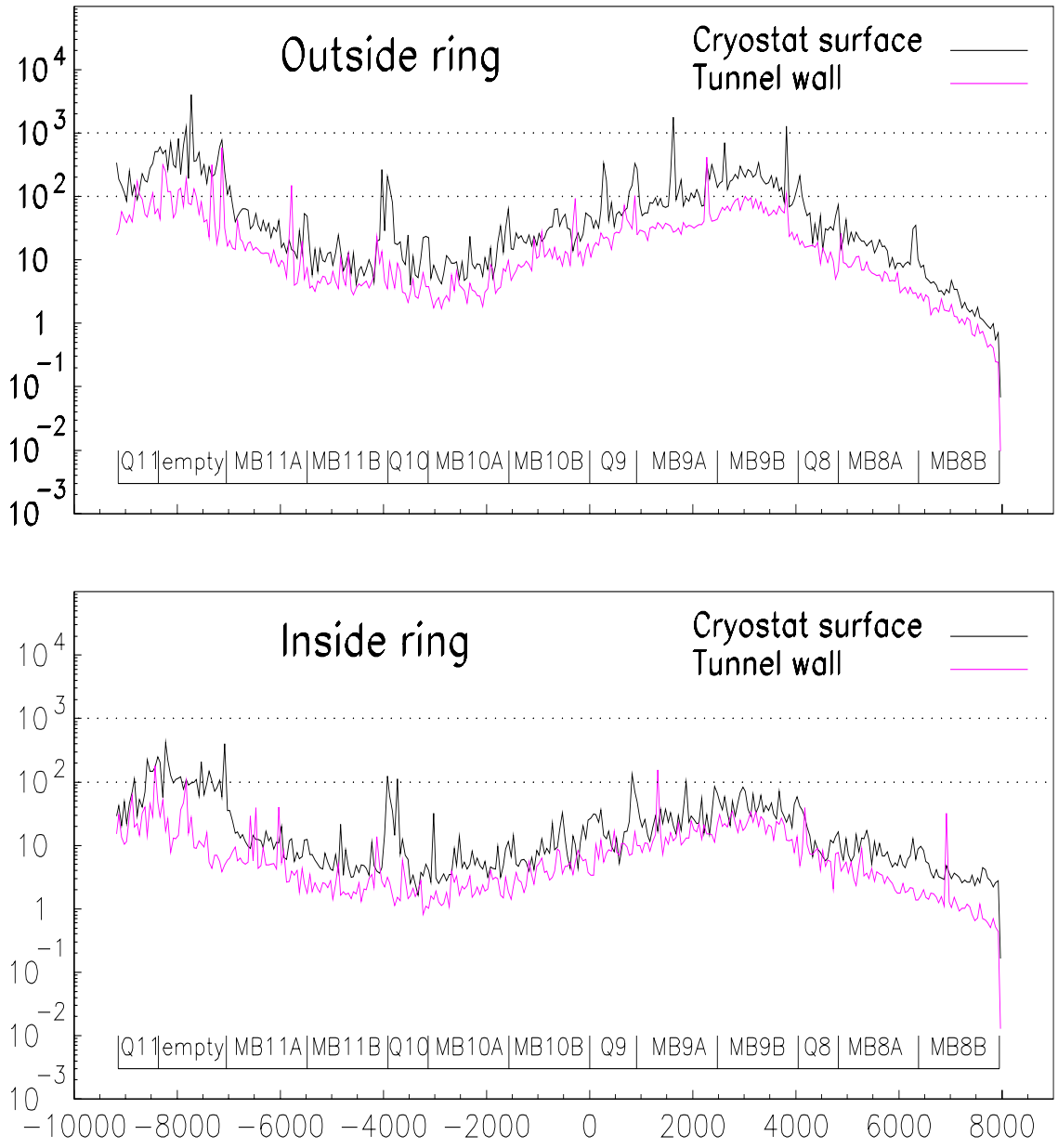

Figure 7: Same as Figure6 but for the dispersion suppressors of Point 5.

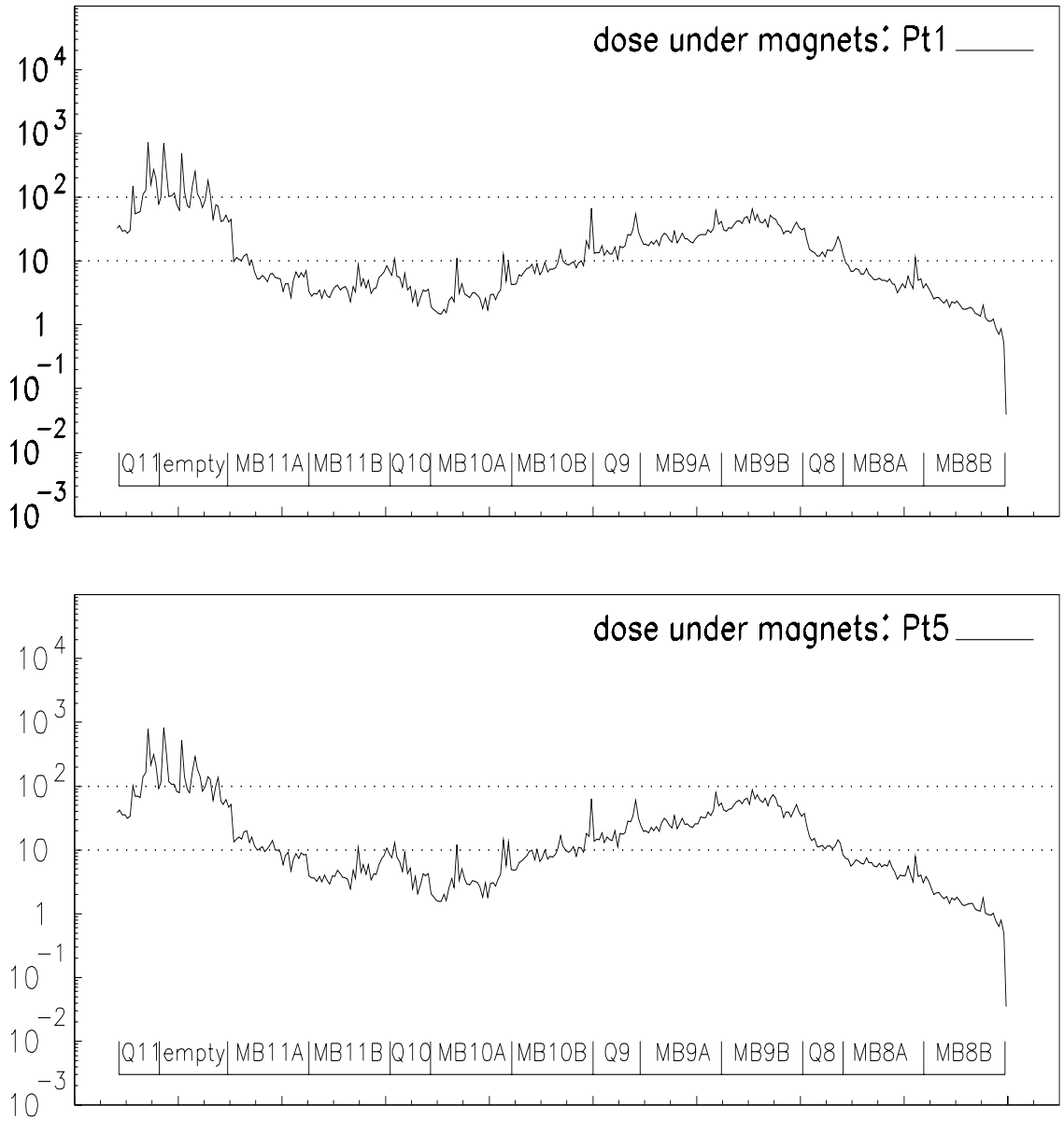

Figure 8: Longitudinal dose distribution (Gy/y) under the magnets of the dispersion suppressors downstream of a) Point1 and b) Point5. These are averaged over a slice of height 30 cm lying between the cryostat and the floor for the Figures 16 and 17. To guide the eye, the horizontal dotted line indicates the 100 Gy/y mark. The schematic under the plot indicates the position of the individual magnets, delimited by their virtual interconnection planes.

4.2.2. Dose to BPMs of dispersion suppressors: Q8-Q11

Annual dose to the Beam Position Monitors of the dispersion suppressors is shown for each quadrupole magnet in Appendix A.5 (Figures 29 (a)-(d) and 30 (a)-(d) for DS1 and DS5 respectively). These plots are averaged over a total height 12 cm above and below the beam-axis to cover the extent of the BPM. Maximum doses are similar for the dispersion suppressors of Points 1 and 5. The BPMs belonging to Q10 tend to have lower maximum doses along the outer beam pipe than for the other quadrupoles. This is due to the low proton point loss rate at this point. Maximum doses close to the beam-pipe for Q8, Q9 and Q11 are of the order several 10^4 Gy / y, whereas for Q10 this value falls to several 10^3 Gy / y. The dose to the BPM is lower for the second beam-line since the dose at this postion does not receive such a large contribution from the point loss interactions, as for the outgoing beam-line. The lower dose region observed for the BPM of Q11 for the second beam-line (for both DS1 & DS5) is an artifact of the Monte-Carlo simulation. This is due to its position at the end of the geometry - since protons are sent down the beam-line starting at the end of the geometry, contributions to the dose at this point arising from interactions upstream in the arcs are not included. Realistic dose values for the second beam-line of Q11 should be similar to those shown in plots (a)-(c) for the other BPMs.

4.3. Dose to the quenchdiodes in the dispersion suppressor regions

Table 1: Summary of dose to the quench diodes in the dispersion suppressors of IR1 and IR5. Values for the dose averaged over the entire diode housing region as well as the dose specifically to the Si in the diodes are given for each magnet. In the DS of IR1 and IR5 the only quadrupole to have a diode is Q11.

lattice element	Average dose over entire diode region Gy / y			lattice element	Doses to Si in diode region Gy / y		
	Pt 1	Pt 5	Beam-gas		Pt 1	Pt 5	Beam-gas
Q11	116.1	127.8	12.9	Q11 Si wafer 1	100.3	134.3	13.2
-	-	-	-	Q11 Si wafer 2	57.7	63.3	11.8
MB11A	32.9	44.3	16.8	MB11A	8.3	10.7	1.5
MB11B	8.3	9.4	6.5	MB11B	1.8	2.3	1.7
MB10A	6.3	6.4	5.0	MB10A	1.2	1.2	0.8
MB10B	10.8	13.3	5.4	MB10B	1.8	1.8	1.8
MB9A	67.6	75.4	5.3	MB9A	15.8	16.7	1.2
MB9B	400.8	497.5	15.7	MB9B	38.3	47.2	1.9
MB8A	25.0	20.0	3.6	MB8A	10.8	9.9	1.3
MB8B	9.2	7.5	5.3	MB8B	5.9	4.6	2.6

Maps of dose due to point losses in the quench diodes for each magnet element are given in Appendix A.6. Figures (31) - (40) show the doses in the dispersion suppressors for both IR1 and IR5. Very little difference is seen between the two regions. To summarise the doses to the magnet diodes, Table 1 shows a) the average annual dose to the entire diode region (*i.e.* averaged over the volume within the diode housing and b) the annual dose to the Si wafers for dispersion suppressors IR1, IR5. The values averaged over the volume of the diode housing for each magnet provide an order of magnitude estimate of the annual dose to individual diodes in the DS regions. The 3rd column of each section (labelled 'Beam-gas') shows the contribution to the dose from beam-gas interactions. This provides an indication of the dose to the quench diodes in the standard arc sections. The results of dose to the Si wafers were obtained from the total energy deposition within the Si region of the simulation. These values are not reliant on the mesh scoring in which bins could contain contributions from other elements within the diode housing; thus this should provide a good estimate of the dose to the sensitive silicon of the diodes and accounts for the large differences seen between the two sets of values.

In general the annual dose to the sensitive silicon components of the quench diodes is very low with exceptions to the diodes of quadrupole Q11 and possibly MB9B. For 10 years of LHC running total doses should not exceed 1 kGy (Si diode of Q11 in Pt5 excepted). The larger dose values seen over the entire diode volume are due to the large dose gradient across the diode volume - there is a strong top:bottom gradient of at least an order of magnitude difference in the doses, with an increase in dose seen towards the front end intermagnet-gap region.

Corresponding values for the neutron fluences above various energy cuts at the position of the quench diodes are given in Table 2 in Section 6.2.

5. Annual dose in the dispersion suppressors of Points 3 & 7

To date no calculation of dose values exists for the dispersion suppressor regions of the cleaning sections IR3 (momentum cleaning) and IR7 (betatron cleaning). This simulation is made difficult in that we do not have full knowledge of the point loss distribution for these regions, which is essential if we are to scale any Monte Carlo simulation results of dose normalised for one interacting proton per metre to give absolute values of annual dose.

Obtaining proton loss distributions for the DS sections of the scraping regions of the LHC ring is more difficult than for the DS regions downstream of the high luminosity interaction points, due to the nature of the collision points. Calculation of proton losses downstream of IR3 and IR7 is made more difficult since the source points are distributed in the collimator jaws of the insertion sections, compared to the unique source point for the experimental interaction regions. This leads to quite large statistical uncertainties in the loss distributions in the DS regions of IR3 and IR7. Another problem is that the point loss distributions downstream of the scraping regions are dependent on the layout of the collimators in these sections. To date, the design of these is not fully fixed making absolute predictions for the proton loss distributions in the DS regions of IR3 and IR7 impossible.

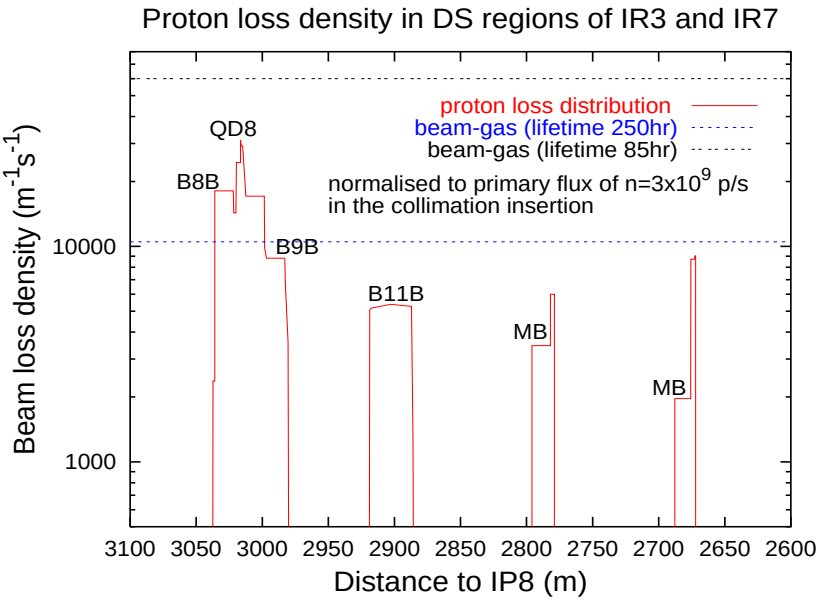

Figure 9: Proton loss density in the dispersion suppressors of IR3 and IR7 as given in [Jea01a]. The longitudinal coordinate has an arbitrary origin at IP8.

However, an indication of the expected proton loss distributions in these regions does exist. This allows us to draw some general conclusions regarding the expected annual dose distributions in the DS regions of IR3 and IR7. Estimation of the expected proton loss rates downstream of the scraping sections of the LHC can be found in [Jea01a]. This data is reproduced in Figure (9), which is normalised to a primary flux of

3×10^9 protons/s in the collimation insertion. [Jea01a] reports that similar integrated loss rates are computed for the betatron and momentum collimation insertions which allow us to use the same differential proton loss distribution for both IR3 & IR7. This data is plotted as a function of distance from the LHC point IP8, which is taken to be an arbitrary origin. The difference in the losses in IR3 and IR7 will be the absolute normalisation of the results, which is not known at present. This estimation of the losses is based on LHC optics verion 5.0. Proton loss distributions are dependent on the layout of the scraper insertion regions, however, no significant changes were seen beyond the extent of the cleaning regions in the long straight sections for higher optics versions[Jea01b]. Therefore this data can be used to give an estimate of losses in the DS sections downstream of the scraper regions for the current LHC version.

Even though proton losses for the scraper regions have a different origin than those for the collision regions, the off-momentum proton losses in the dispersion suppressors are very similar. This is shown in Figure (9) where we see a very similar proton loss distribution downstream of the scraper regions, as that seen downstream of the high luminosity interaction points (see Figure (1)) *i.e.* losses occur in the same magnets. We note that the point loss magnitude is much less than that in IR1 & IR5. The maximum point loss densities reach ~ 3 times higher than the beam-gas loss rate in the standard arc and dispersion suppressors as given for the LHC Design Machine (blue dotted line in Figure (9)). In fact, the magnitude of point losses beyond MB9 in the DS and arc sections of IR3 and IR7 is lower than that of the beam-gas interaction rate. Thus for these regions, beam-gas interactions can be considered to be the dominant contribution to the total dose; point losses are essentially negligible.

This implies that we expect to see similar point loss dose distributions in the dispersion suppressors of the scraper regions as those shown in Figure (3), but with a magnitude similar to that of the beam-gas dose. The dominant contribution to the annual dose from beam-gas interactions will have a similar distribution to that shown in Figure (4). *It is important to remember that the exact normalisation is not known for these losses. Thus the contribution from point losses could be significantly higher than discussed here if a large normalisation factor is found to be required at a later date.* If so, it should be possible to scale the dose distributions as presented in Figure (3) for IR1 & IR5 to obtain an estimate of the dose in the scraper region dispersion suppressors, as long as the loss distribution does not significantly alter. Similarly plots of dose due to beam-gas contributions can be scaled if necessary. In the opinion of the author, in the light of the present information given by the expected point loss rates in Figure (9), further explicit Monte-Carlo simulation of the dispersion suppressor regions of IR3 and IR7, which would take many months of computing time, is not warrented.

6. Radiation environment in the DS regions 1 & 5

Electronics equipment and machine components placed in the LHC tunnel will also be susceptible to the high energy particles found around the machine. To enable estimation of possible SEE effects, it is necessary to know the radiation environment in which the equipment will be placed. Thus, this section presents values for the fluence : dose ratios to be expected in DS1 and DS5; the maps and full information of which can be found in Appendix B. Using these ratio maps in combination with the relevant dose maps given in Appendix A, values for the total annual particle fluences at a position in the LHC tunnel are readily obtained.

6.1. Fluence:dose ratios in the dispersion suppressors DS1 & DS5

Maps of the ratio particle fluence : dose are shown in Appendix B for neutrons, protons, charged pions and total summed hadrons above five specific energy cuts: 100 keV, 1 MeV, 20 MeV, 50 MeV and 100 MeV. Neutrons above 100 keV are responsible for causing bulk damage in Si and the higher energy hadrons are responsible for causing Single Event Upsets (SEUs).

It is found that the radiation environment, characterised by the ratio R=fluence / dose, for the machine section in DS1 and DS5 is the same, with variations of only a few percent seen between the two data sets. A

larger variation is observed for protons close to the cryostat on the outside of the LHC ring such that values for the proton ratio above all energy cuts in DS5 are between 2-4 times larger than those of DS1. This will be due to the difference in the proton loss distributions of the two sections, as the losses occur in the outgoing beam-line close to the outside of the LHC ring. However, since the ratio maps are plotted with each decade split into 3 colour grades, this variation is indistinguishable between maps for DS1 or DS5, thus, only one set of ratio maps is given. The results plotted in this report specifically use data for DS1, but are equally valid for both DS1 and DS5.

The radiation environment in the dispersion suppressors is not completely uniform. To give an overview, Appendix B.1. shows the longitudinal ratio distribution above and below the dispersion suppressor magnet string for neutrons and hadrons for all energy cuts (Figures (41) and (44)), as well as the individual proton and charged pion contributions above the energy cuts 100 keV and 100 MeV (Figures (42) and (43)). Very little drop is seen in the proton and charged pion distributions between these energy cuts.

It is observed that the environment between MB11A and MB8B is the same as that for the LHC arc sections (see fluence : dose maps in [Fyn01a]). Here we observe essentially uniform ratios in the vicinity of dipole magnets, quadrupoles and intermagnet gaps, allowing us to average over these regions to obtain a characteristic value of R alongside a dipole (n $>$ 100 keV: $\sim 5 \times 10^{10}$ cm^{-2}, h $>$ 100 MeV: $\sim 2 \times 10^{9}$ cm^{-2}), quadrupole (n $>$ 100 keV: $\sim 5 \times 10^{10}$ cm^{-2}, h $>$ 100 MeV: $\sim 2 \times 10^{9}$ cm^{-2}) and intermagnet gap (n $>$ 100 keV: $\sim 3 \times 10^{10}$ cm^{-2}, h $>$ 100 MeV: $\sim 1 \times 10^{9}$ cm^{-2}) respectively. It should be noted that the ratios found in the vicinity of the missing magnet and Q11 are lower than these values. We expect $\sim 3 \times 10^{9}$ cm^{-2} and $\sim 1 \times 10^{10}$ cm^{-2} for neutrons $>$ 100 keV, with these values falling to $\sim 2 \times 10^{8}$ cm^{-2} and $\sim 4 \times 10^{8}$ cm^{-2} for hadrons $>$ 100 MeV in the region of the missing magnet and Q11 respectively.

The distributions above / below the magnet string are very similar to those found in the beam-axis plane, as the ratio is found to be reasonably radially symetric about the machine. To give an indication of the variation in the ratio in the LHC tunnel, Appendix B.2. shows cross sectional cuts through the tunnel for the individual magnet components: Q11, the missing magnet, a typical dipole, quadrupole and intermagnet gap (Figures (45) - (54)), for all neutron and hadron energy cuts. These plots are obtained by averaging over the length of the individual magnets and for the case of a "typical" magnet element by averaging further over the individual magnet component values, *e.g.* the value for a dipole is obtained by averaging over the averaged value obtained for MB11A - MB8B. The data plotted for Q11 and the missing magnet is obtained by averaging over the data along the length of the relevant section. Generally, variations of a $\sim$ few tens % are observed in performing this averaging - however, larger variations are seen when averaging over the region of the missing magnet in which a much less uniform ratio distribution is observed. Reasonable radial symmetry is observed in the tunnel alongside magnet components, with slightly lower ratios seen towards the outside of the tunnel in the beam-axis plane for the low energy neutrons. Larger deviations from uniformity are seen in the vicinity of the missing magnet where the ratio increases by approximately an order of magnitude between the surface of the cryostat and the tunnel wall.

To give a quantitative overview of the variation in the fluence : dose ratios found in the LHC dispersion suppressors, Appendix B.3. provides tables of the ratio at specific positions in the LHC tunnel: specifically for positions alongside the cryostat, both inside and outside the LHC ring, at the tunnel wall inside and outside the ring, under the magnet string and for 3 heights above the magnet. These values should be used with the corresponding dose at these positions in DS1 and DS5 to give the required annual particle fluence. Full data is given for neutrons, hadrons and the individual proton and charged pion contributions for each energy cut (Figures (55) - (59)). To give an idea of the statistical uncertainity on these values from averaging over the data along the length of a magnet component / over dipole magnets etc., the column, $\pm$ %, gives the standard error on the mean in taking the average, and the column, sd %, keeps track of the standard deviation of the values averaged - specifically the largest value between the standard deviation obtained in averaging over the magnet component data sets, or the combined error of the standard deviations on the 'raw' data being averaged over. It can be seen that the data alongside dipole / quadrupole magnets is essentially uniform with small deviations of a few tens %. The largest errors are obtained in averaging over the data to give a "characteristic" value for the missing magnet and gap sections of the machine (up to $\sim$ 70%).

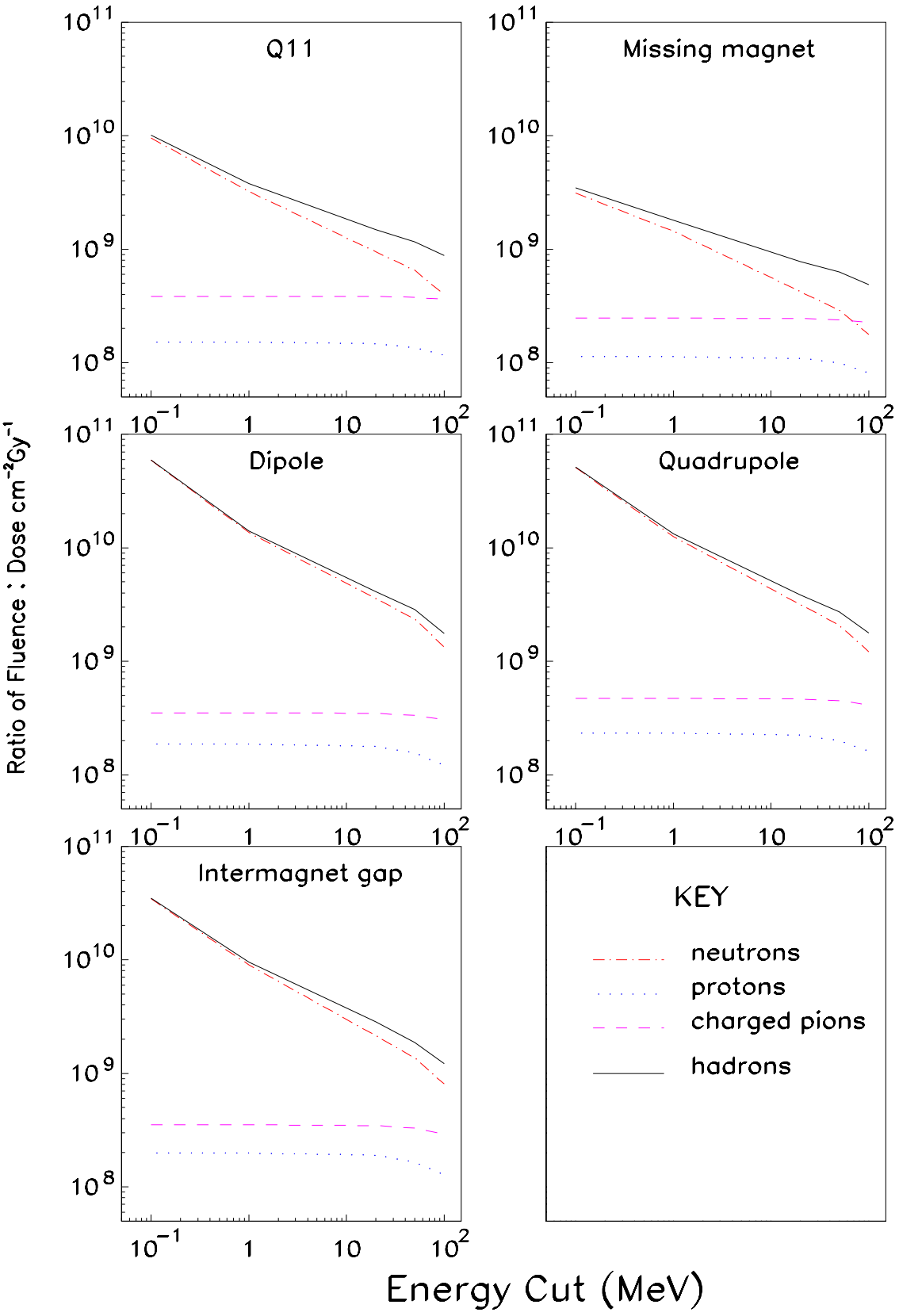

Figure 10: Ratios of fluence:dose as a function of the particle energy cut. Summary curves are shown for neutrons, protons, charged pions and total summed hadrons above a given energy cut. The individual plots show the radiation environment in the vicinity of Q11, the missing magnet, a dipole, a quadrupole (not Q11) and the intermagnet gap regions for the dispersion suppressors of DS1 and DS5. Values are taken from the averaged data in Figures (55) - (59).

A summary of the radiation environment for each of the magnet components is shown in Figure (10), plotted as a function of the particle energy cut. These can be used to obtain information on particle fluences in the LHC tunnel for any arbitrary particle energy cut. In order to obtain a representative value for the ratio in the tunnel at the position of a given magnet component, the average of all data has been performed. The quantitative values for producing these summary plots are given in the "average ratio" rows of Figures (55) - (59). It is useful to note that, the ratio values in the region of the missing magnet are representative of any position in the LHC machine in which one finds the bare beamline and not just the dispersion suppressors. Similarly, the values for a "typical" dipole, quadrupole and intermagnet gap are representative of these components placed elesewhere in the machine *e.g* LHC arc sections.

6.2. Neutron fluences at the position of the quench diodes

To estimate whether the observed particle fluences in the vicinity of the dispersion suppressor magnets will cause problems for the sensitive quench diodes, Table 2 shows the annual neutron fluence (neutrons / cm^2) for each of the quench diodes in both dispersion suppressor sections. Values are given for the usual energy cuts where neutrons > 100 keV are responsible for causing bulk damage in Si, and the higher energy neutrons are a source of SEEs.

It is noted that the highest neutron fluences are found at the same position as the regions of highest dose in the dispersion suppressor sections *i.e.* at the positions of highest proton point loss. Thus fluences of $\sim$2-4 $\times 10^{12}$ neutrons > 100 keV / cm^2 can be expected at the positions of the quench diodes in MB9A and MB9B. All other diodes will see lower neutron fluences. Values are similar for the diodes in DS1 & DS5, especially in sections of the dispersion suppressors which see a radiation environment similar to that of the LHC arcs (MB11B-MB10B). At the positions of maximum proton point loss, DS5 will see slightly higher neutron fluences than the same position in DS1.

7. Summary

In this study we have performed a detailed Monte-Carlo simulation of the dispersion suppressor sections of LHC points 1 and 5, to determine the expected total annual dose and fluence : dose ratios from both point losses (the dominant factor) and beam-gas interactions. Individual dose and fluence : dose ratio maps for various cuts through the dispersion suppressor geometry are given in Appendix A and Appendix B respectively.

The plots presented here are shown as the average over a number of scoring layers, and summary plots are obtained by taking a further average over a number of different components, *e.g* dipole magnets to give a "typical" value in the vicinity of a dispersion suppressor dipole. This averaging is the dominant cause of uncertainty in the results presented here, depending on the uniformity of the dose or ratio data. It is found that the largest uncertainties arise when considering the intermagnet gap, or missing magnet sections due to the more non-uniform distributions in these areas. Generally, uncertainites of a few tens percent are obtained in averaging over data in the vicinity of magnet elements, which can increase up to a factor 2 in the gap / missing magnet regions.

Doses in the tunnel and magnets of the dispersion suppressors:

The expected total annual dose distributions from point losses in the dispersion suppressors of Points 1 and 5 are very similar. The DS magnets downstream of Point 5 will however see slightly higher doses and extended hotter regions than Point 1 since the loss density downstream of Point 5 is the larger. The dose study presented here remains valid as long as the proton loss distributions for the DS regions remain valid *i.e.* if the optics in the inner regions of IR1 or IR5 change, then the loss distributions downstream will also change.

Table 2: Neutron fluences above various energy cuts, at the postion of the quench diodes in the dispersion suppressors of IR1 and IR5. Values are the averaged annual fluence over the entire diode housing volume.

Diode	Annual Neutron Fluence $> E_{cut}$ ($cm^{-2}.yr^{-1}$)				
	Dispsersion Suppressor DS1				
	100 keV	1 MeV	20 MeV	50 MeV	100 MeV
Q11	2.9×10^{11}	1.4×10^{11}	4.9×10^{10}	3.5×10^{10}	2.3×10^{10}
MB11A	6.5×10^{11}	2.1×10^{11}	5.7×10^{10}	3.8×10^{10}	2.2×10^{10}
MB11B	2.6×10^{11}	6.4×10^{10}	1.6×10^{10}	1.1×10^{10}	7.3×10^{9}
MB10A	1.6×10^{11}	4.5×10^{10}	1.1×10^{10}	7.8×10^{9}	4.5×10^{9}
MB10B	3.2×10^{11}	8.7×10^{10}	2.3×10^{10}	1.7×10^{10}	9.2×10^{9}
MB9A	1.9×10^{12}	5.3×10^{11}	1.3×10^{11}	9.1×10^{10}	5.4×10^{10}
MB9B	2.9×10^{12}	7.7×10^{11}	1.8×10^{11}	1.2×10^{11}	6.5×10^{10}
MB8A	1.0×10^{12}	3.0×10^{11}	7.8×10^{10}	5.1×10^{10}	2.9×10^{10}
MB8B	3.1×10^{11}	8.2×10^{10}	2.0×10^{10}	1.3×10^{10}	7.6×10^{9}
	Dispsersion Suppressor DS5				
	100 keV	1 MeV	20 MeV	50 MeV	100 MeV
Q11	3.0×10^{11}	1.5×10^{11}	5.2×10^{10}	3.7×10^{10}	2.4×10^{10}
MB11A	9.0×10^{11}	2.9×10^{11}	7.7×10^{10}	5.2×10^{10}	3.0×10^{10}
MB11B	2.8×10^{11}	6.9×10^{10}	1.6×10^{10}	1.2×10^{10}	7.5×10^{9}
MB10A	1.7×10^{11}	4.7×10^{10}	1.1×10^{10}	8.2×10^{9}	4.8×10^{9}
MB10B	3.8×10^{11}	1.1×10^{11}	3.0×10^{10}	2.2×10^{10}	1.2×10^{10}
MB9A	2.0×10^{12}	5.8×10^{11}	1.5×10^{11}	1.0×10^{11}	5.9×10^{10}
MB9B	3.8×10^{12}	9.8×10^{11}	2.3×10^{11}	1.6×10^{11}	8.4×10^{10}
MB8A	6.6×10^{11}	1.9×10^{11}	4.9×10^{10}	3.2×10^{10}	1.8×10^{10}
MB8B	2.4×10^{11}	6.3×10^{10}	1.5×10^{10}	1.0×10^{10}	5.9×10^{9}

In general if equipment to be installed in the dispersion suppressor regions of Points 1 and 5 is able to withstand doses of a few hundred gray per year, *i.e. minimum* of 10^3 Gy for 10 years of LHC running then it should be able to survive. However, it is likely that some very localized regions in the dispersion suppressors will see even higher doses - possibly reaching thousands of gray per year which will most probably cause a problem for components situated at these points if they are only radiation hard to a few hundred Gy / y. For equipment to be placed under the magnet string a limit of 10^2 Gy / y should ensure that equipment will survive in all locations under the magnet string except under the empty cryostat region - here a limit of at least 10^3 Gy / y will be required. On a more local basis, considering the distribution of dose along the DS magnets then the "high" dose areas are limited to a couple of dipoles, the missing magnet and Q11 regions. Other regions, alongside the magnets MB11A-MB10B will see annual doses $\ll$100 Gy / y, *i.e.* regions with comparable doses to the LHC standard arc sections will be found in the DS sections. A summary of the required dose levels equipment will need to be able to survive is given for the different magnet elements in the DS regions in Table 3. These are explicitly for the left dispersion suppressor section; to obtain the required resistance of equipment in the vicinity of the individual magnets in the right dispersion suppressors, the magnet labels A and B should be interchanged. The localization of the hot-spots and the non-symmetric nature of the dose distribution shows that the positioning of equipment / electronics in the DS regions will be very important. Equipment to be positioned on the outside of the LHC ring will receive higher annual doses than that situated inside the ring. This is because point losses occur in the outgoing proton direction from the interaction point which for both Points 1 and 5 is in the beam-pipe closest to the outer tunnel wall.

The highest doses in the DS section are found in the vicinity of the missing magnet. Here the only material surrounding the beam-pipes in which the radiation can interact is the cryostat. This region could

Table 3: Required minimum dose for radiation hardness of equipment to be installed in the DS sections of IR1 and IR5. Doses are given for the vicinity of each magnet in the DS. For the magnets in the DS sections to the right of the IP the magnet labels A and B should be interchanged.

Magnet	Required minimum radiation resistance of equipment in DS regions Gy / y
MB8A	several
Q8	several tens
MB9B	several hundreds
MB9A	100
Q9	several tens
MB10B	several tens
MB10A	several
Q10	several tens
MB11B	several tens
MB11A	several tens
missing	$\sim$ 1000
Q11	several hundreds

pose a problem to equipment to be installed in its vicinity as doses of hundreds of gray reach the tunnel wall (in other regions of the DS, doses of $\sim$100 Gy / y are limited to positions near the inter-magnet gaps). In some localized regions of the missing magnet section doses reach thousands of gray per year. This also allows radiation to reach the quadrupole Q11 downstream before it interacts in the material of the magnet. A possible solution to reduce the dose in this region would be to include extra material around the beam-pipes, *e.g.* a non-functioning magnet, as the radiation would interact with the dense iron before reaching the cryostat surface. This would result in much lower doses outside the cryostat in this area.

Doses to quenchdiodes:

To observe the dose in the region of the sensitve quench diodes, additional information was included in the geometry of the simulation to include the sensitive components such as the silicon wafers and the general positioning of components inside the diode housing. It was found that relatively low doses of a few tens gray per year will be found inside the diode housing volumes, with even lower doses to the sensitive silicon wafers for all diodes excepting those of quadrupole Q11 and dipole MB9B. These regions correspond to the dispersion suppressor sections with the maximum dose contribution from point losses. Doses to the diodes in DS1 and DS5 will be similar. Explicitly, dose contributions to the diodes from beam-gas interactions are in the range $\sim$ few-20 Gy / y averaged over the diode housing volume and $\sim$ 1-10 Gy / y in the silicon wafers, with the higher doses seen by the quadrupole diodes. These values will be similar to the doses to the quench diodes in the standard LHC arc sections. It should be noted that a strong top:bottom dose gradient will be observed across the volume of the quench diodes *i.e.* there can be an order of magnitude difference seen in the dose at the top of the diode volume than at the bottom.

Doses in the dispersion suppressors of IR3 & IR7:

No explicit simulation has been made to calculate the doses in the dispersion suppressors downstream of the scraping regions. However, the expected proton point loss densities in these regions are comparible to loss rates associcated with collisions between circulating protons and residual gas pressure [Jea01a], thus we can expect to see annual doses in the DS regions of IR3 and IR7 with similar point loss distributions to those shown in Figure (3) but with a maximum magnitude similar to that of beam-gas interaction dose rates *i.e.* generally a few gray per year. This estimation is made with the proviso that final normalisation

of the proton point losses in these regions may differ, such that these regions may pose more of a radiation problem than the currently available loss data indicates.

Particle fluences in the dispersion suppressors:

In order that estimation can be made of Single Event Effect problems occuring with the equipment placed in the tunnel in the vicinity of the dispersion suppressors, it is necessary to have an idea of the radiation environment it will be placed in. Details of the radiation environments of DS1 and DS5 are given in Appendix B of this report in the form of fluence : dose maps. The high energy particle fluences have been presented in this way since it is found that the ratio R = fluence / dose is the same for both dispersion suppressors. Absolute magnitudes of neutron, proton, charged pion, as well as the total summed hadron, fluences can readily be obtained by combining the ratio data with the dose data presented in Appendix A at a given position in the LHC tunnel.

Typical ratio values of fluence : dose can be obtained for standard dipole and quadrupole magnets: a value of $\sim 5 \times 10^{10} \mathrm{cm}^{-2}\mathrm{Gy}^{-1}$ is found for neutron fluences $> 100\,\mathrm{keV}$, which falls to $\sim 2 \times 10^{9}\ \mathrm{cm}^{-2}\mathrm{Gy}^{-1}$ for hadrons $> 100\,\mathrm{MeV}$. These values are also representative of the fluence : dose ratio seen at other postitions in the LHC machine, such as the standard arc sections [Fyn01a]. Ratios corresponding to the missing magnet section and quadrupole Q11 of the dispersion suppressor regions are lower than these values by up to an order of magnitude. Detailed values of the fluence : dose ratios are provided in Figures (55) - (59) for five different energy cuts, for each particle species and for differing positions in the LHC tunnel. A summary of the data showing the ratio as a function of the particle energy cut is given in Figure (10). This can be used to determine absolute particle fluences in the dispersion suprressors for any arbitrary energy cut, which when combined with further information on nuclear interaction probabilities [Huh00] can provide estimates of SEU rates expected for the electronics placed in the LHC tunnel.

References

[Ajg00] I. Ajguirei, I. Baichev and J. B. Jeanneret, *Beam losses far downstream of the high luminosity interaction points of LHC*, LHC Project Report 398.

[Bai99] I. Baichev, J. B. Jeanneret and G. R. Stevenson, *Beam losses far downstream of the high luminosity interaction points of LHC - intermediate results*, LHC Project Note 208.

[Bai00] I. Baichev, *Proton losses in the dispersion suppressors of IR1 and IR5 of LHC*, LHC Project Note 240.

[Fas01a] A. Fassò, A. Ferrari and P. R. Sala, *Electron-photon Transport in FLUKA: Status*, in Proc. Monte Carlo 2000 Conf., Lisbon, 23-26 October 2000, Eds A. Kling, F. Barao, M. Nakagawa, L. Tavora, P.Vaz (Berlin: Springer) pp. 159-164 (2001).

[Fas01b] A. Fassò, A. Ferrari and P. R. Sala, *FLUKA: Status and Prospectives for Hadronic Applications*, in Proc. Monte Carlo 2000 Conf., Lisbon, 23-26 October 2000, Eds A. Kling, F. Barao, M. Nakagawa, L. Tavora, P.Vaz (Berlin: Springer) pp. 995-960 (2001).

[Fyn01] C. A. Fynbo and G. R. Stevenson, *Annual dose in the standard LHC arc section*, CERN Engineering Specification, LHC-S-ES-0001, (2001).

[Fyn01a] C. A. Fynbo, *Radiation Environment in the Main Ring of the LHC*, LHC Project Seminar, 22 / 11 / 2001.

[Huh00] M. Huhtunen, F. Faccio, *Computational method to estimate Single Event Upset rates in an accelerator environment*, Nucl. Inst. and Methods in Physics Research A, 450 155-172 (2000).

[Jea01a] B. Jeanneret, *Beam losses in the dispersion suppressors of IR3 and IR7*, LHC Project Note 253.

[Jea01b] B. Jeanneret, Private communication, November 2001.

[Ste97] G. R. Stevenson, Preliminary FLUKA simulation of dose to quench diodes in the LHC arcs, Summer 1997 - unpublished.

[Huh96] M. Huhtinen and G. R. Stevenson, *Doses around the LHC beam-pipe due to beam-gas interactions in a long straight section*, CERN-LHC Project Note 39 (1996).

[Ost01] R. Ostojic, *LHC Layout Version 6.3*, Engineering Change Order - Class I, LHC-LS63-EC-0001 rev 1.0.

[Pot95a] K. Potter and G. R. Stevenson, *Source intensities for use in the radiological assessment of the effect of proton losses at the scrapers and around the main ring of the LHC*, CERN Internal Report TIS–RP / IR / 95–16 (1995), CERN AC / 95–04(DI), LHC Note 322.

[Pot95b] K. Potter, H. Schönbacher and G. R. Stevenson, *Estimates of dose to components in the arcs of the LHC due to beam-loss and beam-gas interactions*, CERN-LHC Project Note 18 (1995).

List of Appendix A figures:

List of Appendix B figures:

Appendix B.1: Fluence : Dose ratios above/below the magnet string

Appendix B.2: Radial fluence : dose ratio distibutions

Appendix B.3: Quantitative fluence : dose ratios

Appendix A.1

Total annual dose due in the dispersion suppressor regions of the high luminosity insertion points IR1 & IR5.

Tunnel Doses

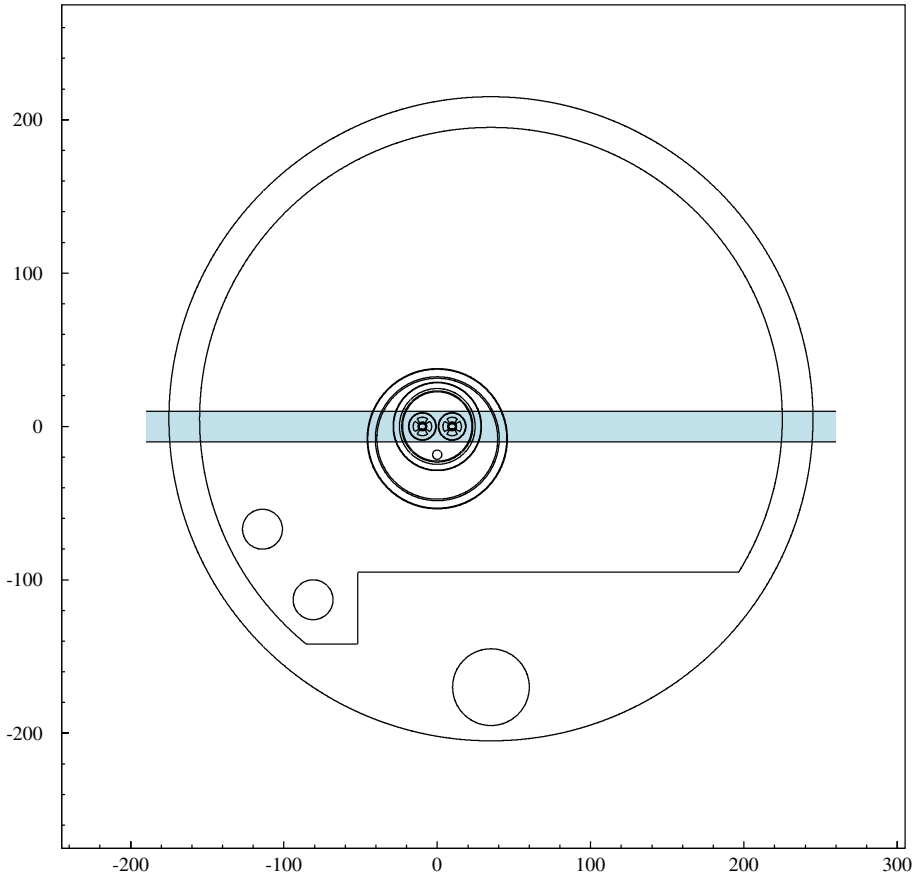

Figure 11: Schematic cross-section of the tunnel in the dispersion suppressors downstream of IP1 and IP5 in the LHC. In the following figures, for those depicting horizontal cuts through the tunnel geometry the doses shown are averaged over a slice 20 cm thick about the beam-axis (shaded region above). For the maxiumum doses in the LHC tunnel (see Appendix A.4) the above slice has a thickness of 4 cm for the inner regions of the LHC magnets.

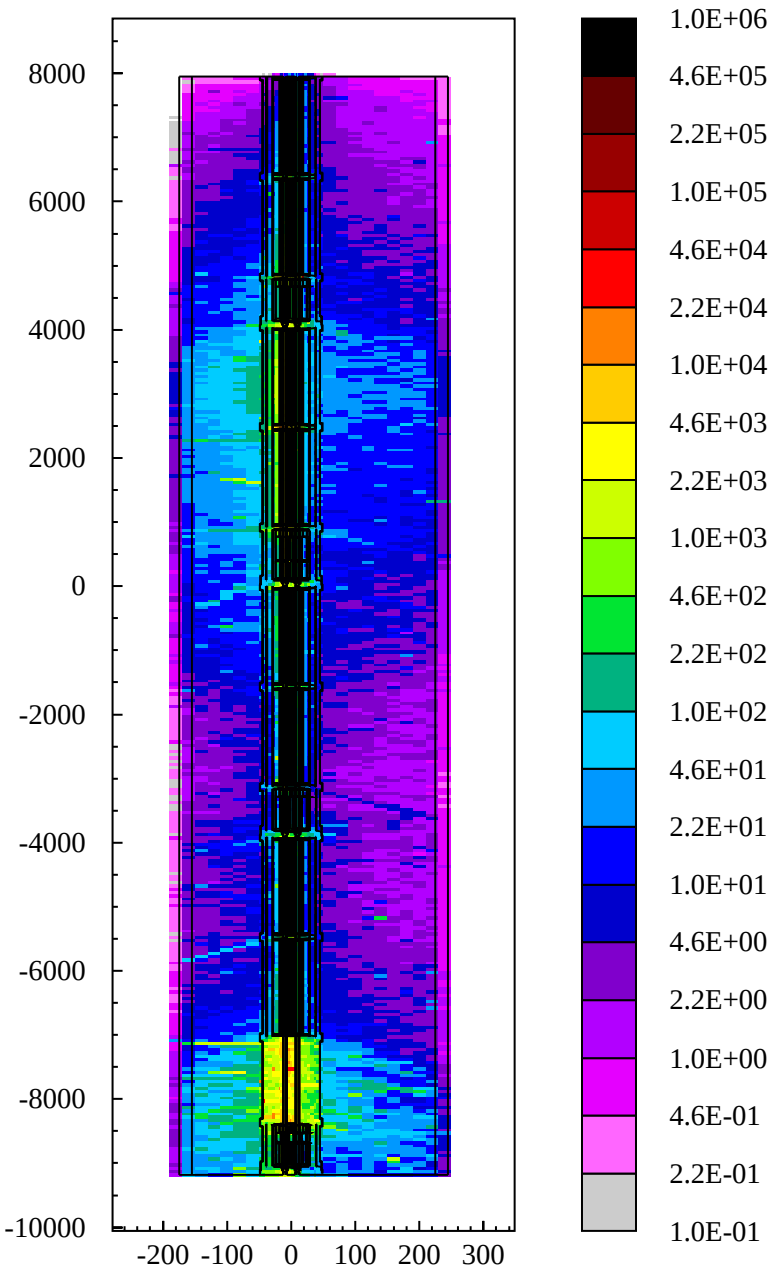

Figure 12: Total annual dose in the LHC tunnel (Gy / y) due to point losses and beam-gas interactions: shown alongside the magnets in the dispersion suppressors of IR1. The outgoing protons from IP1 are in the outer beam-pipe. The plot shows the dose for a horizontal cut averaged over a slice 20 cm about the beam-axis (see Figure 11). The dose contribution due to point losses was obtained by weighting the FLUKA results of dose per interacting proton by the proton loss density (red solid line) of Figure 1.

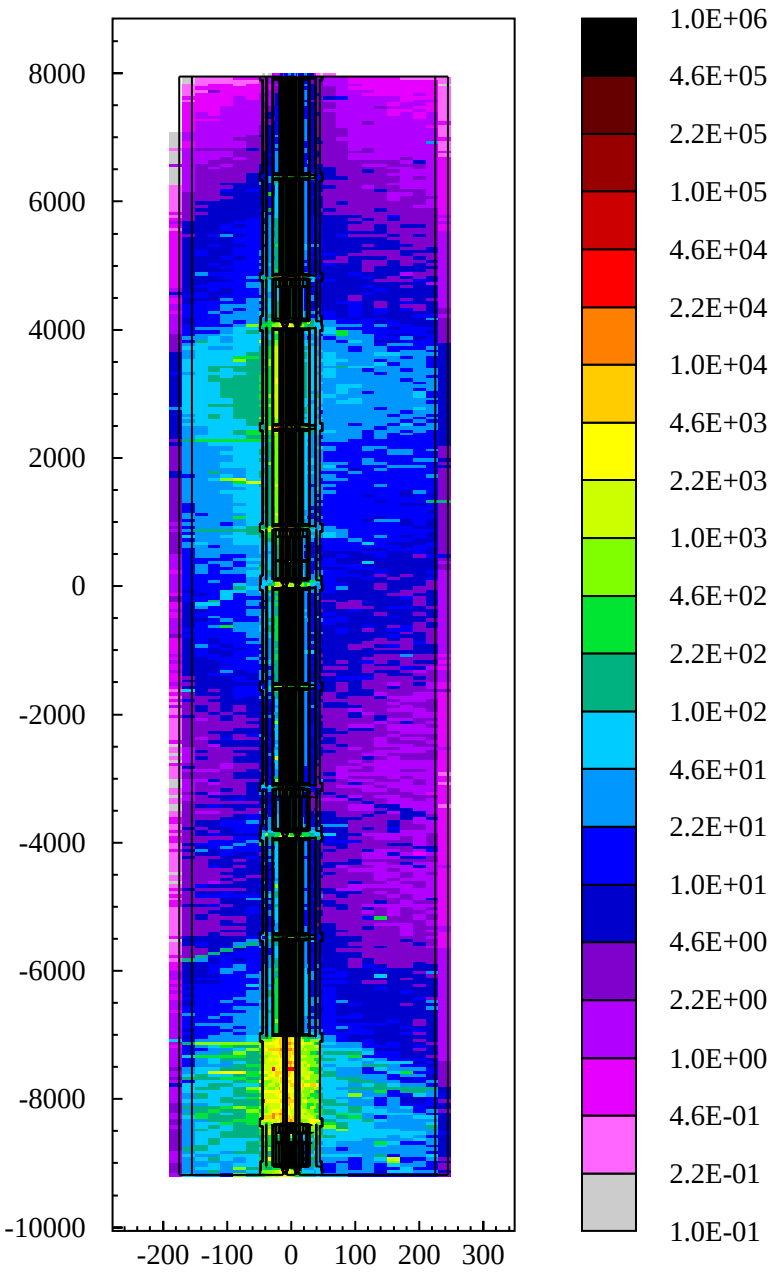

Figure 13: Total annual dose in the LHC tunnel (Gy / y) due to point losses and beam-gas interactions: shown alongside the magnets in the dispersion suppressors of IR5. The outgoing protons from IP1 are in the outer beam-pipe. The plot shows the dose for a horizontal cut averaged over a slice 20 cm about the beam-axis (see Figure 11). The dose contribution due to point losses was obtained by weighting the FLUKA results of dose per interacting proton by the proton loss density (blue dashed line) of Figure 1.

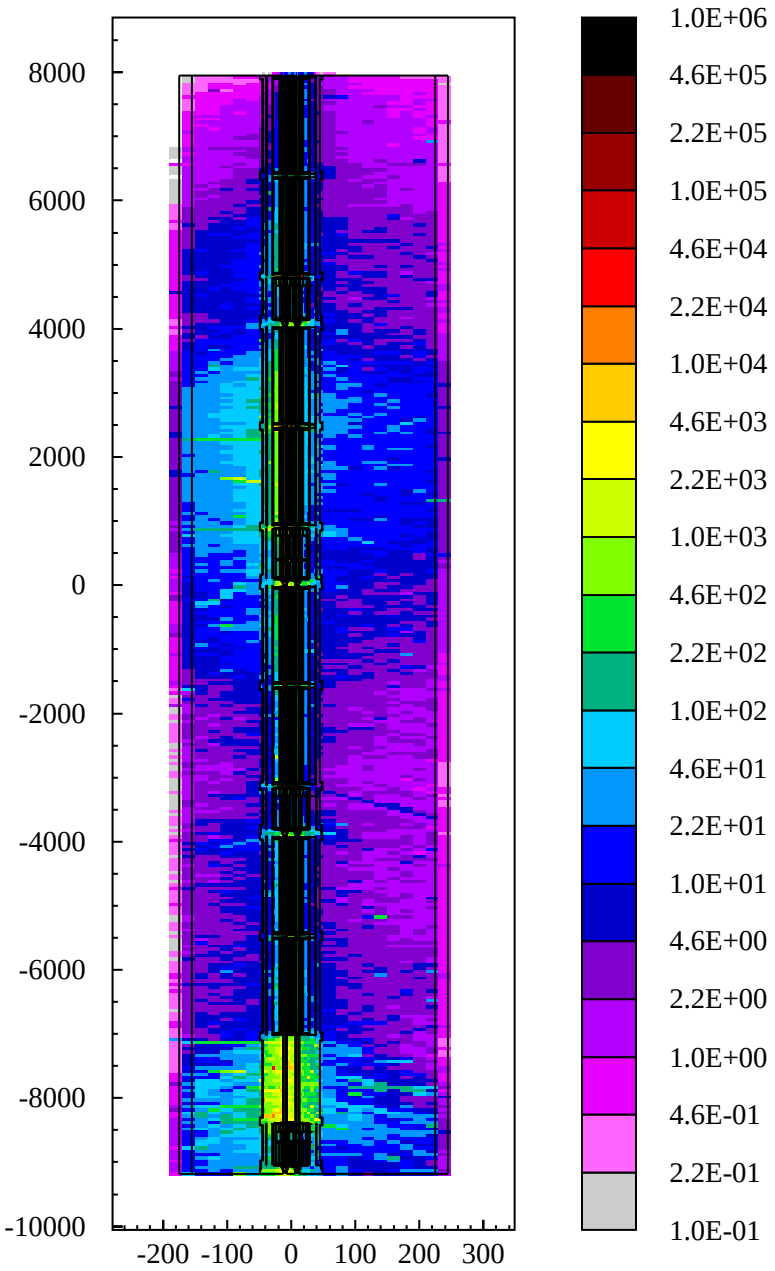

Figure 14: Total annual dose in the LHC tunnel (Gy / y) due to point losses and beam-gas interactions: shown alongside the magnets in the dispersion suppressors for the case when no distinction is made between the beam-crossing orientations of Points 1 or 5. The outgoing protons from the IP are in the outer beam-pipe. The plot shows the dose for a horizontal cut averaged over a slice 20 cm about the beam-axis (see Figure 11). The annual doses were obtained by weighting the FLUKA results of dose per interacting proton by the proton loss density (black double dashed line) of Figure 1.

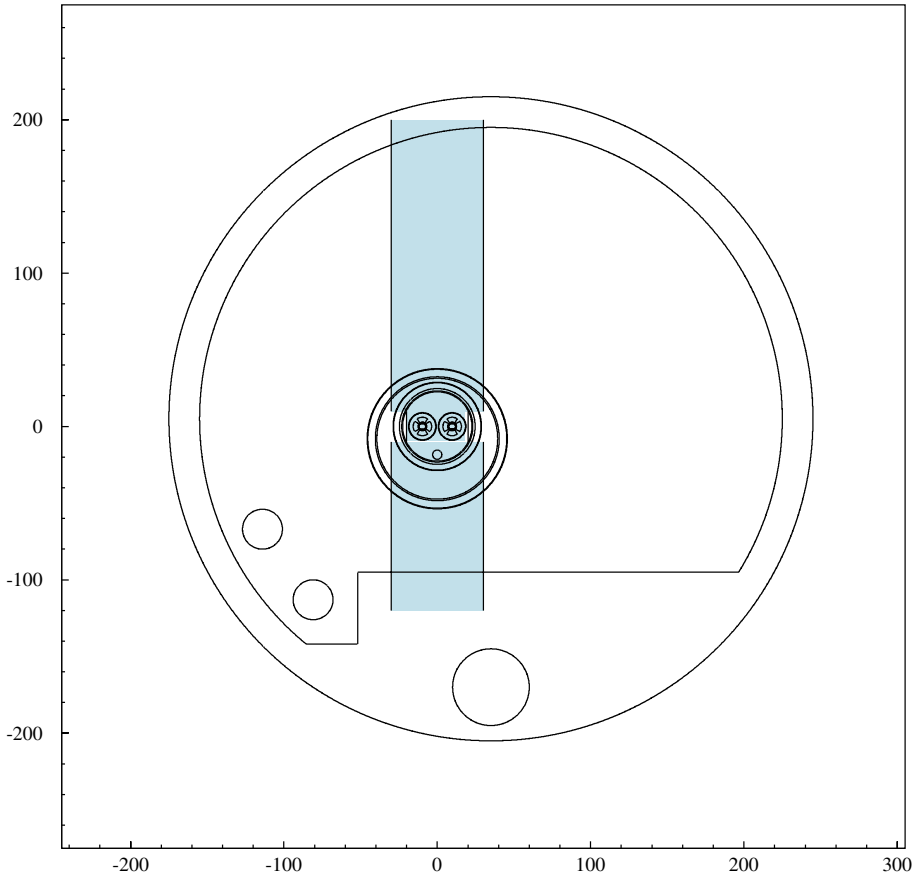

Figure 15: Schematic cross-section of the tunnel in the dispersion suppressors downstream of IP1 and IP5 in the LHC. In the following figures showing the dose above and below the magnet strings, the doses are averaged over the bins covering a width of 60 cm about the central point between the beam lines (40 cm in the inner regions surrounding the beam-pipes) as shown by the shaded region above.

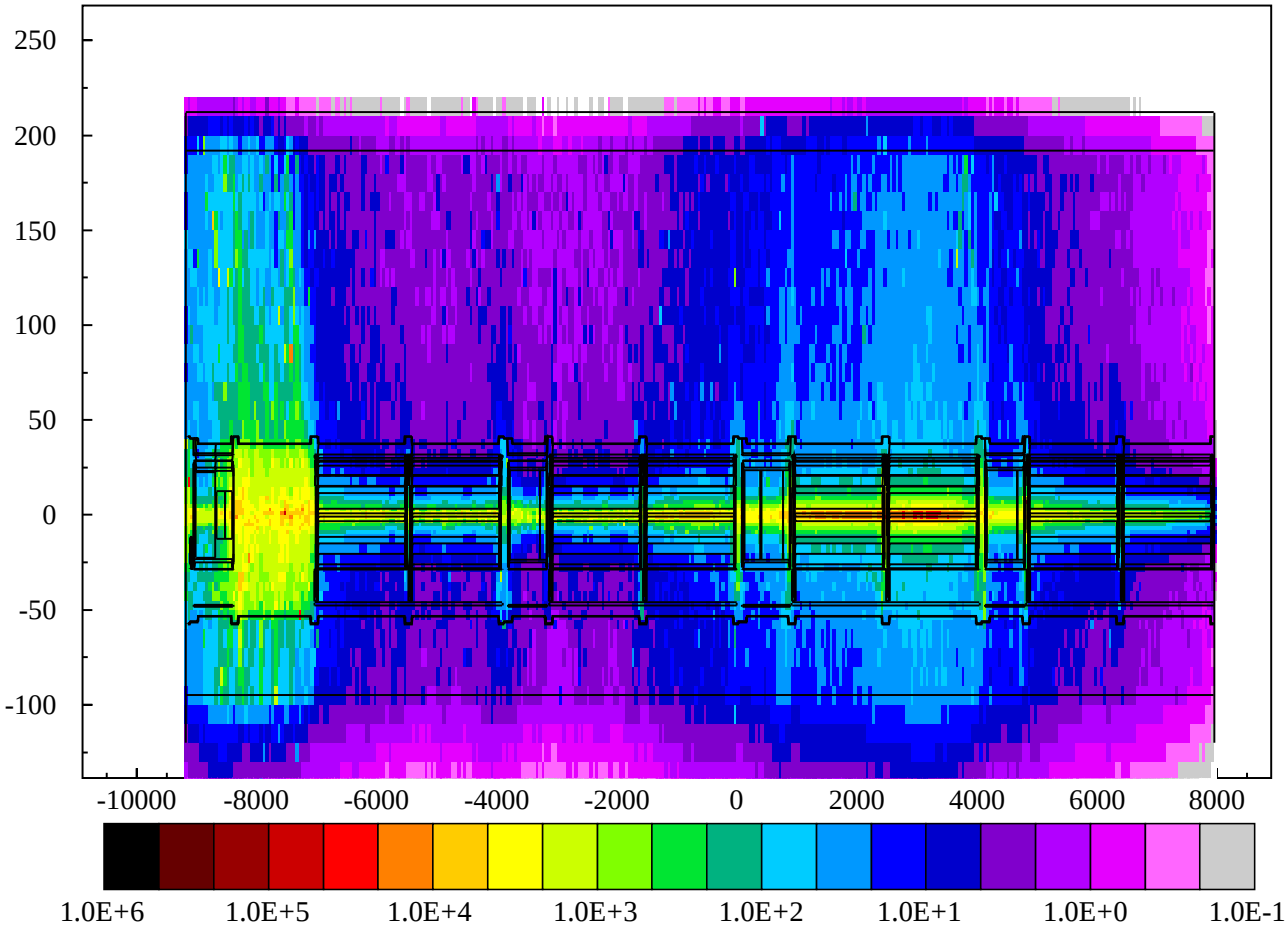

Figure 16: Total annual dose (Gy / y) above and below the magnet string in the dispersion suppressors of IR1. Doses are the average over the shaded region shown in Figure 15. The annual doses were obtained by weighting the FLUKA dose per interacting proton results by the proton loss given by the red solid line of Figure 1.

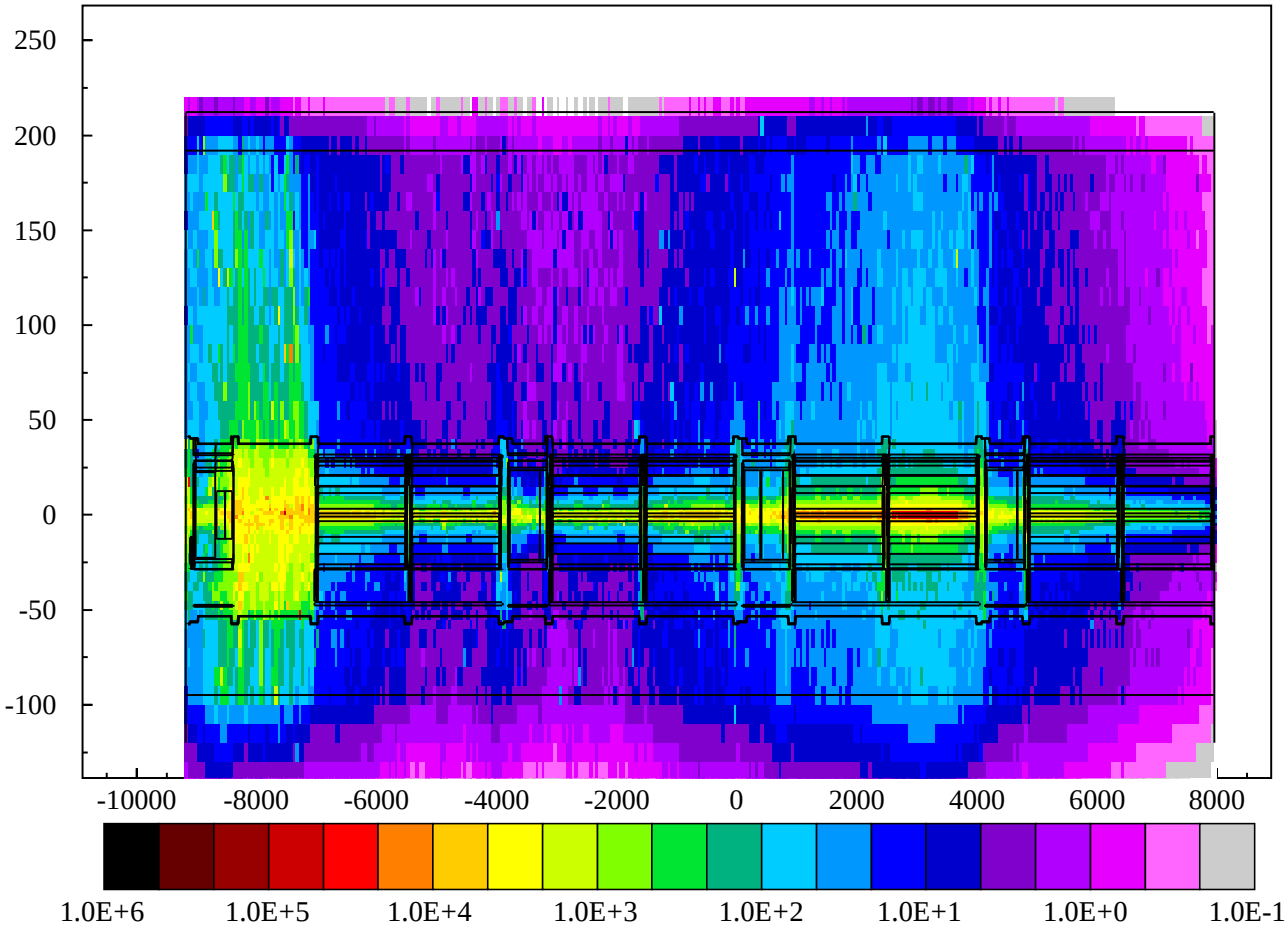

Figure 17: Total annual dose (Gy / y) above and below the magnet string in the dispersion suppressors of IR5. Doses are the average over the shaded region shown in Figure 15. The annual doses were obtained by weighting the FLUKA dose per interacting proton results by the proton loss given by the blue dashed line of Figure 1.

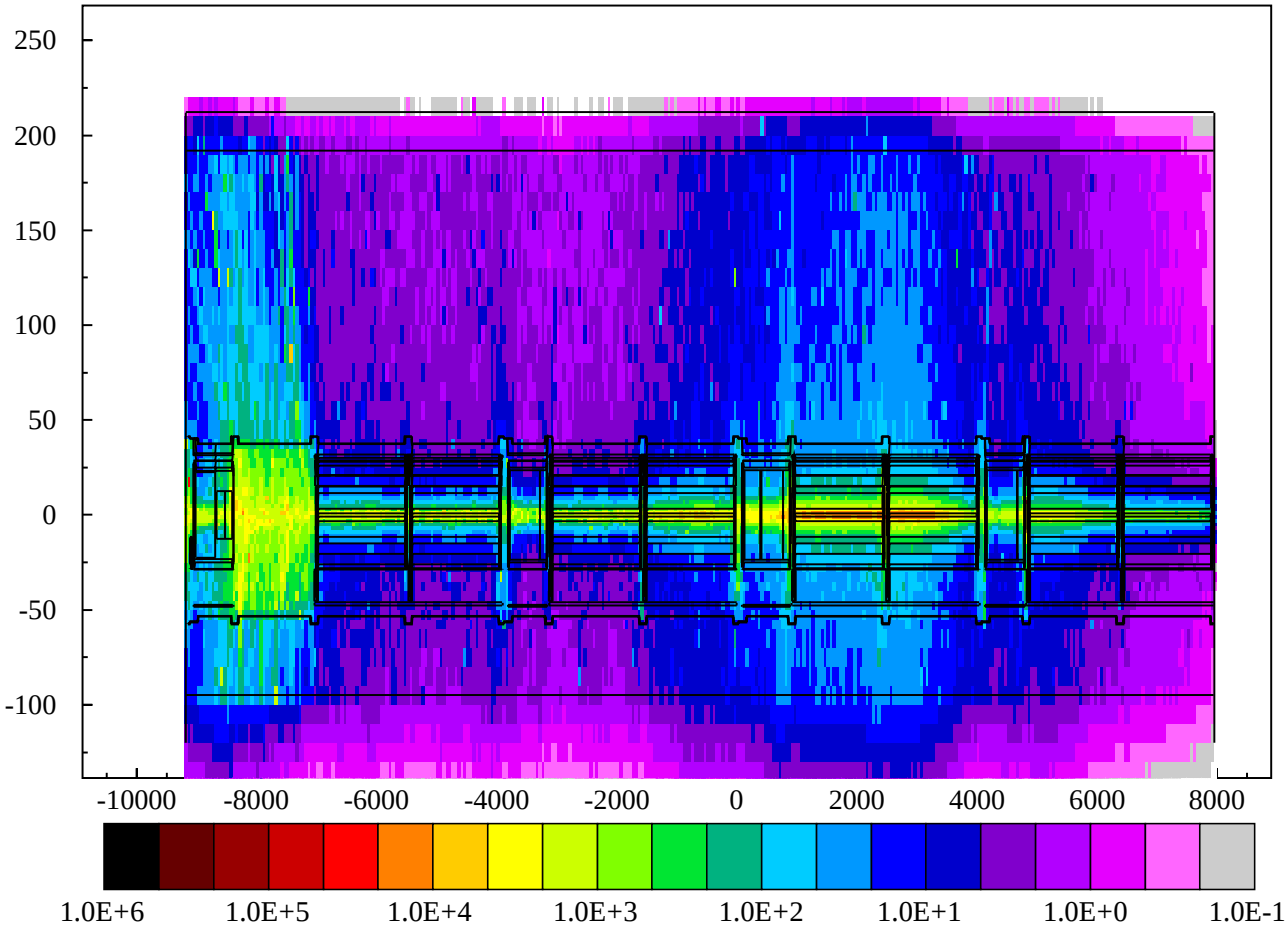

Figure 18: Total annual dose (Gy/y) above and below the magnet string in the dispersion suppressors when no distinction is made between the beam-crossing orientations of IP1 or IP5. Doses are the average over the shaded region shown in Figure 15. The annual doses were obtained by weighting the FLUKA dose per interacting proton results by the proton loss given by the black double dashed line of Figure 1.

Appendix A.2

Total annual dose in the floor of the tunnel for DS1 & DS5

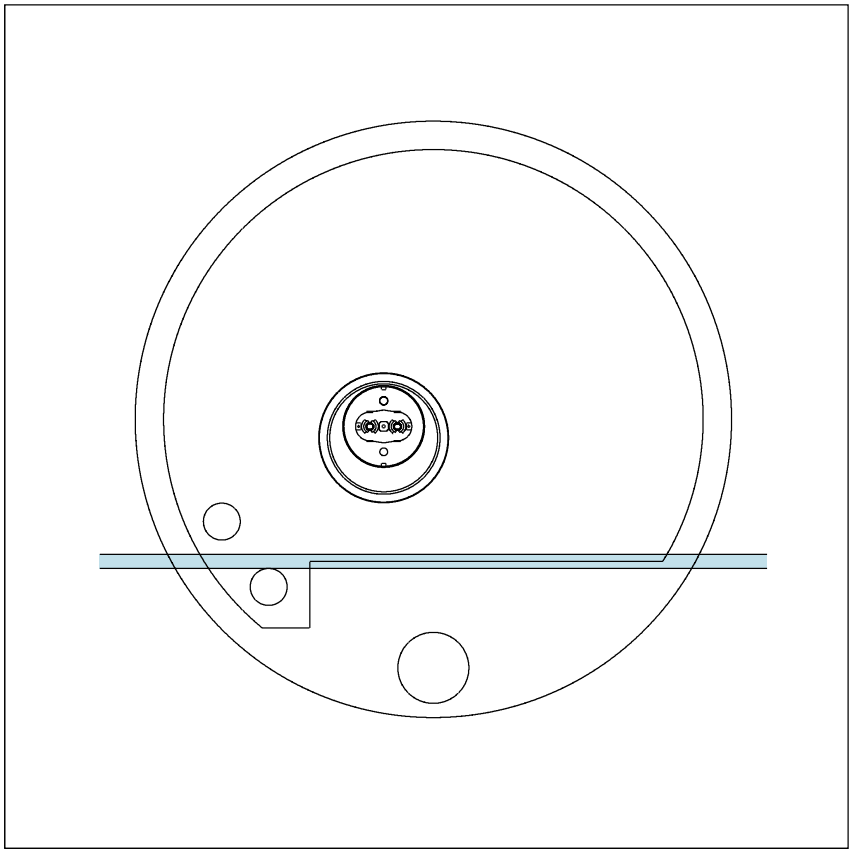

Figure 19: Cut taken to show the annual doses in the floor of the LHC tunnel in the region of the arc cell (shown by the shaded region above). This corresponds to the scoring bin lying across the air / floor interface: specifically covering a depth of 0-5cm below the concrete floor surface, and 0-5cm above the floor in air.

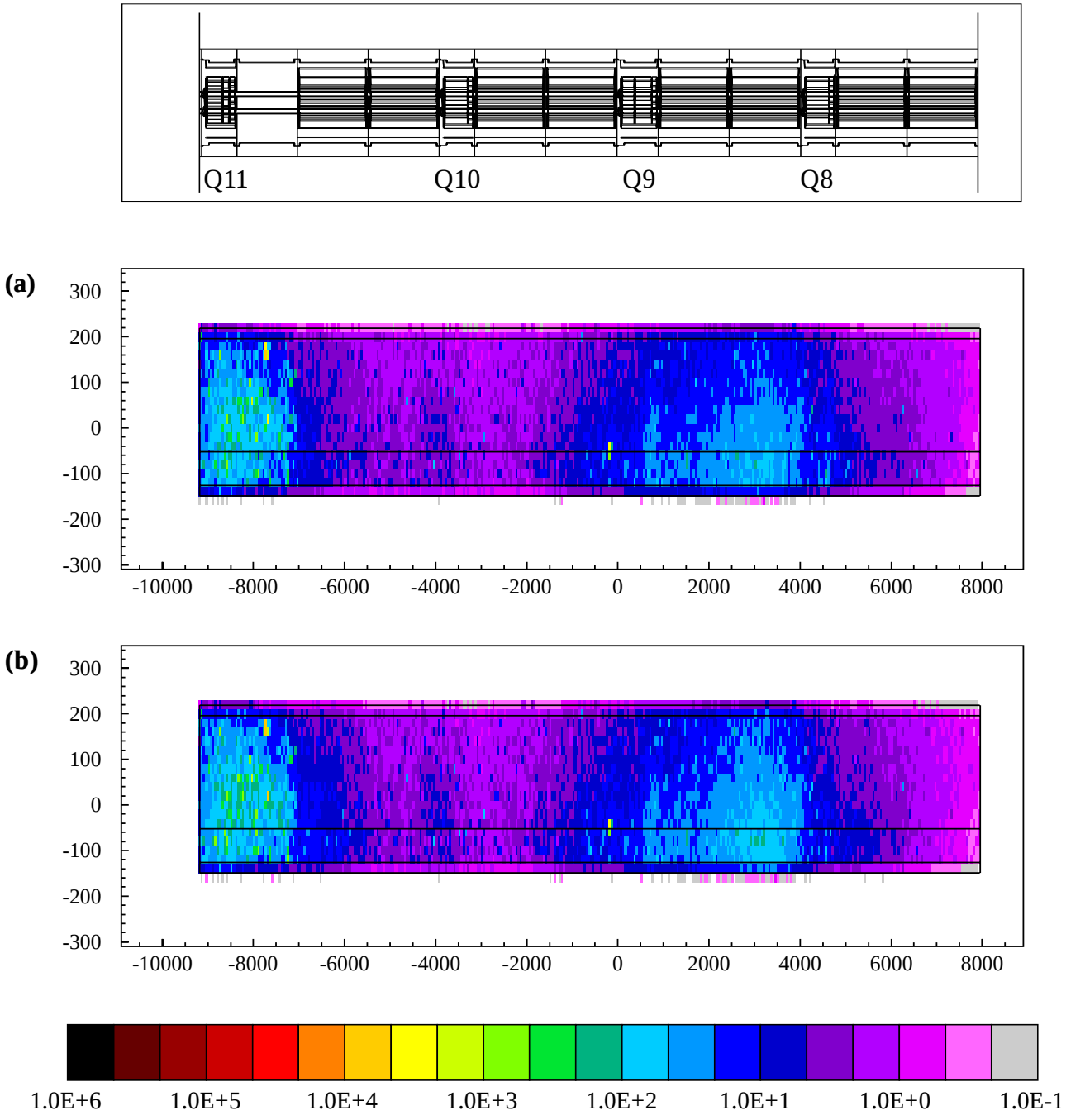

Figure 20: Annual dose in floor alongside DS magnet string (Gy / y). The plots shown correspond to the scoring bin as shown in Figure (19). The top schematic diagram shows the magnet positions relative to the floor. The horizontal line at approximately -50 shows the edge of the floor step. The concrete floor is correspondingly above this line. Figure (a) shows the annual dose in DS1 and Figure (b) shows the annual dose in DS5.

Appendix A.3

Maximum dose in the LHC tunnel for the dispersion suppressors DS1 & DS5

Cross sectional cuts through the LHC tunnel

Cross sectional cuts through LHC tunnel - DS1

MB9B

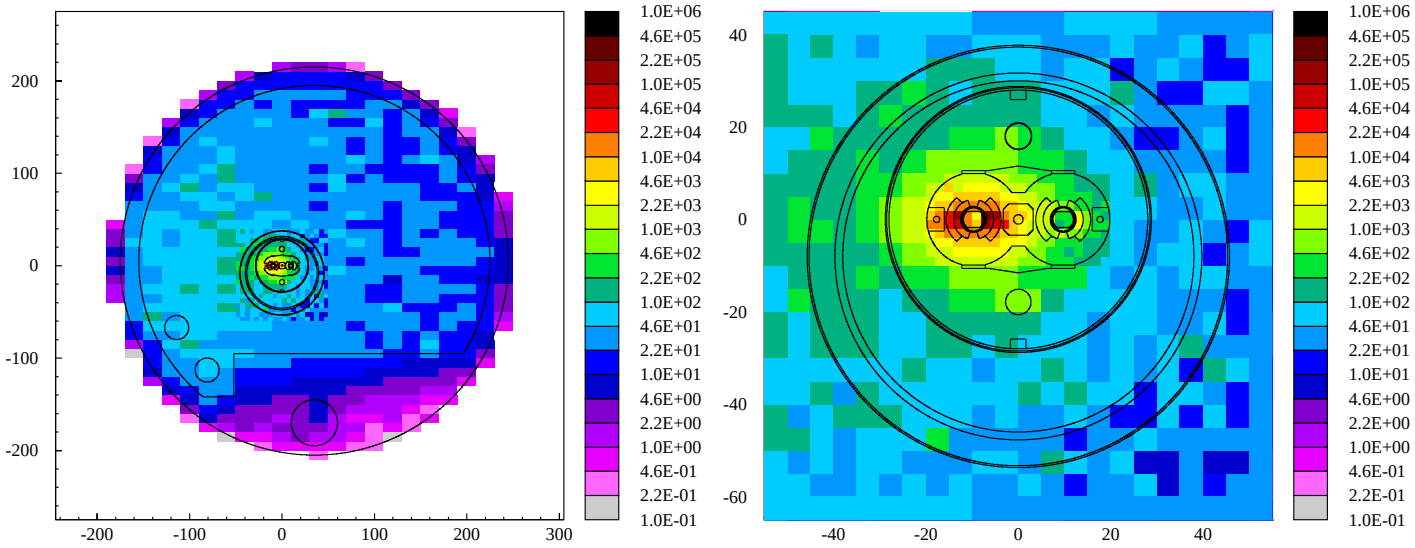

Q11

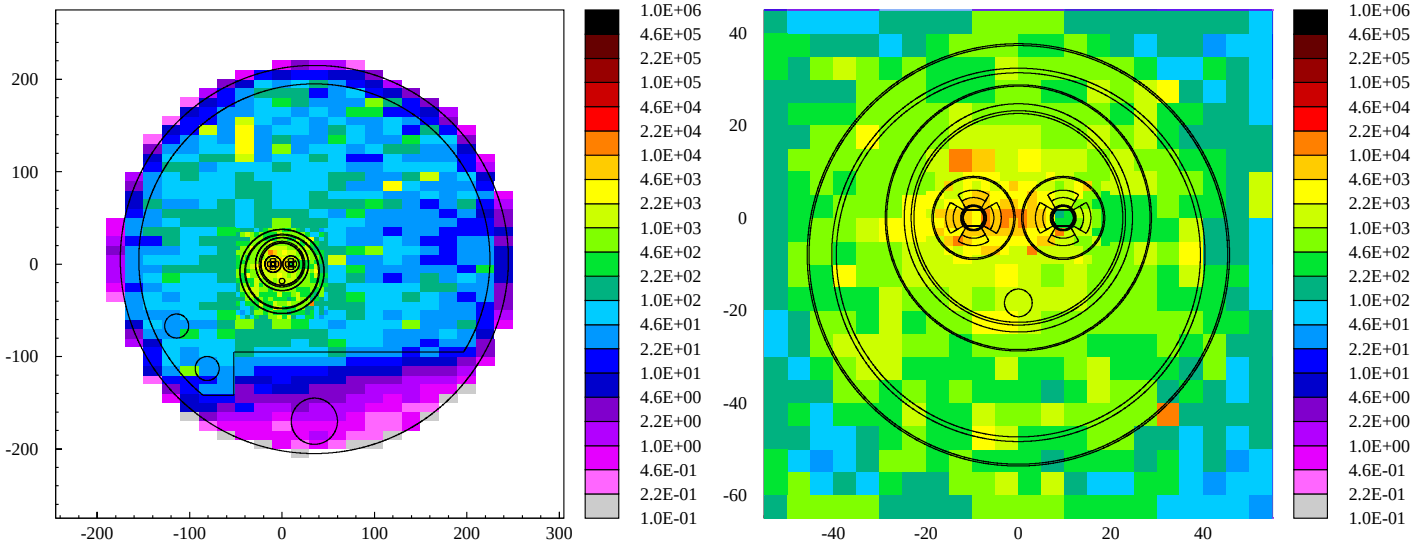

Figure 21: Radial distribution of annual dose (Gy/y) in the LHC tunnel of the dispersion suppressors DS1. This is shown for the regions of highest dose at the position of MB9B and Q11 for the entire tunnel and to the inner magnet components. The cut through MB9B (top) is specifically for the scoring bin at a longitudinal position of 3250-3300 cm, and the scoring bin for Q11 (bottom) is at a longitudinal position of -8450--8400 cm. These postions correspond to the coordinate system of Figure (2).

Cross sectional cuts through LHC tunnel - DS5

MB9B

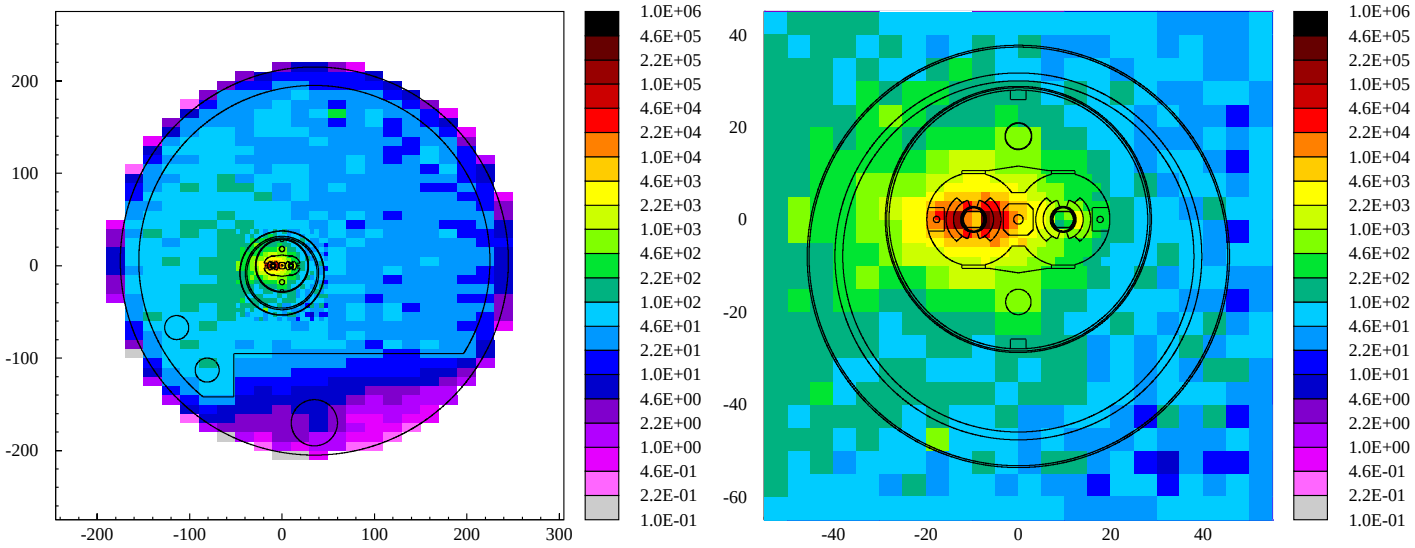

Q11

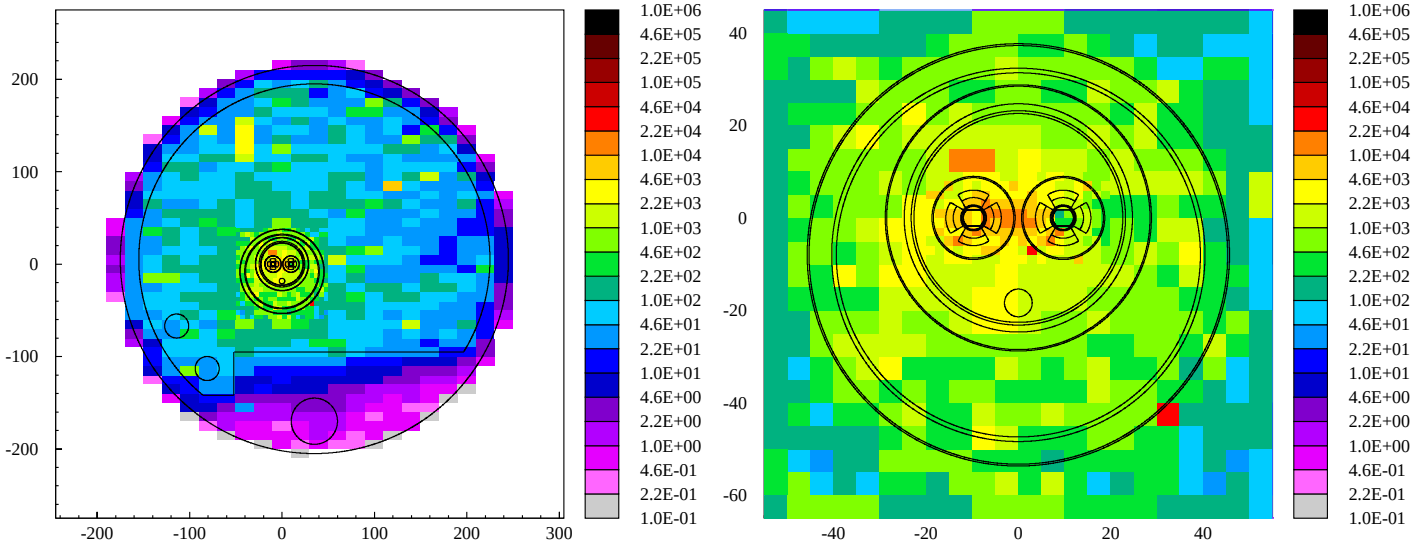

Figure 22: Radial distribution of annual dose (Gy/y) in the LHC tunnel of the dispersion suppressors DS5. This is shown for the regions of highest dose at the position of MB9B and Q11 for the entire tunnel and to the inner magnet components. The cut through MB9B (top) is specifically for the scoring bin at a longitudinal position of 3250-3300 cm, and the scoring bin for Q11 (bottom) is at a longitudinal position of -8450--8400 cm. These postions correspond to the coordinate system of Figure (2).

Appendix A.4

Maximum dose in the inner regions of the dispersion suppressor magnets of the high luminosity insertion points IR1 & IR5.

Dose to beamline and magnet coils

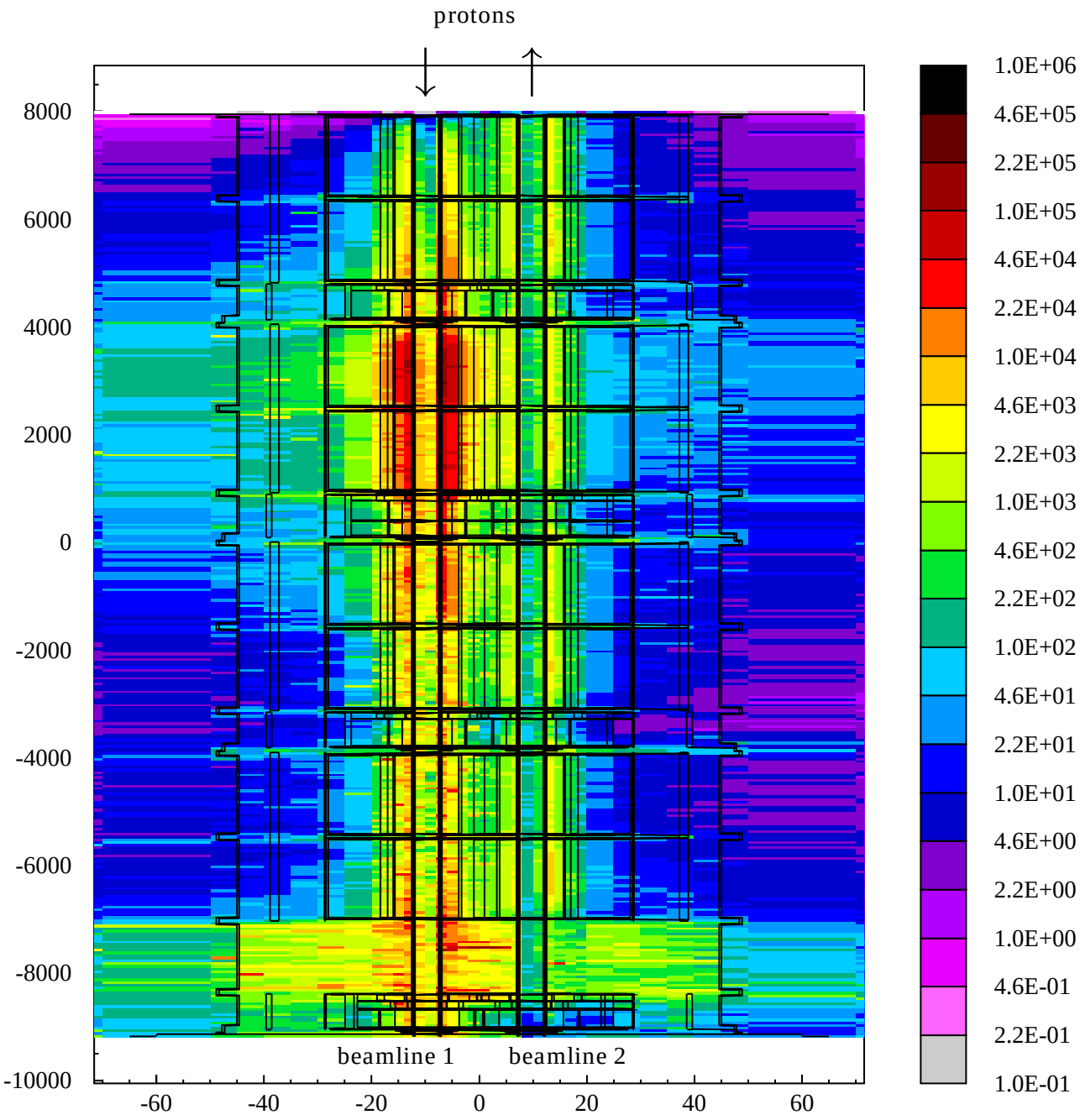

Figure 23: Longitudinal distribution of maximum dose (Gy / y) due to point losses in the inner regions of the magnets in the dispersion suppressors of IR1. The plot shows the dose for a horizontal cut averaged over a slice 4 cm about the beam-axis (maximum doses occur radially out along the beam axis). The annual doses were obtained by weighting the FLUKA results of dose per interacting proton by the proton loss given by the red solid line of Figure 1.

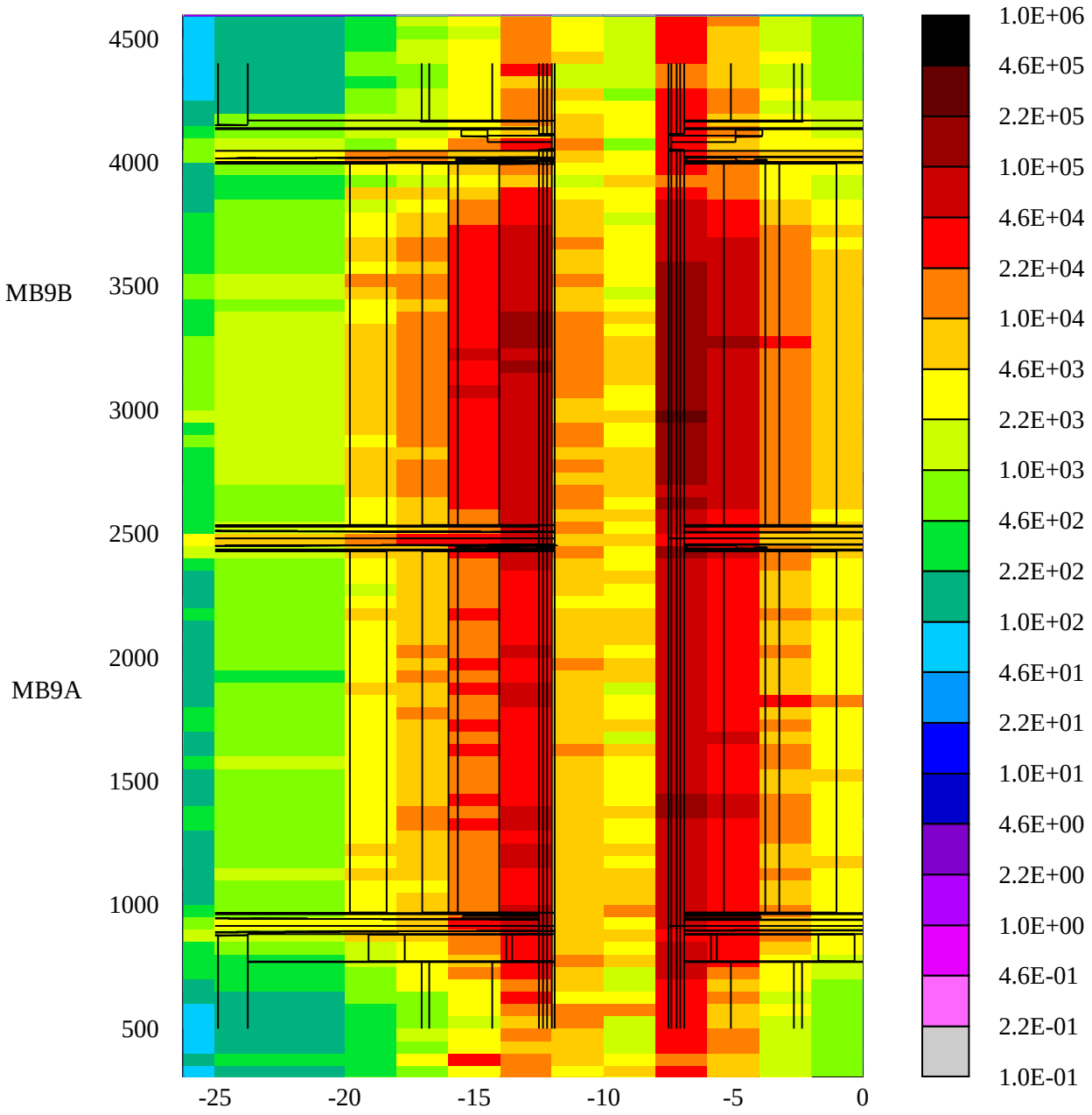

Figure 24: Maximum annual dose (Gy / y) in the inner regions of the dipole magnets MB9A / MB9B in the dispersion suppressors of IR1 - specifically covering beamline 1 and the surrounding dipole coils (enlargement of inner section of magnets from Figure 21). The plot shows the dose for a horizontal cut averaged over a slice 4 cm about the beam-axis. The point loss contribution was obtained by weighting the FLUKA results of dose per interacting proton by the proton loss given by the red solid line of Figure 1.

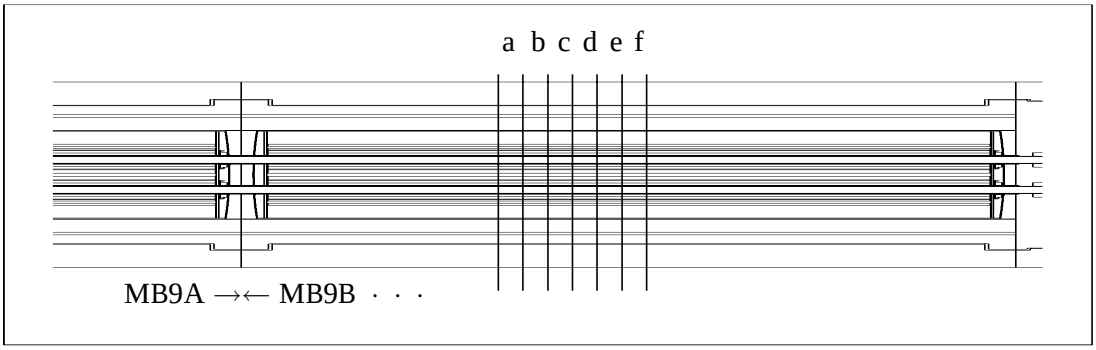

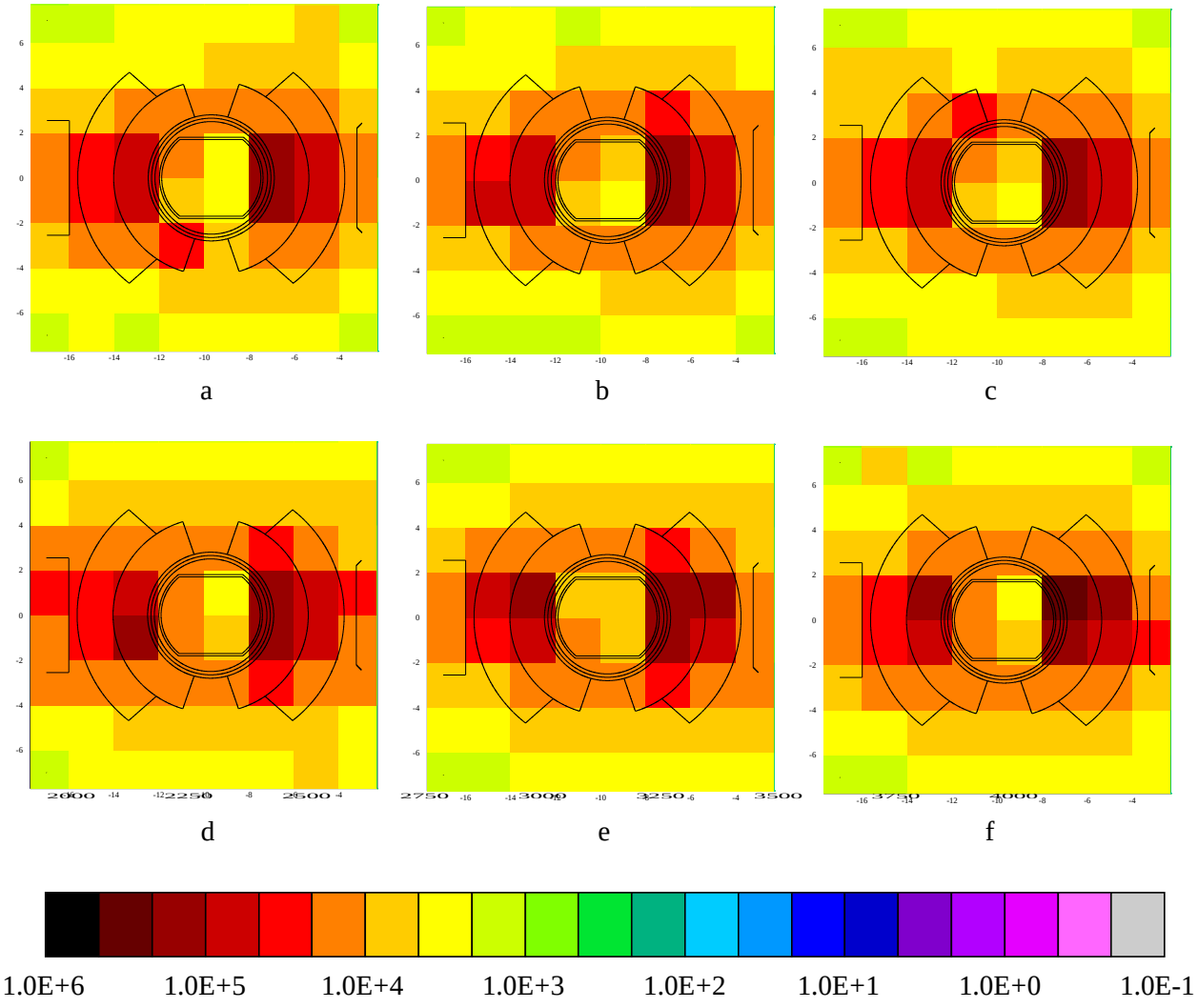

Figure 25: Selection of cross-sectional slices showing maximum dose (Gy / y) in the coils and beam-line of the dipole magnet MB9B in the dispersion suppressors of IR1. This is for the outgoing proton direction beam-line. The proton loss distribution used is taken from [Bai00] for a rate of 3.5×10^8 inelastic interactions per second in the IP. The total proton loss in IR1 is 1.1 $\times 10^7$ s^{-1}. Each slice corresponds to the labelled slice in the top schematic diagram.

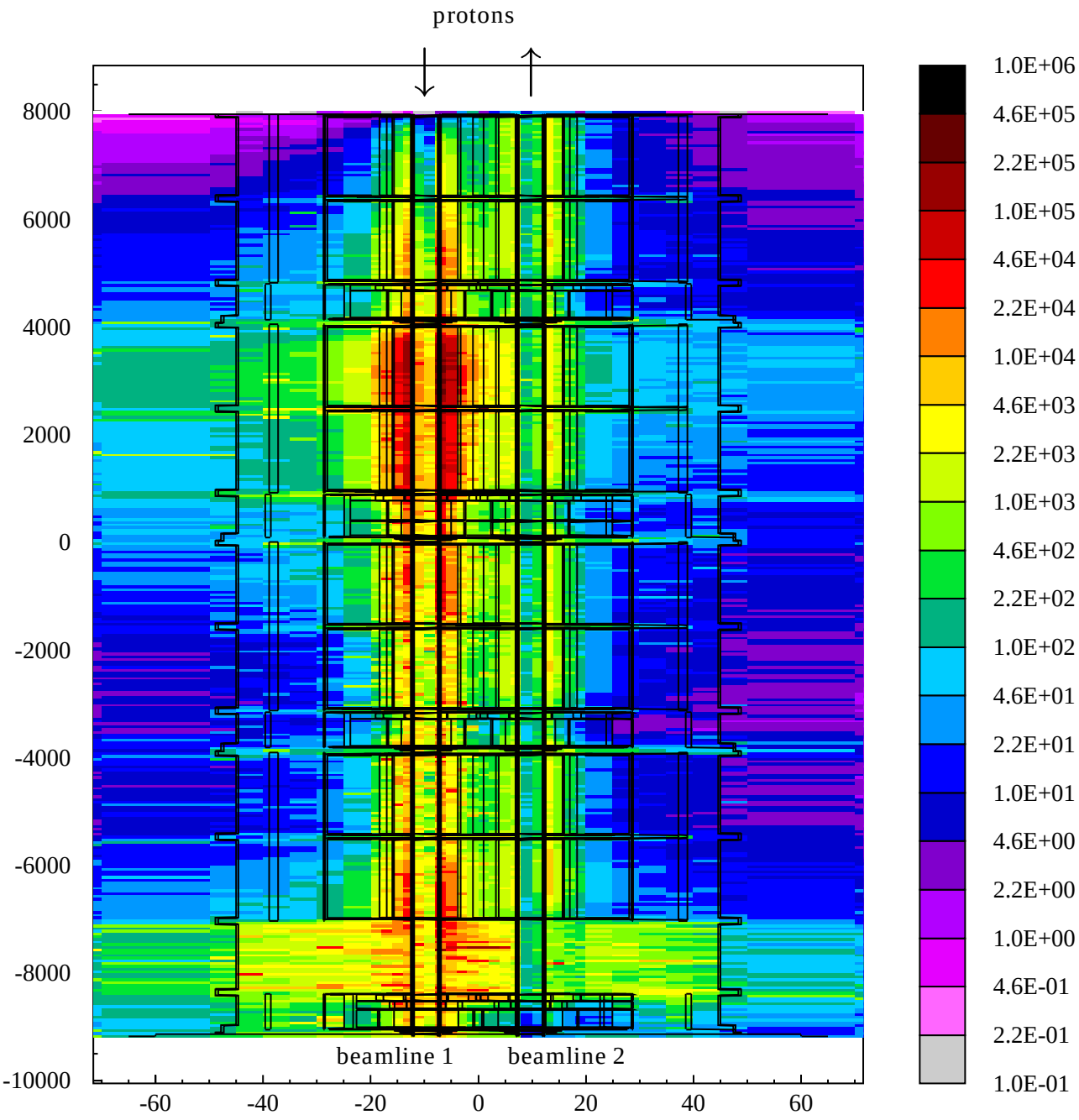

Figure 26: Longitudinal distribution of maximum dose (Gy / y) due to point losses in the inner regions of the magnets in the dispersion suppressors of IR5. The plot shows the dose for a horizontal cut averaged over a slice 4 cm about the beam-axis (maximum doses occur radially out along the beam axis). The annual doses were obtained by weighting the FLUKA results of dose per interacting proton by the proton loss given by the blue dashed line of Figure 1.

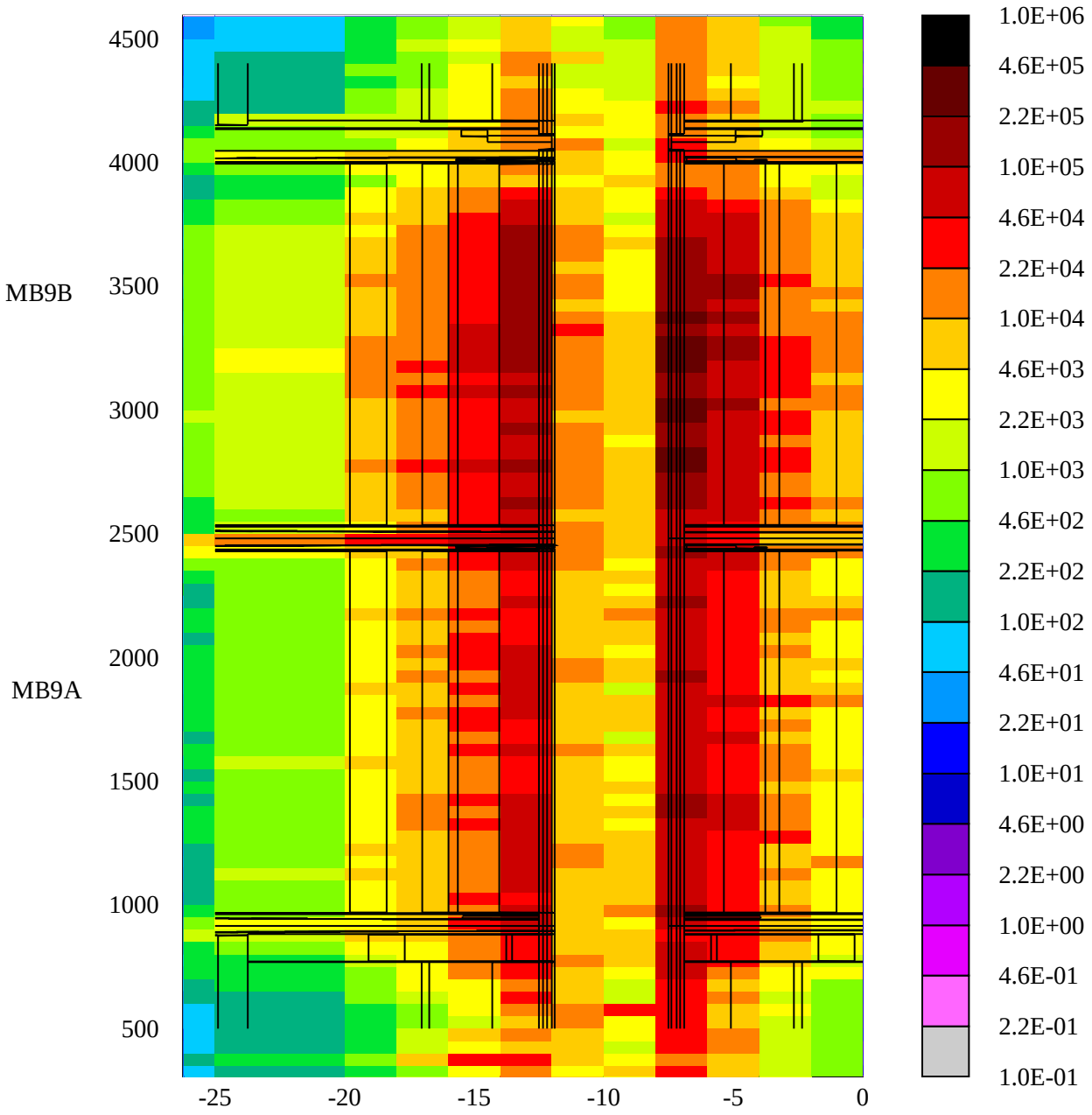

Figure 27: Maximum annual dose (Gy / y) in the inner regions of the dipole magnets MB9A / MB9B in the dispersion suppressors of IR5 - specifically covering beamline 1 and the surrounding dipole coils (enlargement of inner section of magnets from Figure 21). The plot shows the dose for a horizontal cut averaged over a slice 4 cm about the beam-axis. The point loss contribution was obtained by weighting the FLUKA results of dose per interacting proton by the proton loss given by the blue dashed line of Figure 1.

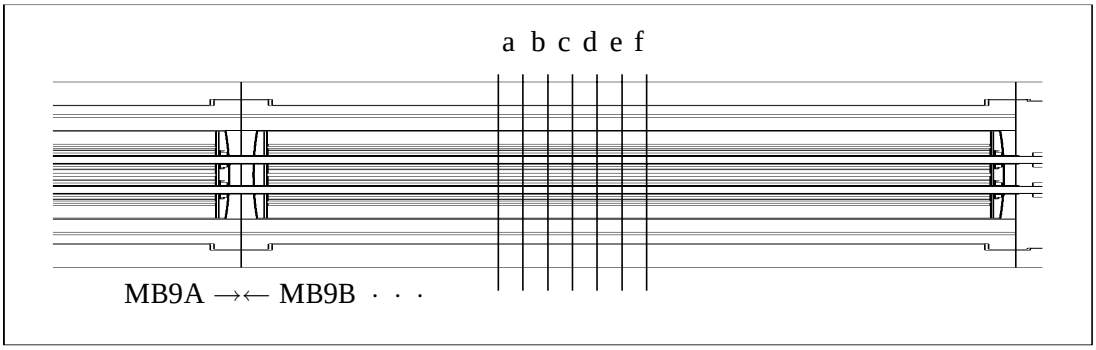

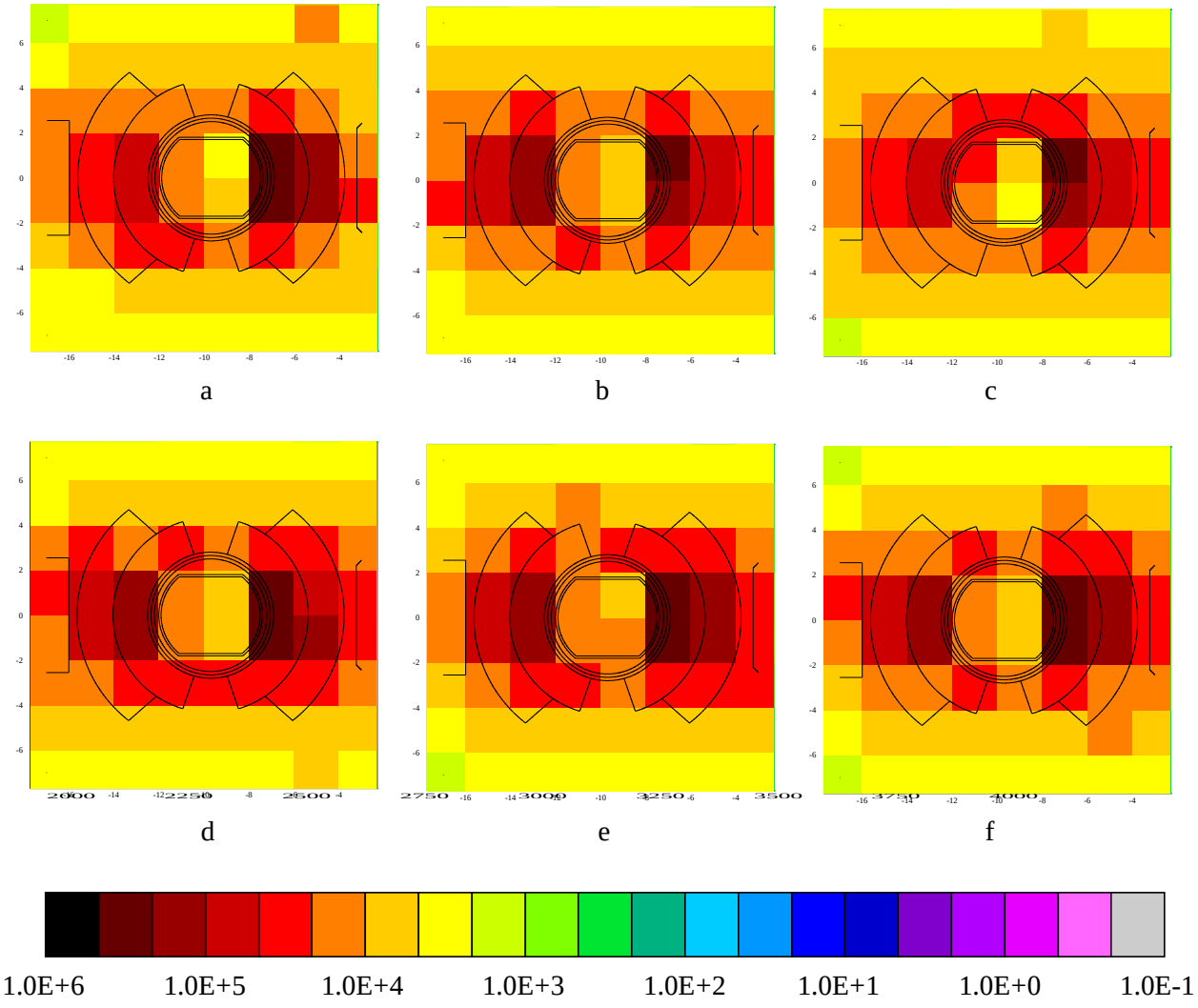

Figure 28: Selection of cross-sectional slices showing maximum dose (Gy / y) in the coils and beam-line of the dipole magnet MB9B in the dispersion suppressors of IR5. This is for the outgoing proton direction beam-line. The proton loss distribution used is taken from [Bai00] for a rate of 3.5×10^8 inelastic interactions per second in the IP. The total proton loss in IR1 is 1.3×10^7 s^{-1}. Each slice corresponds to the labelled slice in the top schematic diagram.

Appendix A.5

Annual dose to the beam position monitors (Q8-Q11)

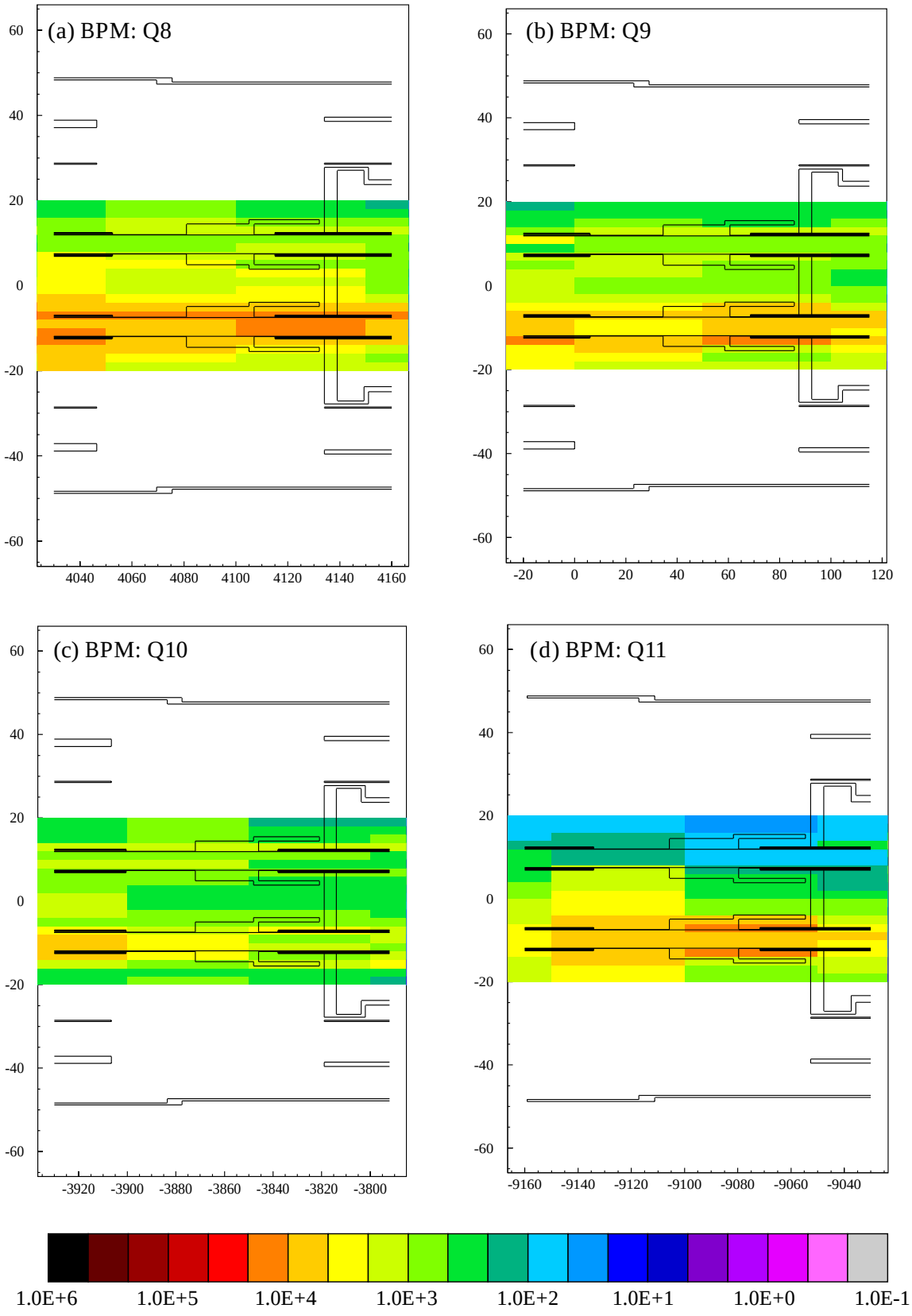

Figure 29: Dose (Gy / y) to the Beam Position Monitors: (a) Q8, (b) Q9, (c) Q10 and (d) Q11 in the dispersion suppressors of IR1. These doses are averaged over a slice of 12cm around the beam-axis covering the radial extent of the BPM. In Figure (d) contributions to the dose from beam-gas interactions and from the upstream arcs are missing due to the start of the FLUKA geometry at this point. Realistic doses for the second beam-pipe would appear similar to those shown in Figures (a)-(c).

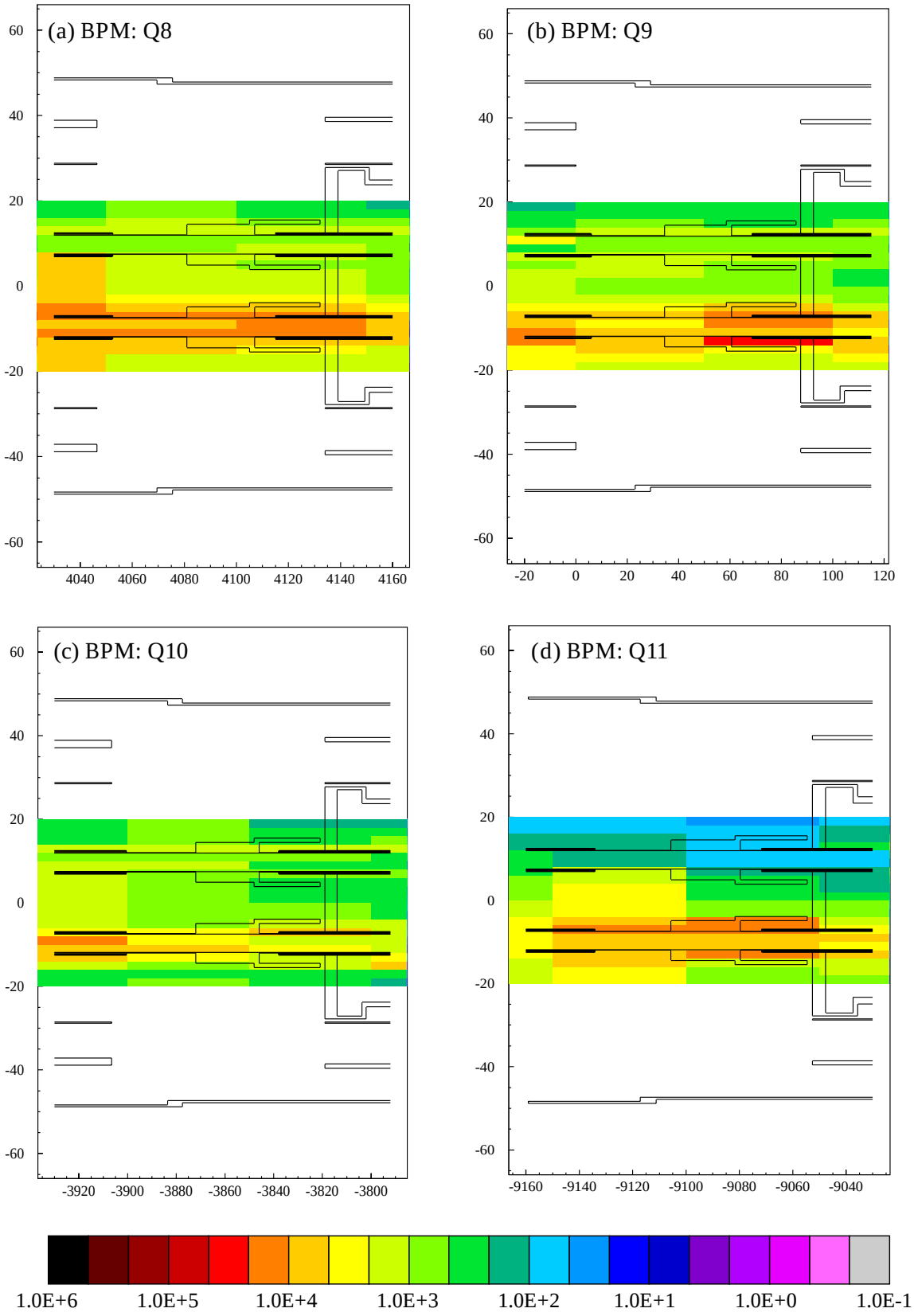

Figure 30: Dose (Gy / y) to the Beam Position Monitors: (a) Q8, (b) Q9, (c) Q10 and (d) Q11 in the dispersion suppressors of IR5 due to point losses. These doses are averaged over a slice of 12cm around the beam-axis covering the radial extent of the BPM. In Figure (d) contributions to the dose from beam-gas interactions and from the upstream arcs are missing due to the start of the FLUKA geometry at this point. Realistic doses for the second beam-pipe would appear similar to those shown in Figures (a)-(c).

Appendix A.6

Annual dose to the quench diodes in the dispersion suppressors of the high luminosity insertion points IR1 & IR5

Dispersion Suppressor Pt1 - diode Q11

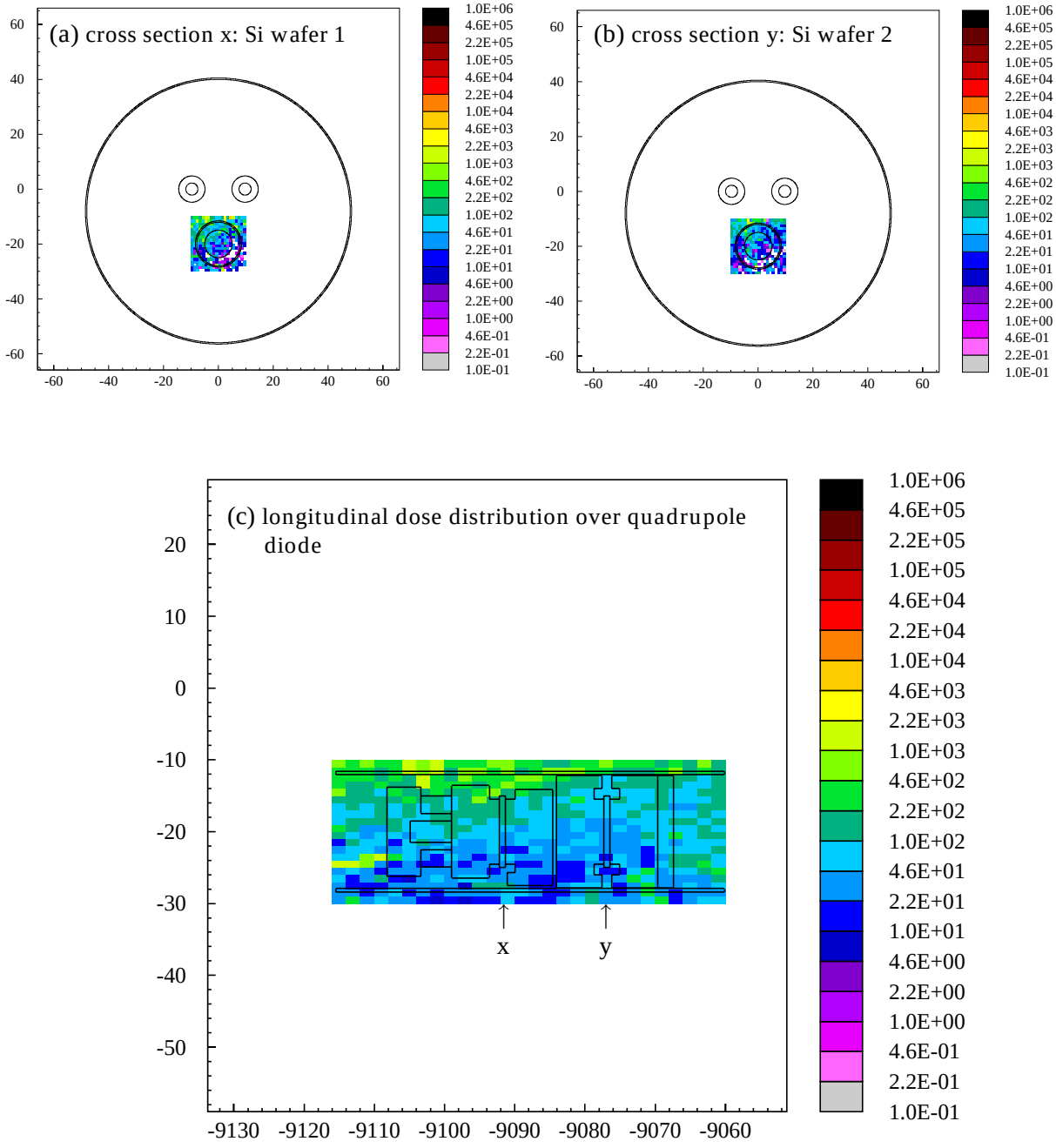

Figure 31: Dose (Gy/y) to the quadrupole diode of Q11 in the dispersion suppressors of IR1. The thin strips labelled “x” and “y” represents the Si in the diode. Plots (a) and (b) show cross sectional cuts through the Si wafer strips x and y respectively. Plot (c) shows the longitudinal dose distribution averaged over the width of the diode housing region.

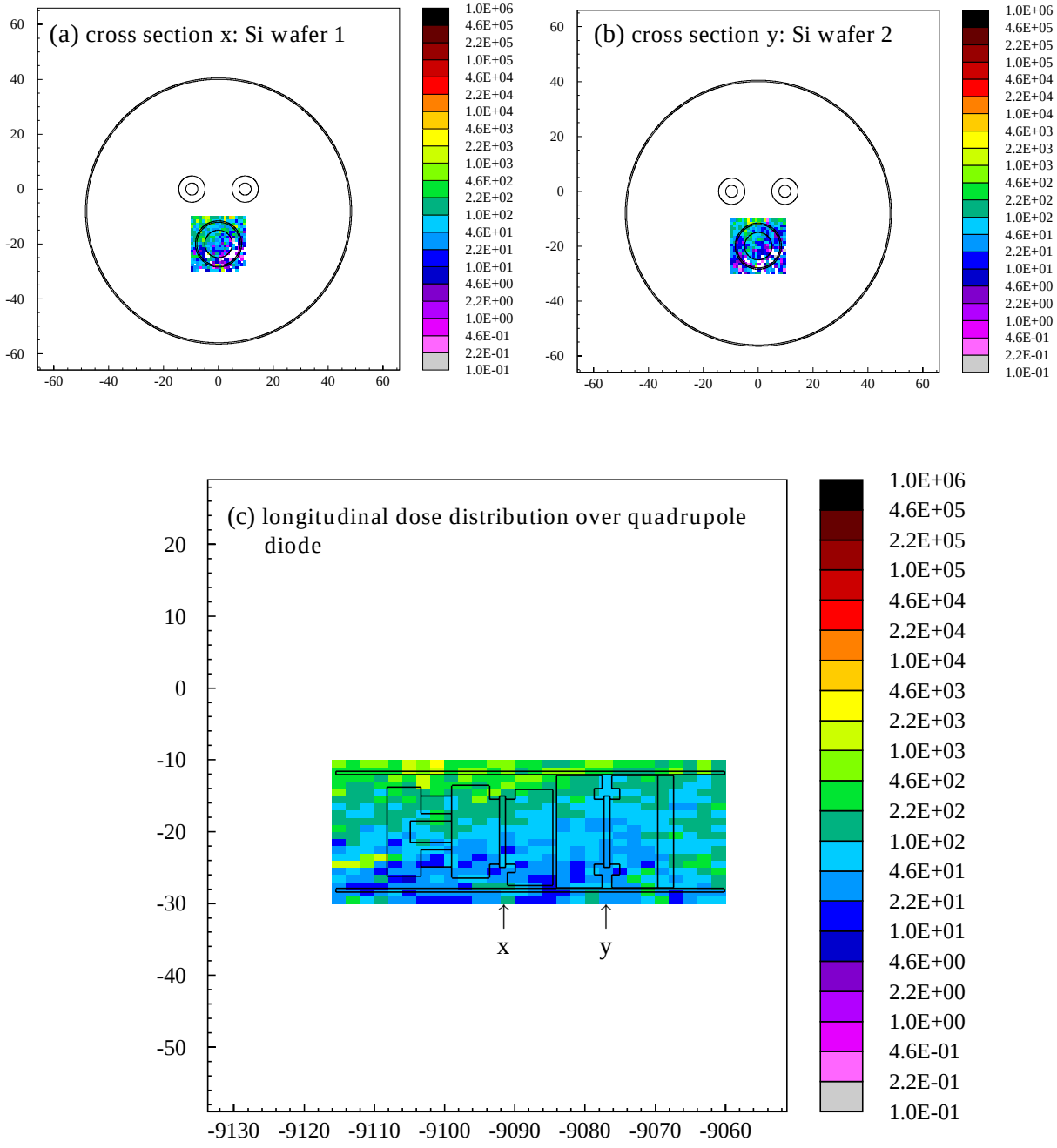

Figure 32: Dose (Gy / y) to the quadrupole diode of Q11 in the dispersion suppressors of IR5 due to point losses. The thin strips labelled “x” and “y” represents the Si in the diode. Plots (a) and (b) show cross sectional cuts through the Si wafer strips x and y respectively. Plot (c) shows the longitudinal dose distribution averaged over the width of the diode housing region.

Dipole diode MB11A

(a) cross section x: Si wafer

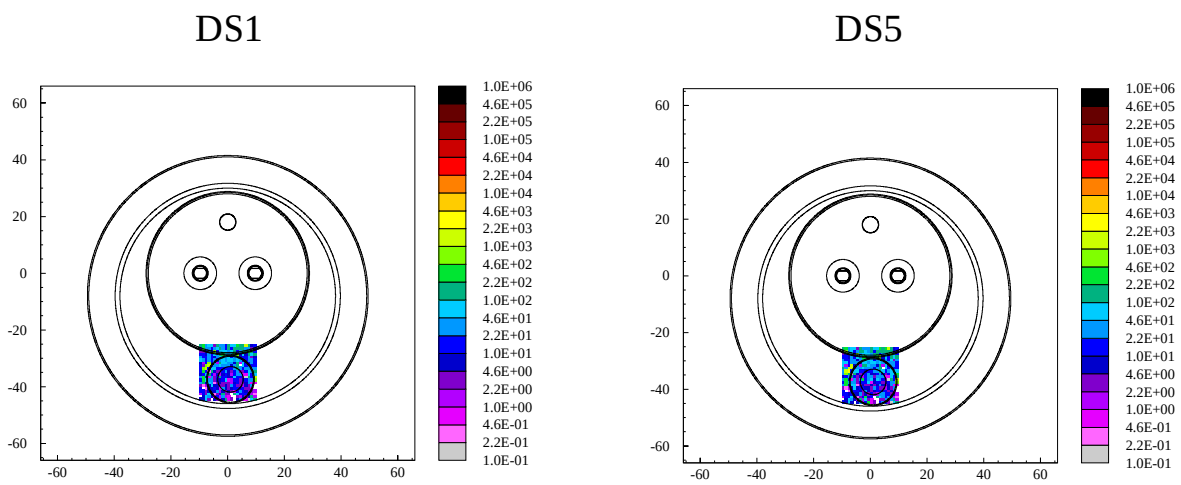

(b) longitudinal dose distribution over dipole diode

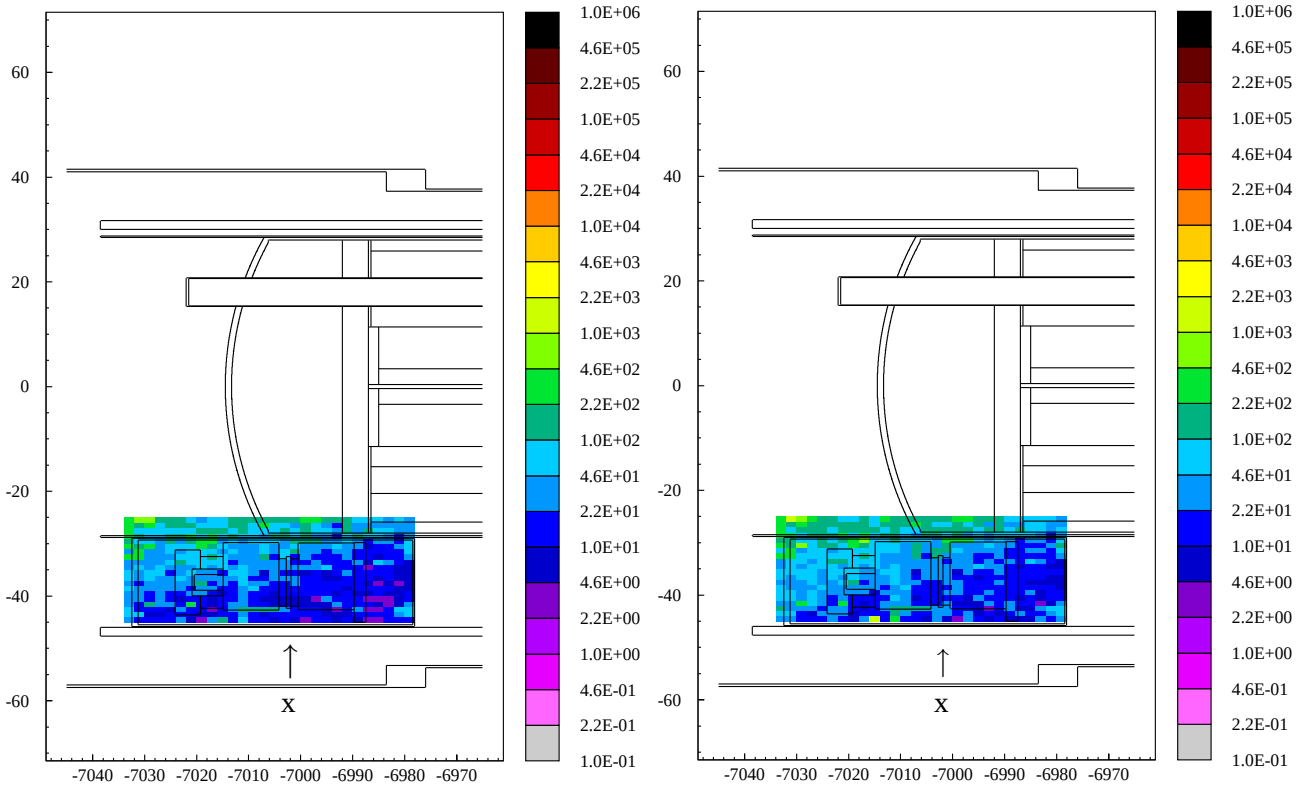

Figure 33: Dose (Gy / y) to the dipole diode of MB11A in the dispersion suppressors of IR1 (left) and IR5 (right). The thin strip labelled “x” represents the Si in the diode. Plot (a) is the cross sectional cut through the Si wafer, (b) shows the longitudinal dose distribution over the diode. These doses are averaged over the width of the dipole diode housing region.

Dipole diode MB11B

(a) cross section x: Si wafer

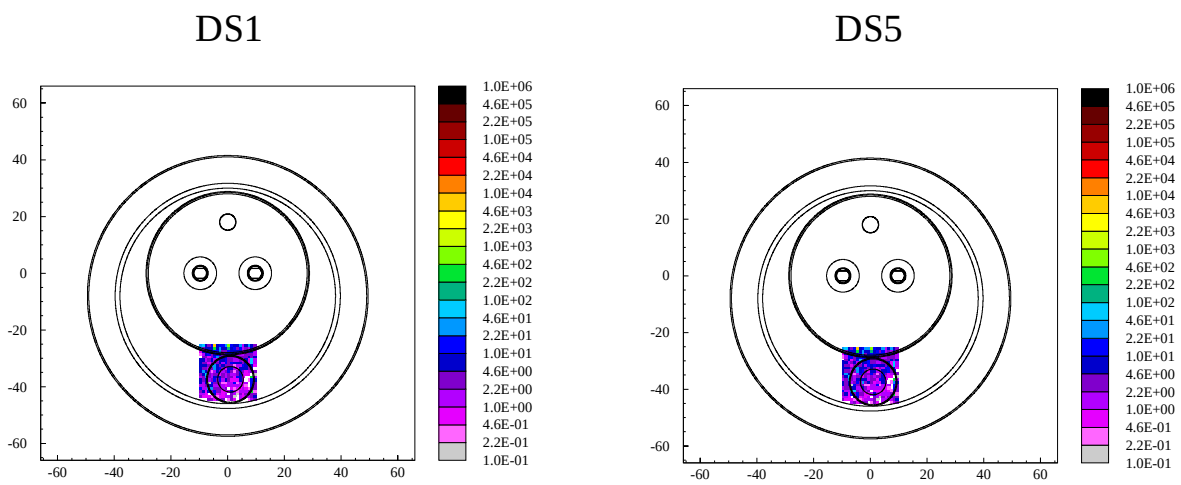

(b) longitudinal dose distribution over dipole diode

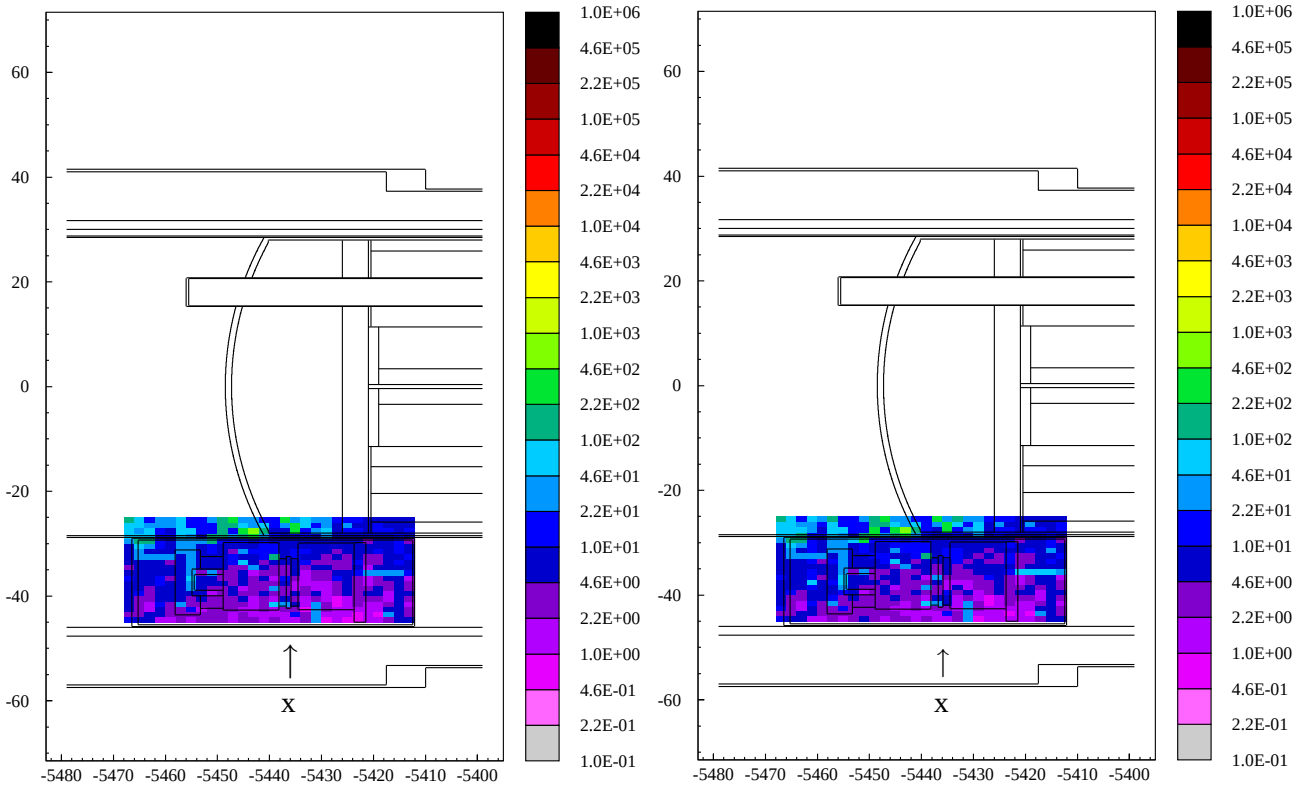

Figure 34: Dose (Gy / y) to the dipole diode of MB11B in the dispersion suppressors of IR1 (left) and IR5 (right). The thin strip labelled “x” represents the Si in the diode. Plot (a) is the cross sectional cut through the Si wafer, (b) shows the longitudinal dose distribution over the diode. These doses are averaged over the width of the dipole diode housing region.

Dipole diode MB10A

(a) cross section x: Si wafer

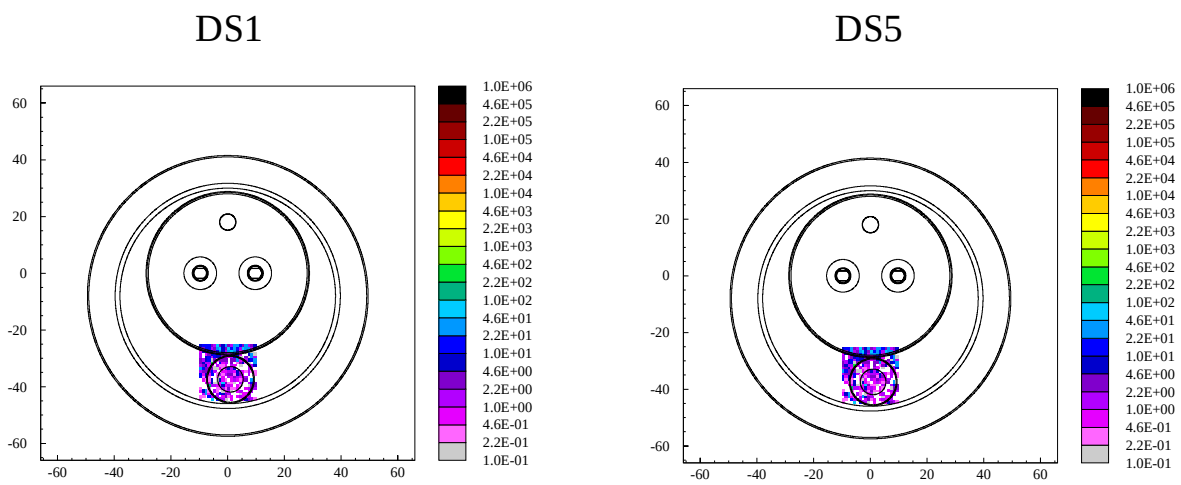

(b) longitudinal dose distribution over dipole diode

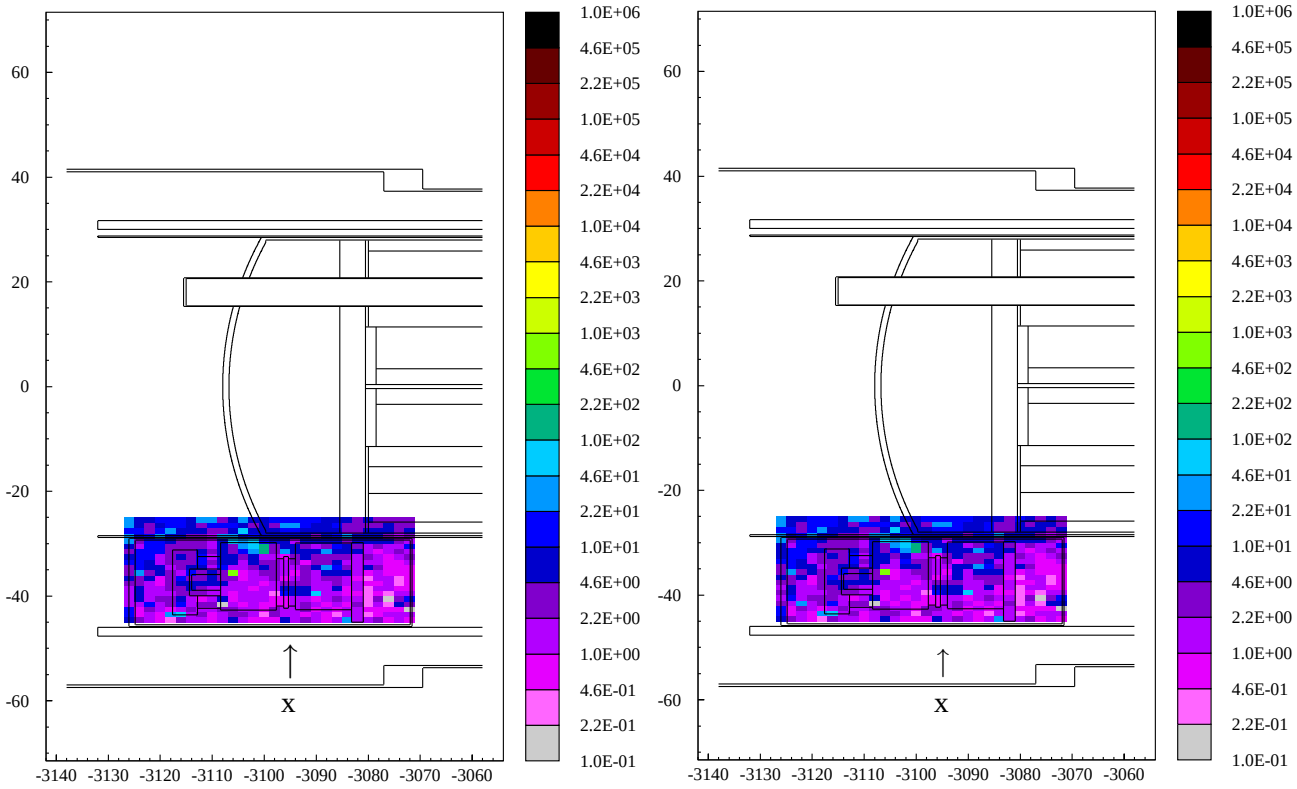

Figure 35: Dose (Gy / y) to the dipole diode of MB10A in the dispersion suppressors of IR1 (left) and IR5 (right). The thin strip labelled “x” represents the Si in the diode. Plot (a) is the cross sectional cut through the Si wafer, (b) shows the longitudinal dose distribution over the diode. These doses are averaged over the width of the dipole diode housing region.

Dipole diode MB10B

(a) cross section x: Si wafer

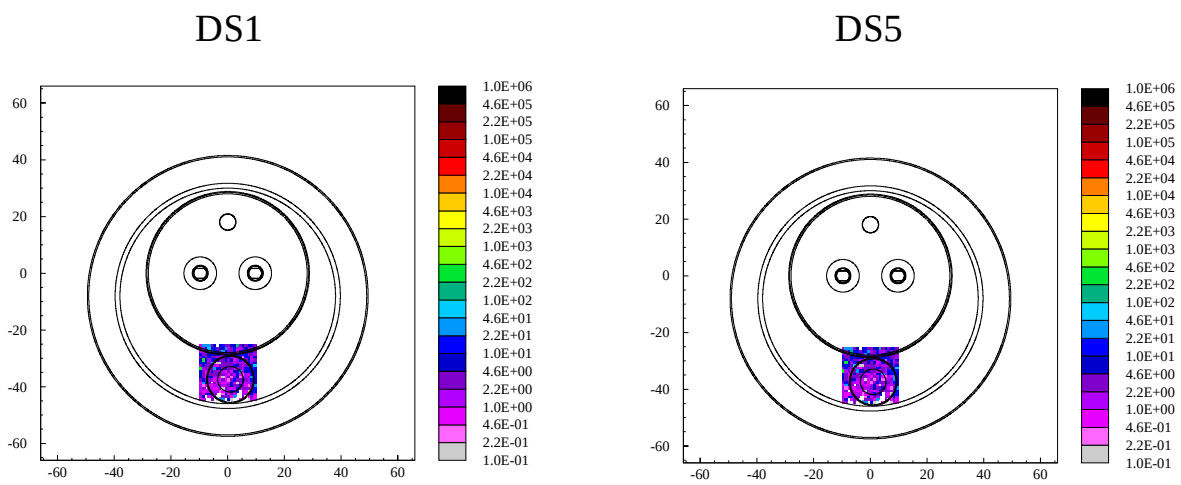

(b) longitudinal dose distribution over dipole diode

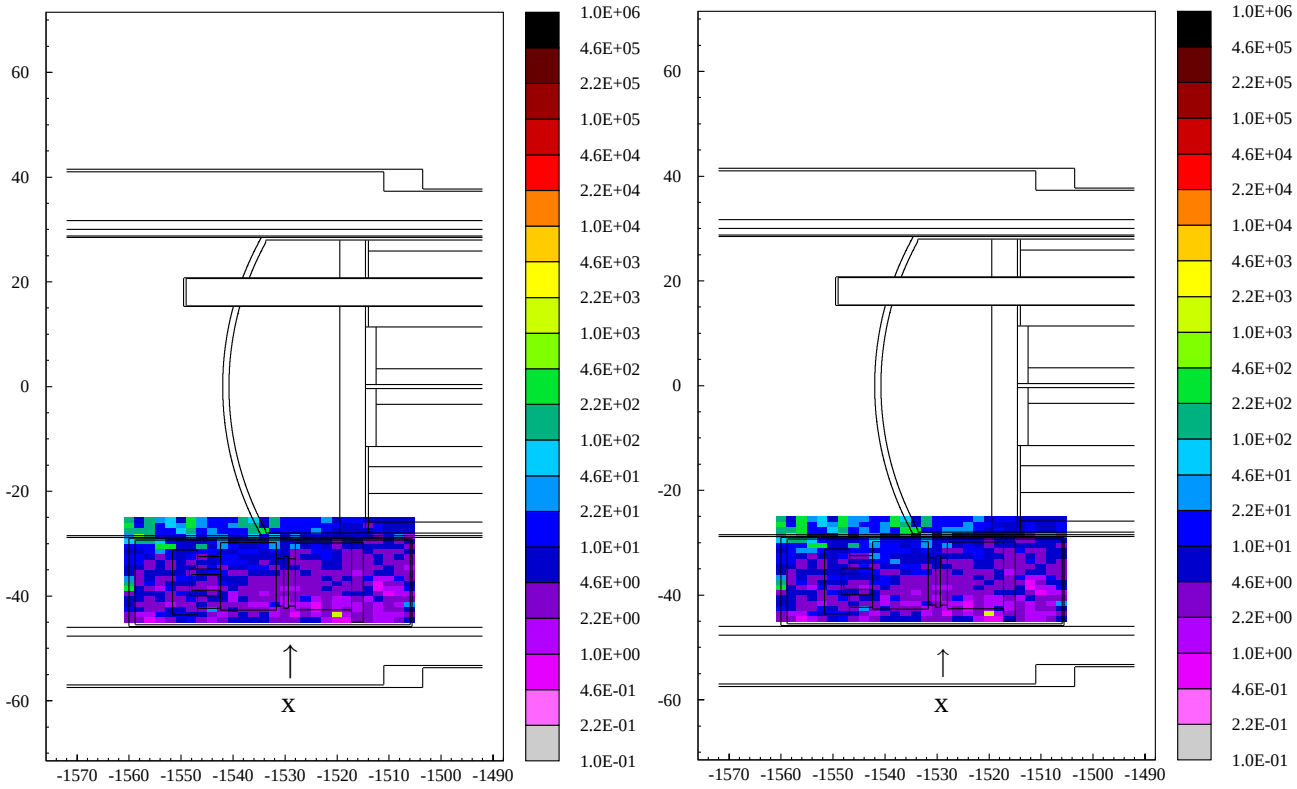

Figure 36: Dose (Gy / y) to the dipole diode of MB10B in the dispersion suppressors of IR1 (left) and IR5 (right). The thin strip labelled “x” represents the Si in the diode. Plot (a) is the cross sectional cut through the Si wafer, (b) shows the longitudinal dose distribution over the diode. These doses are averaged over the width of the dipole diode housing region.

Dipole diode MB9A

(a) cross section x: Si wafer

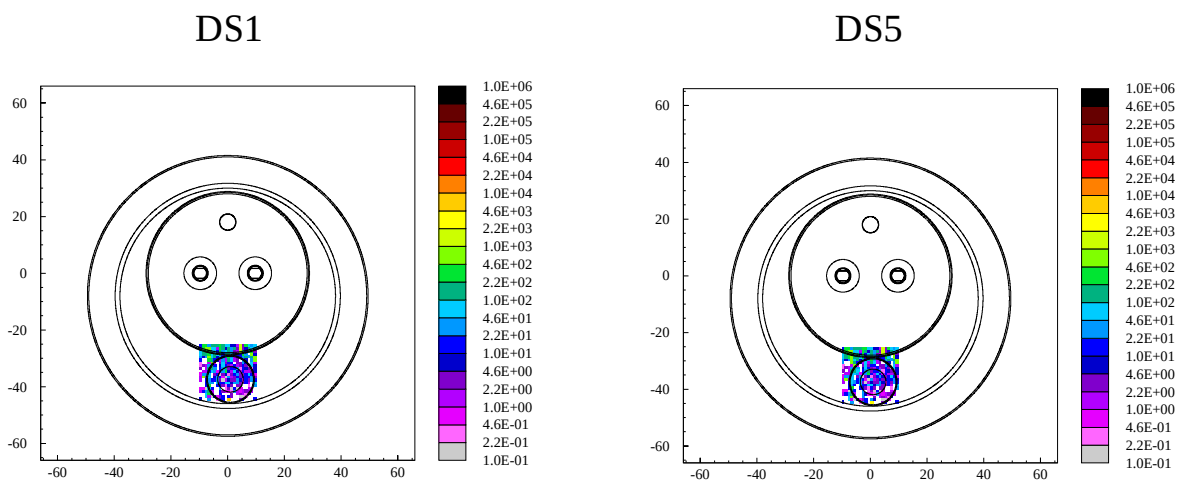

(b) longitudinal dose distribution over dipole diode

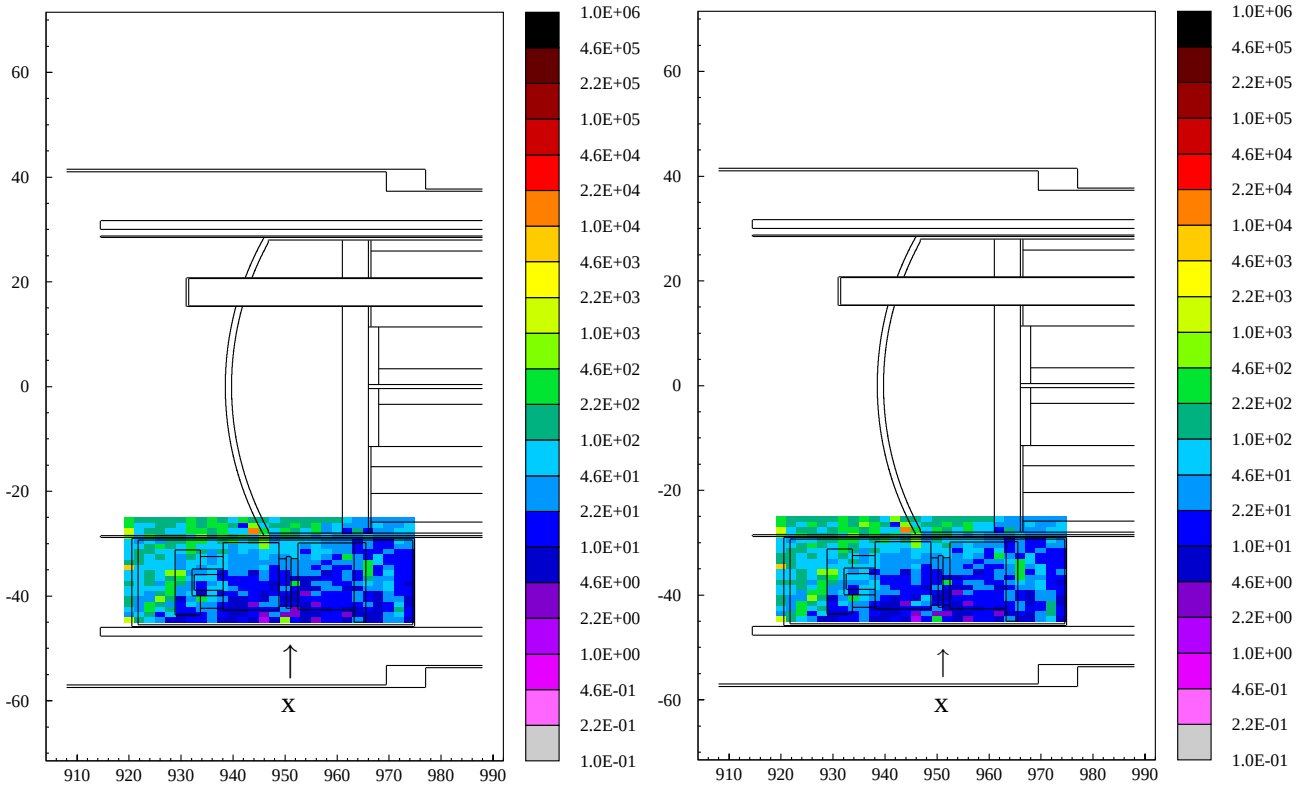

Figure 37: Dose (Gy / y) to the dipole diode of MB9A in the dispersion suppressors of IR1 (left) and IR5 (right). The thin strip labelled “x” represents the Si in the diode. Plot (a) is the cross sectional cut through the Si wafer, (b) shows the longitudinal dose distribution over the diode. These doses are averaged over the width of the dipole diode housing region.

Dipole diode MB9B

(a) cross section x: Si wafer

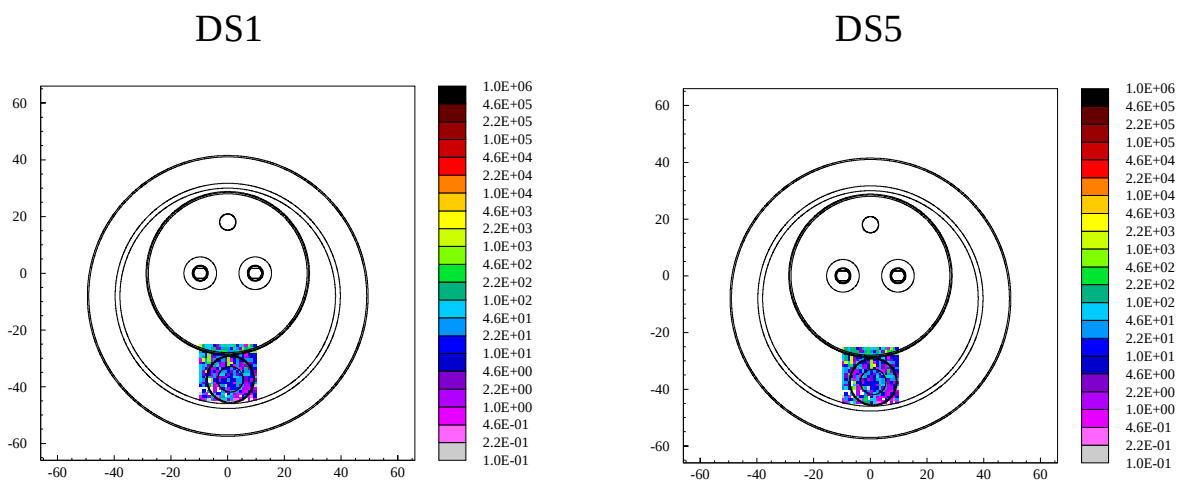

(b) longitudinal dose distribution over dipole diode

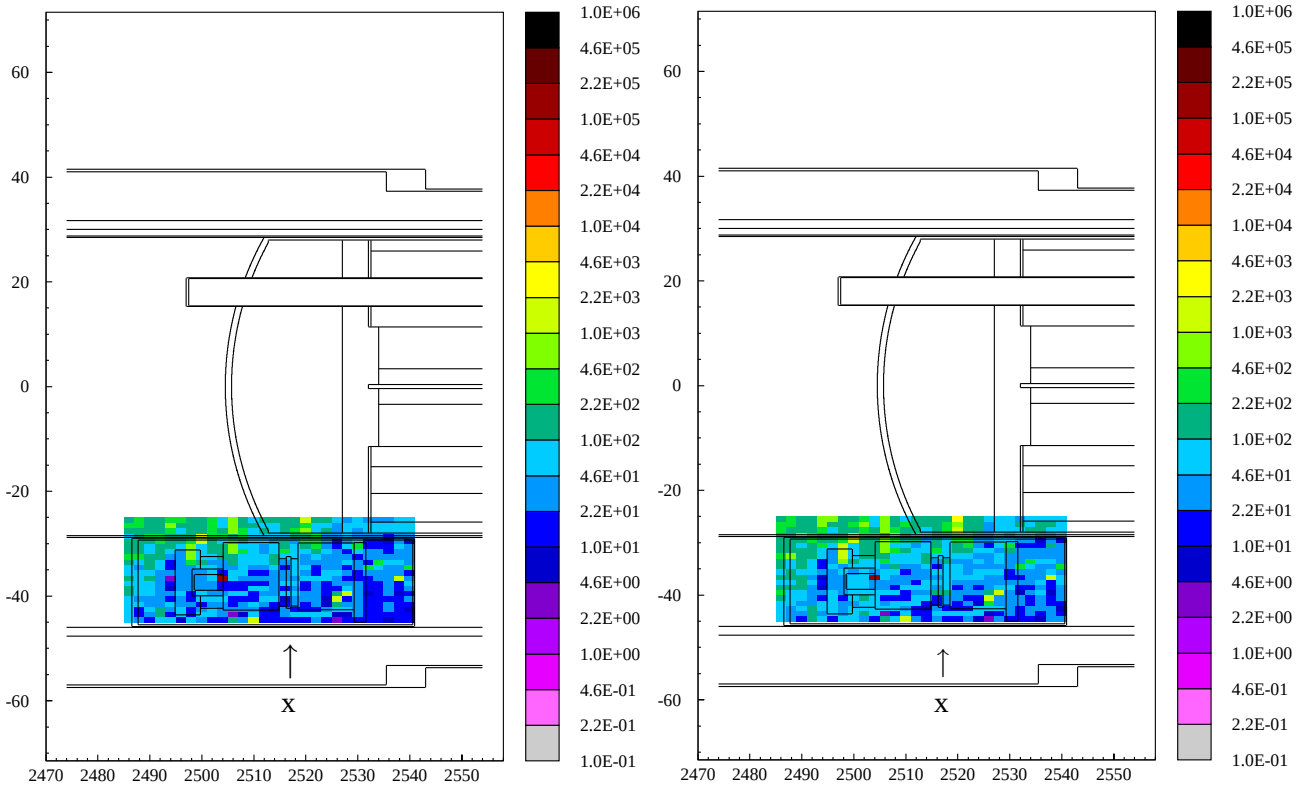

Figure 38: Dose (Gy / y) to the dipole diode of MB9B in the dispersion suppressors of IR1 (left) and IR5 (right). The thin strip labelled “x” represents the Si in the diode. Plot (a) is the cross sectional cut through the Si wafer, (b) shows the longitudinal dose distribution over the diode. These doses are averaged over the width of the dipole diode housing region.

Dipole diode MB8A

(a) cross section x: Si wafer

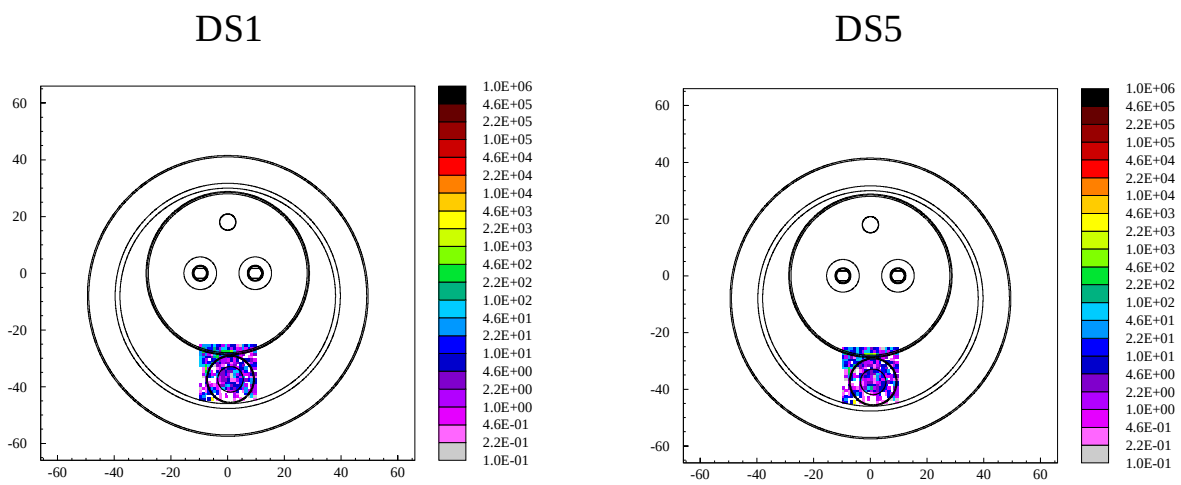

(b) longitudinal dose distribution over dipole diode

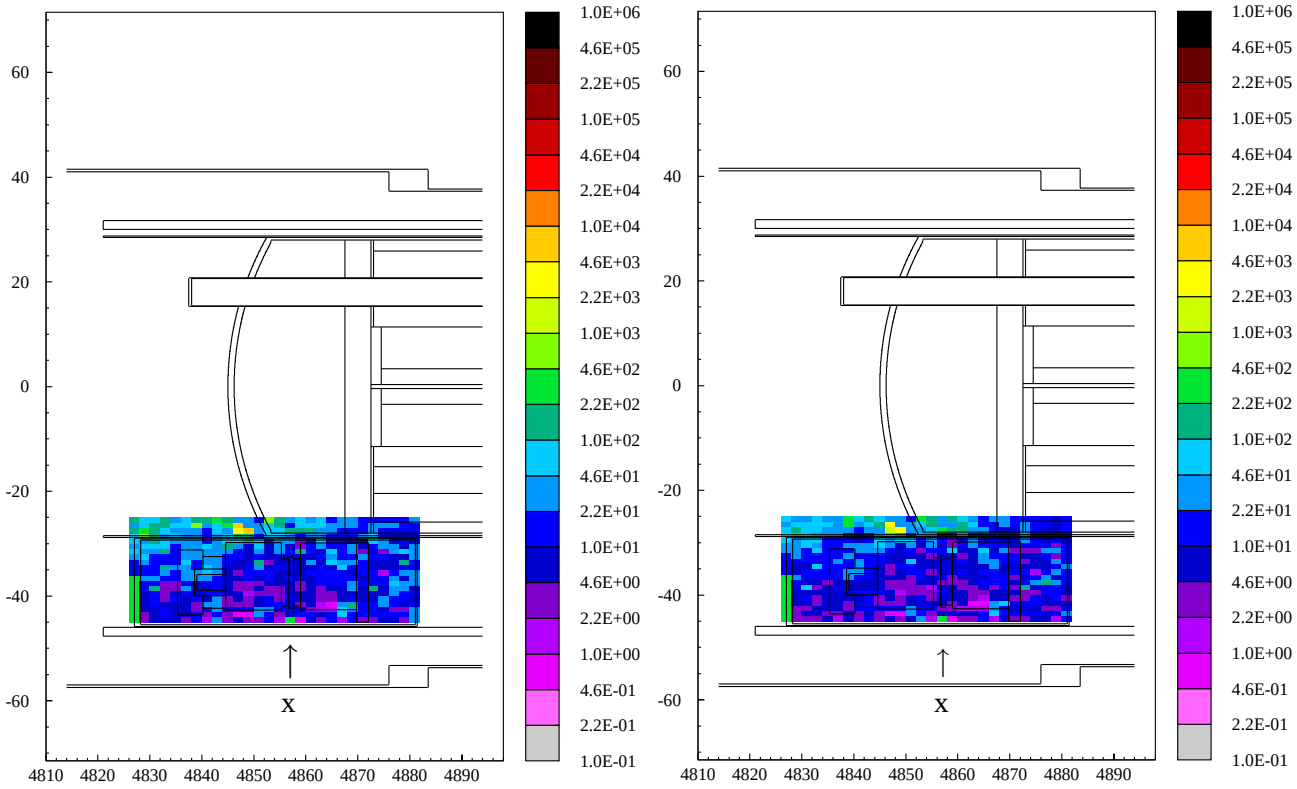

Figure 39: Dose (Gy / y) to the dipole diode of MB8A in the dispersion suppressors of IR1 (left) and IR5 (right). The thin strip labelled “x” represents the Si in the diode. Plot (a) is the cross sectional cut through the Si wafer, (b) shows the longitudinal dose distribution over the diode. These doses are averaged over the width of the dipole diode housing region.

Dipole diode MB8B

(a) cross section x: Si wafer

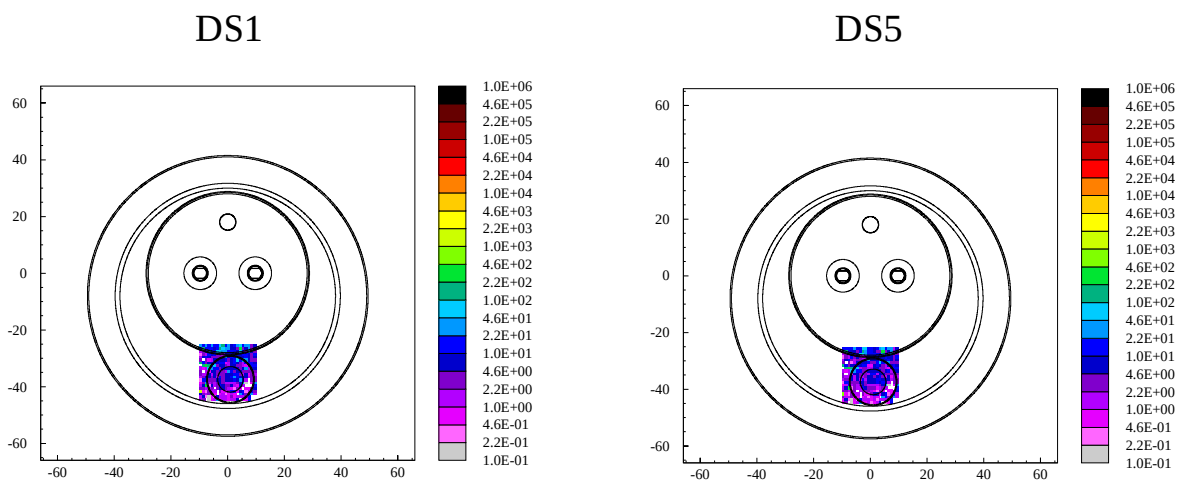

(b) longitudinal dose distribution over dipole diode

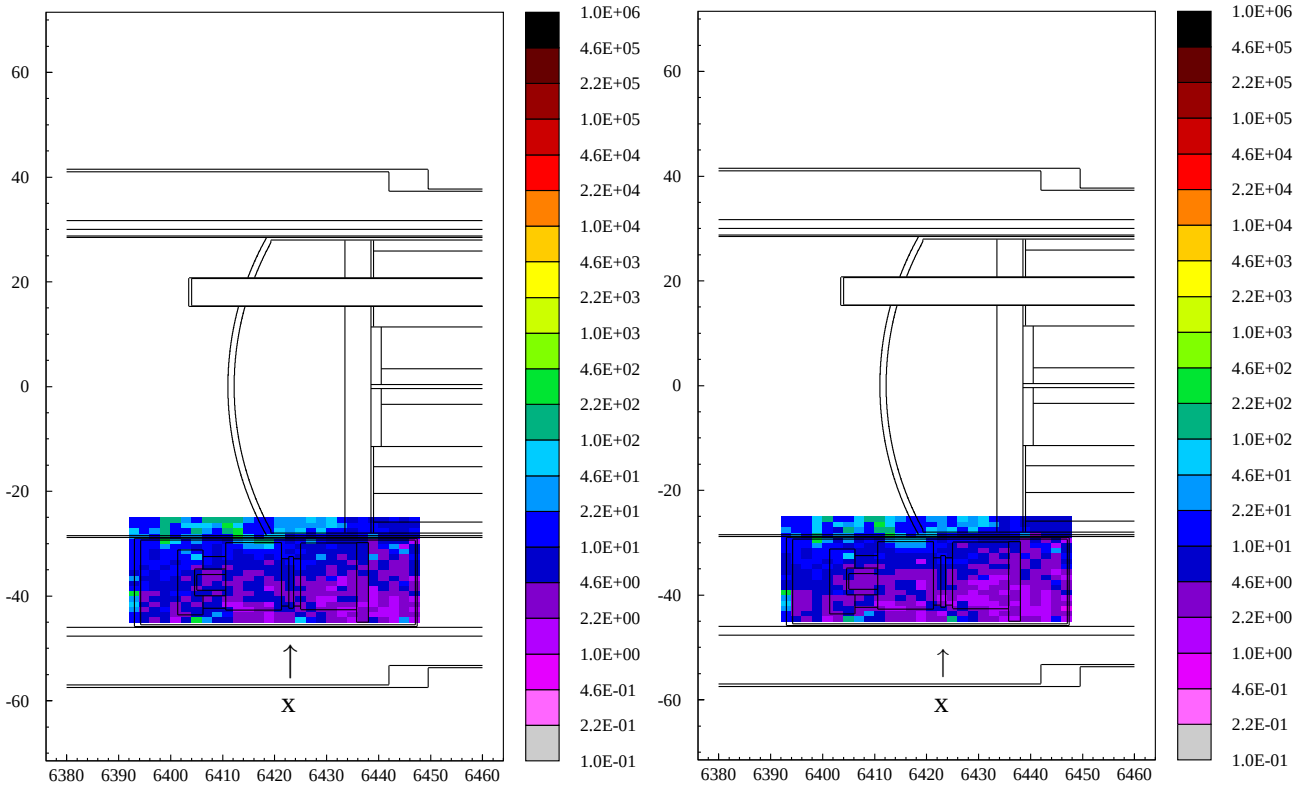

Figure 40: Dose (Gy / y) to the dipole diode of MB8B in the dispersion suppressors of IR1 (left) and IR5 (right). The thin strip labelled “x” represents the Si in the diode. Plot (a) is the cross sectional cut through the Si wafer, (b) shows the longitudinal dose distribution over the diode. These doses are averaged over the width of the dipole diode housing region.

Appendix B

Radiation Environment in the dispersion suppressors of the high luminosity insertion points IR1 & IR5

Fluence : Dose ratios

Appendix B.1

Longitudinal fluence : dose distributions
above & below the dispersion suppressor magnet string

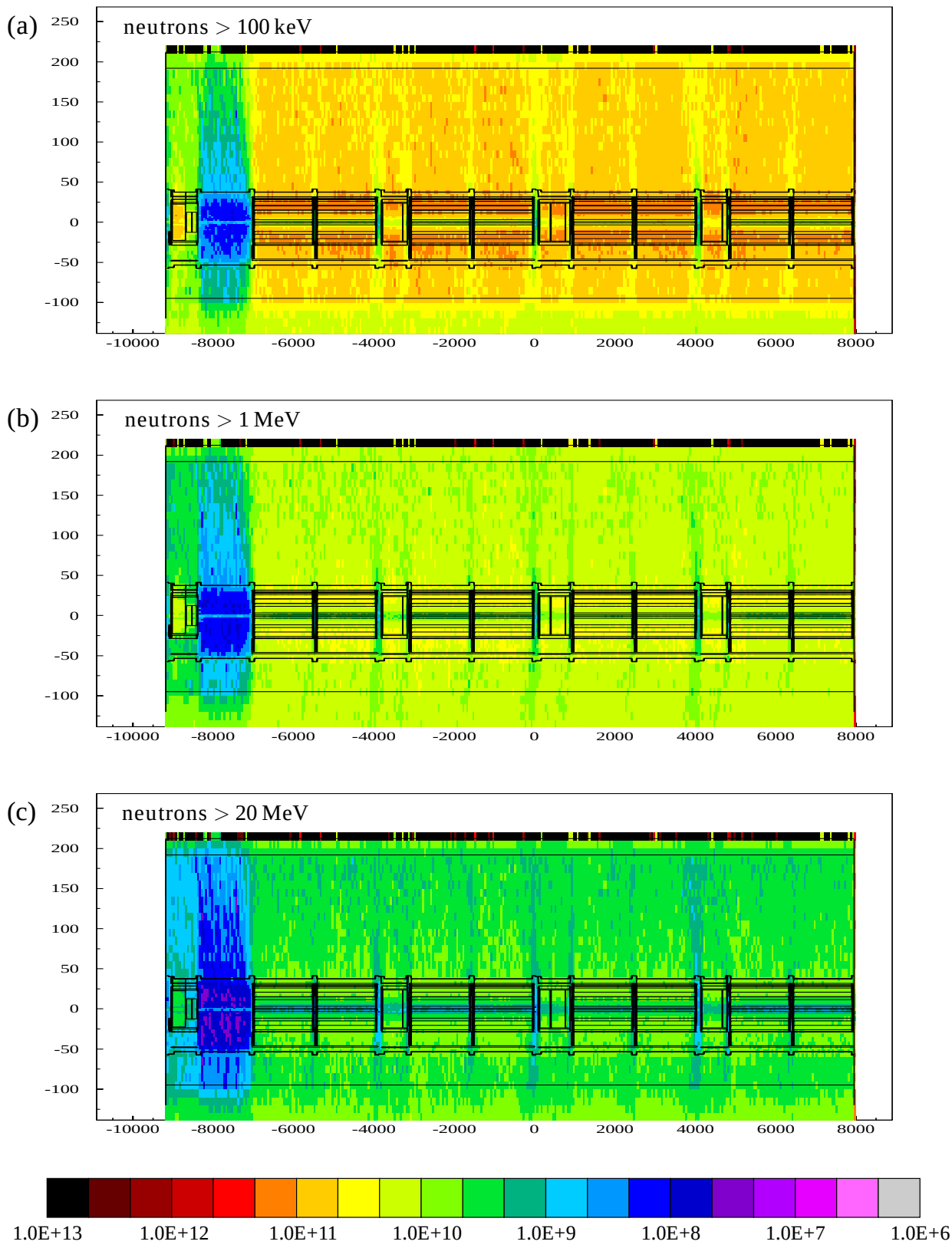

Figure 41: Fluence : Dose ratios above & below the magnet string of DS1 & DS5 a) neutrons > 100 keV, b) neutrons > 1 MeV and c) neutrons > 200 MeV. See full text next page.

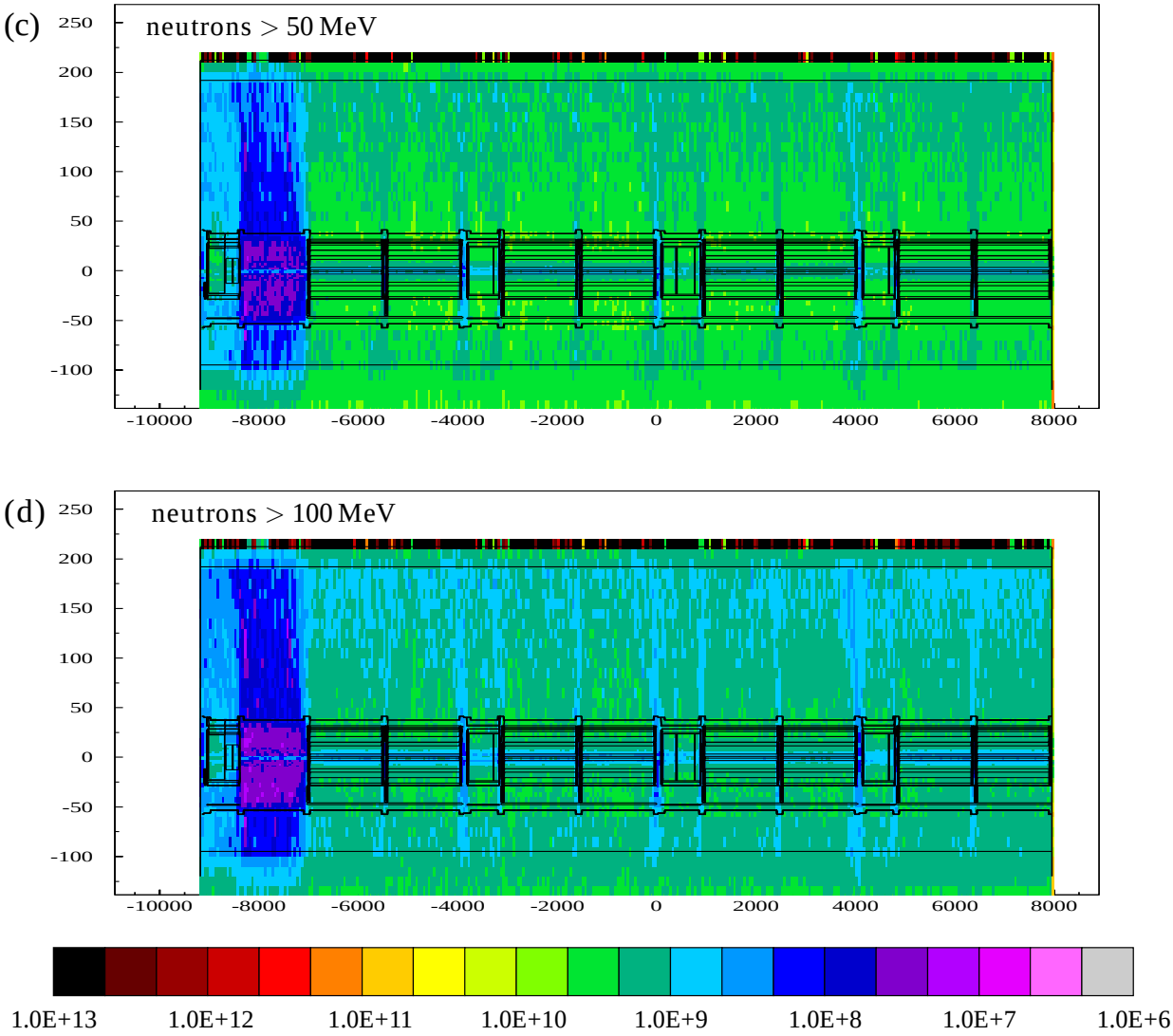

Figure 41: Neutron fluence : dose ratio distributions above and below the magnet string in the dispersion suppressors of DS1 & DS5. Values are the same for both dispersion suppressor sections. Absolute values for the annual neutron fluence can be obtained by combining these plots with the corresponding annual dose maps for DS1 (Figure 16) and DS5 (Figure 17). Plots (a)-(e) are shown for various neutron energy cuts: a) neutrons $>$ 100 keV (responsible for bulk damage in Si), b) neutrons $>$ 1 MeV, c) neutrons $>$ 20 MeV, d) neutrons $>$ 50 MeV and e) neutrons $>$ 100 MeV. The latter are responsible for SEUs.

Fluence:Dose ratios above & below magnet string ($cm^{-2}Gy^{-1}$)

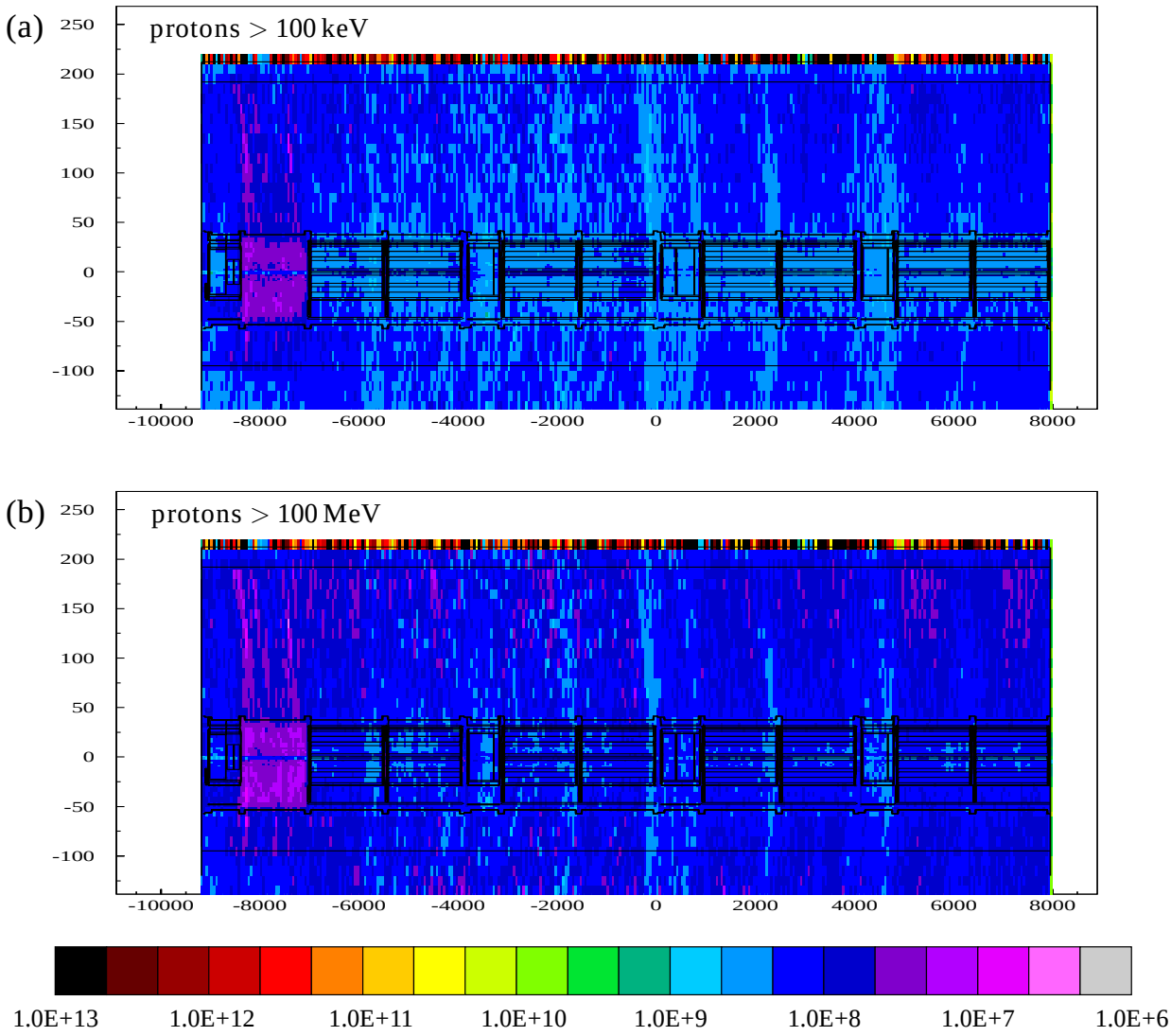

Figure 42: Proton fluence : dose ratio distributions above and below the magnet string in the dispersion suppressors of DS1 & DS5. Values are the same for both dispersion suppressor sections. Absolute values for the annual proton fluence can be obtained by combining these plots with the corresponding annual dose maps for DS1 (Figure 16) and DS5 (Figure 17). Plots (a) & (b) are shown for the two energy cuts: a) protons $>$ 100 keV and b) protons $>$ 1 MeV. There is very little difference in the ratio of fluence : dose for protons between these energy cuts.

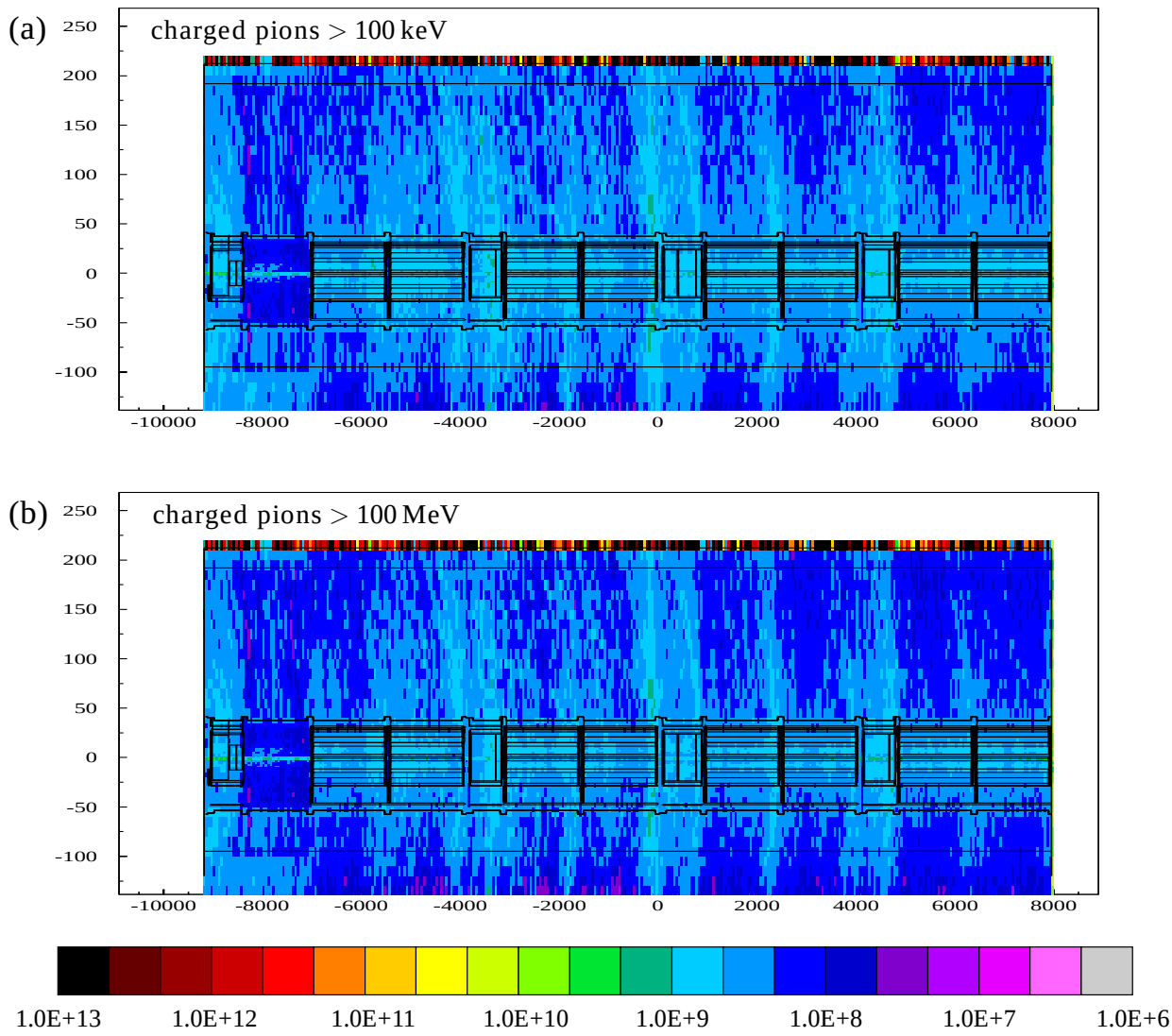

Figure 43: Charged pion fluence : dose ratio distributions above and below the magnet string in the dispersion suppressors of DS1 & DS5. Values are the same for both dispersion suppressor sections. Absolute values for the annual pion fluence can be obtained by combining these plots with the corresponding annual dose maps for DS1 (Figure 16) and DS5 (Figure 17). Plots (a) & (b) are shown for the two energy cuts: a) charged pions $>$ 100 keV and b) charged pions $>$ 1 MeV. There is very little difference in the ratio of fluence : dose for charged pions between these energy cuts.

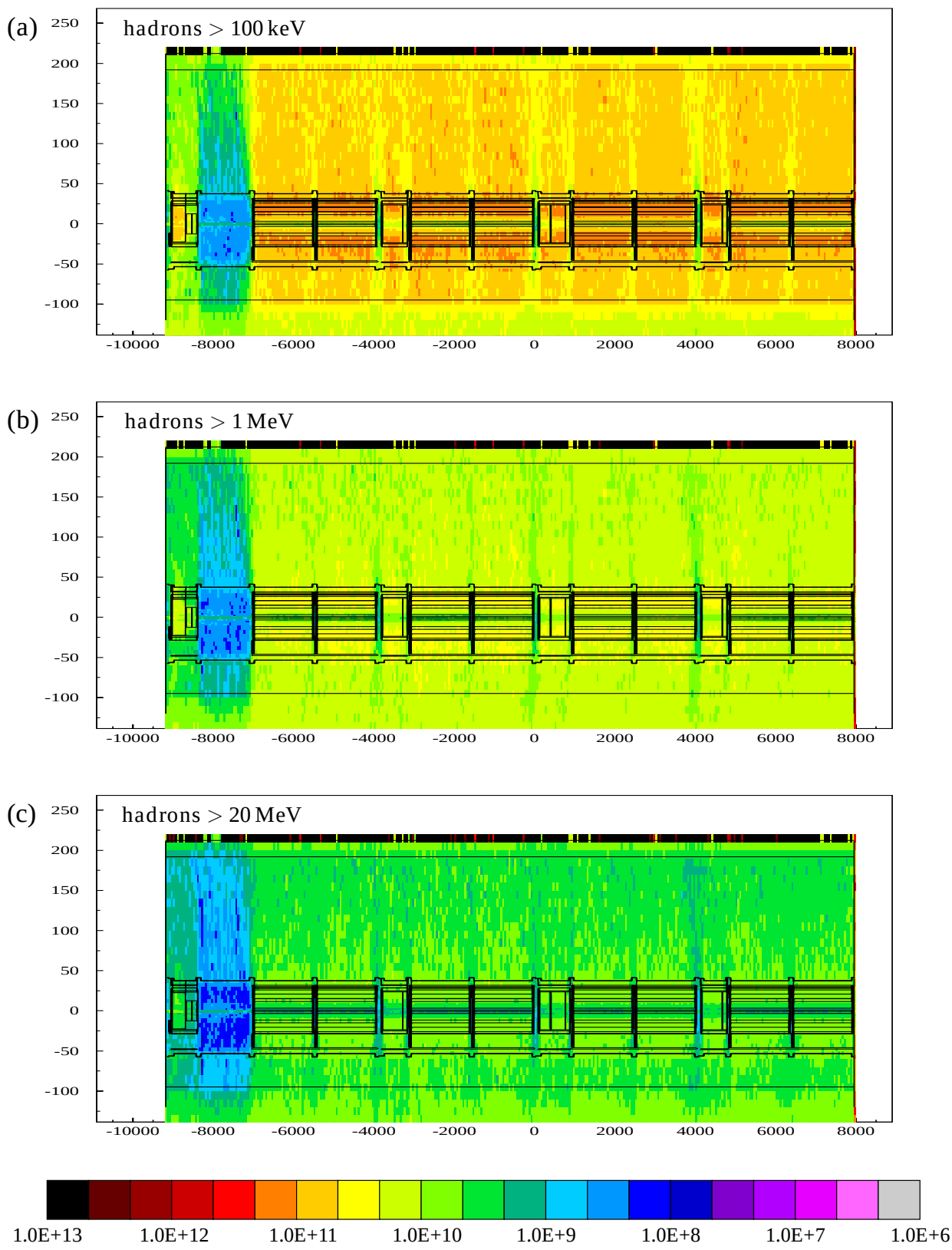

Figure 44: Fluence : Dose ratios above & below the magnet string of DS1 & DS5 a) hadrons > 100 keV, b) hadrons > 1 MeV and c) hadrons > 200 MeV. See full text next page.

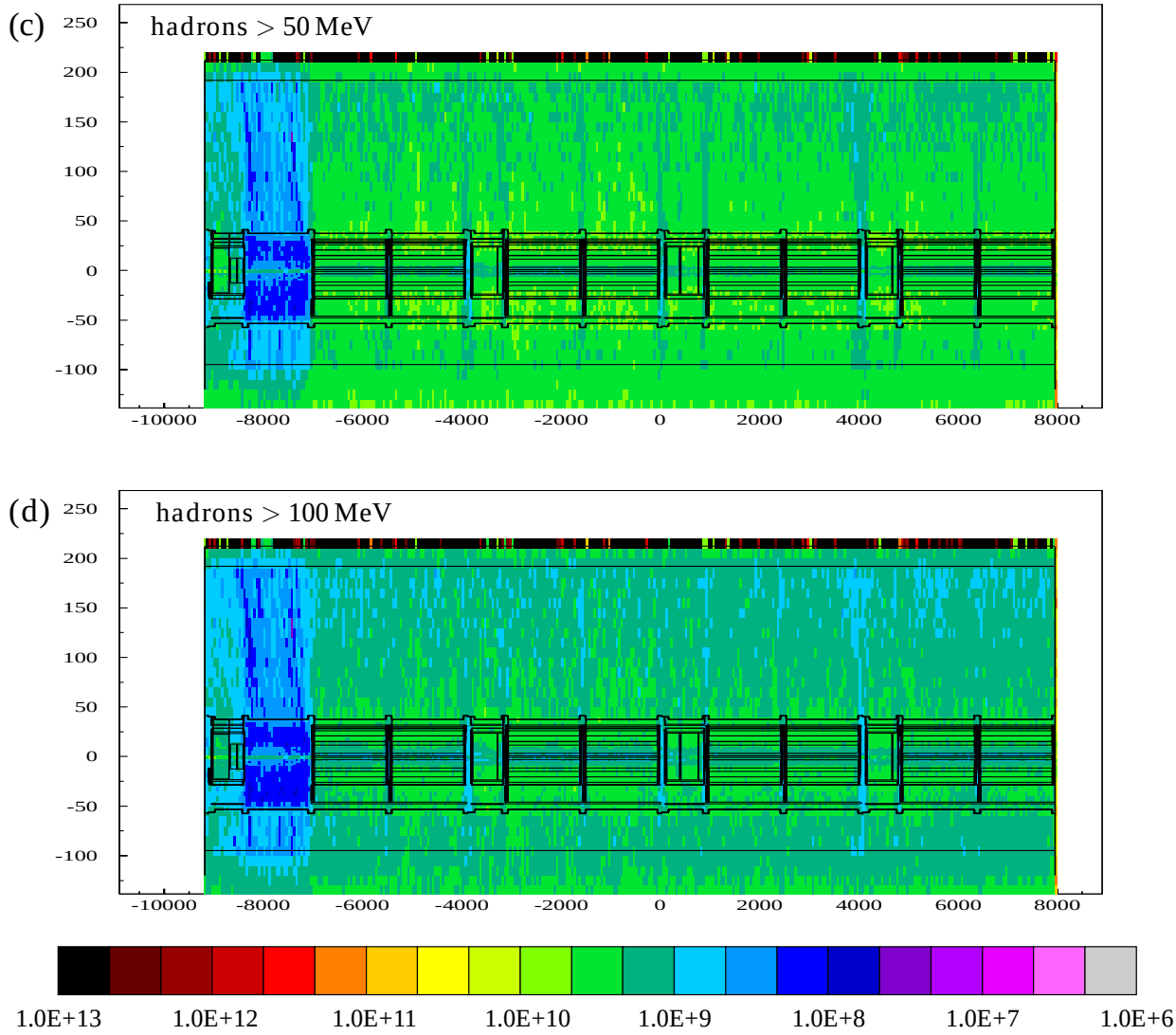

Figure 44: Hadron fluence : dose ratio distributions above and below the magnet string in the dispersion suppressors of DS1 & DS5. Values are the same for both dispersion suppressor sections. Absolute values for the annual hadron fluence can be obtained by combining these plots with the corresponding annual dose maps for DS1 (Figure 16) and DS5 (Figure 17). Plots (a)-(e) are shown for various hadron energy cuts: a) hadrons $>$ 100 keV (responsible for bulk damage in Si), b) hadrons $>$ 1 MeV, c) hadrons $>$ 20 MeV, d) hadrons $>$ 50 MeV and e) hadrons $>$ 100 MeV. The latter are responsible for SEUs.

Appendix B.2

Radial fluence : dose distributions in the LHC tunnel

Neutron Fluence:Dose ratios in LHC tunnel at Q11

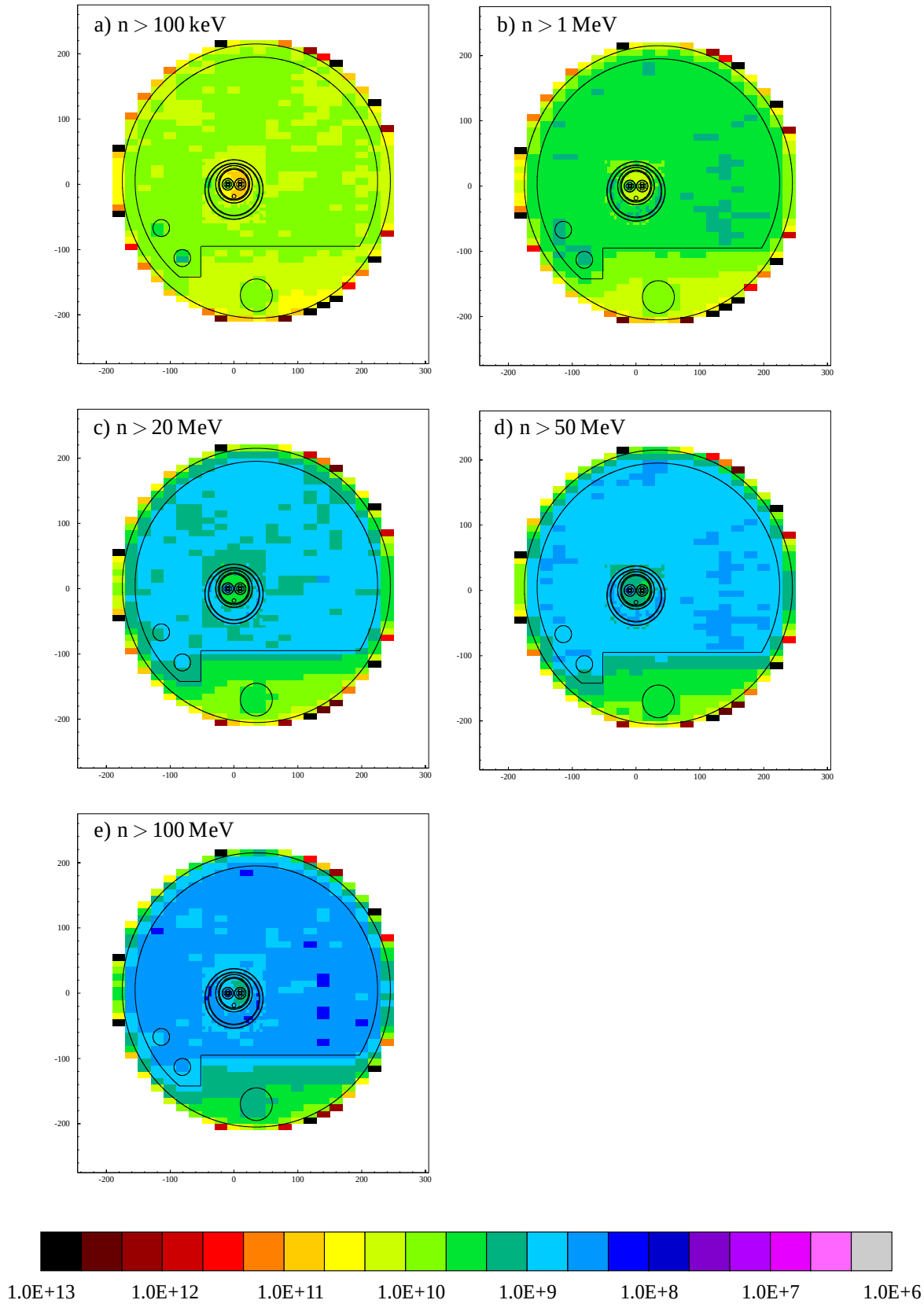

Figure 45: Radial fluence : dose distributions ($cm^{-2}Gy^{-1}$) in the LHC tunnel for neutrons above various energy cuts in the vicinity of Q11 for DS1 & DS5.

Hadron Fluence:Dose ratios in LHC tunnel at Q11

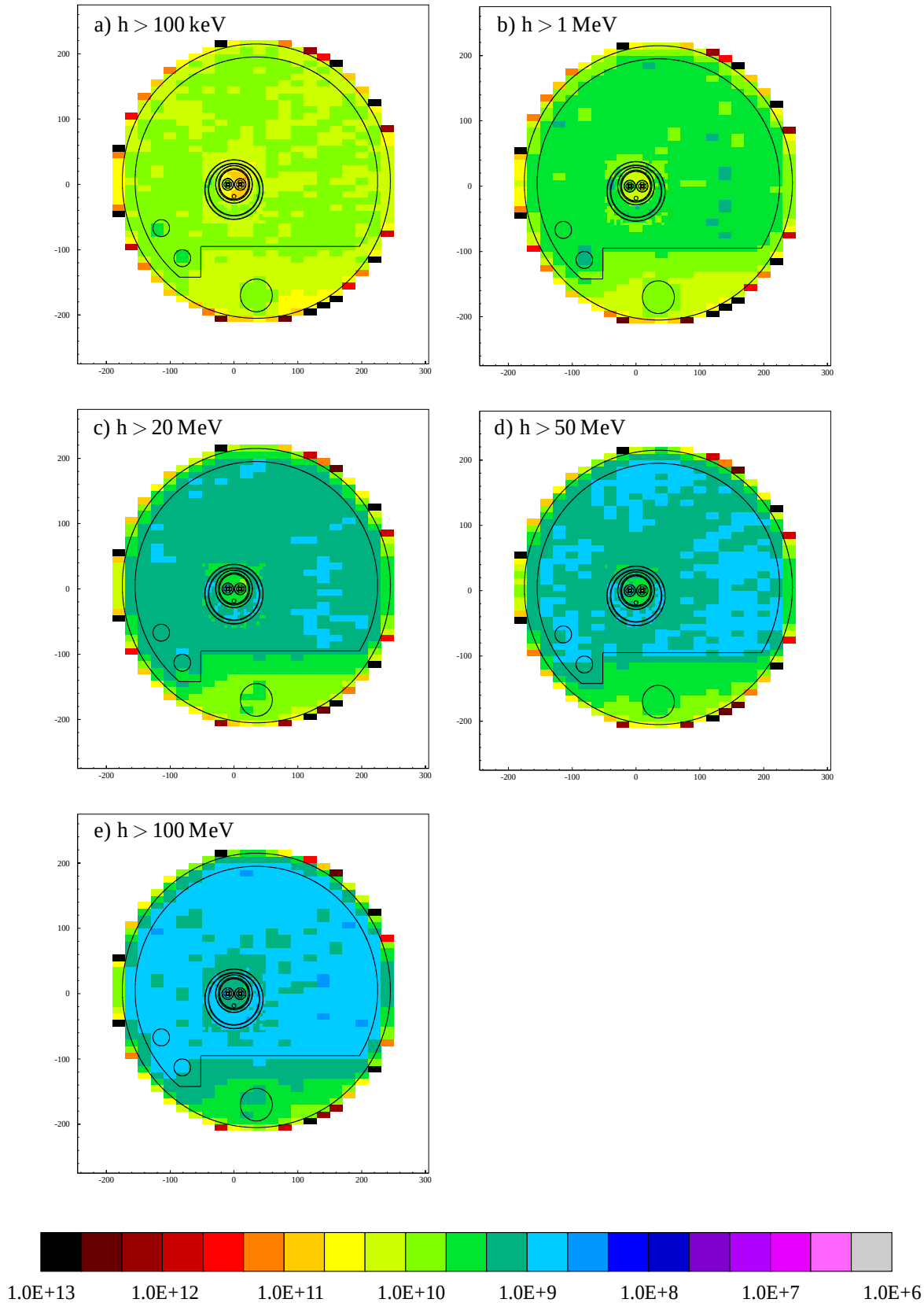

Figure 46: Radial fluence : dose distributions ($cm^{-2}Gy^{-1}$) in the LHC tunnel for total summed hadrons ($n+p+\pi^{\pm}$) above various energy cuts in the vicinity of Q11 for DS1 & DS5.

Neutron Fluence:Dose ratios in LHC tunnel at missing magnet

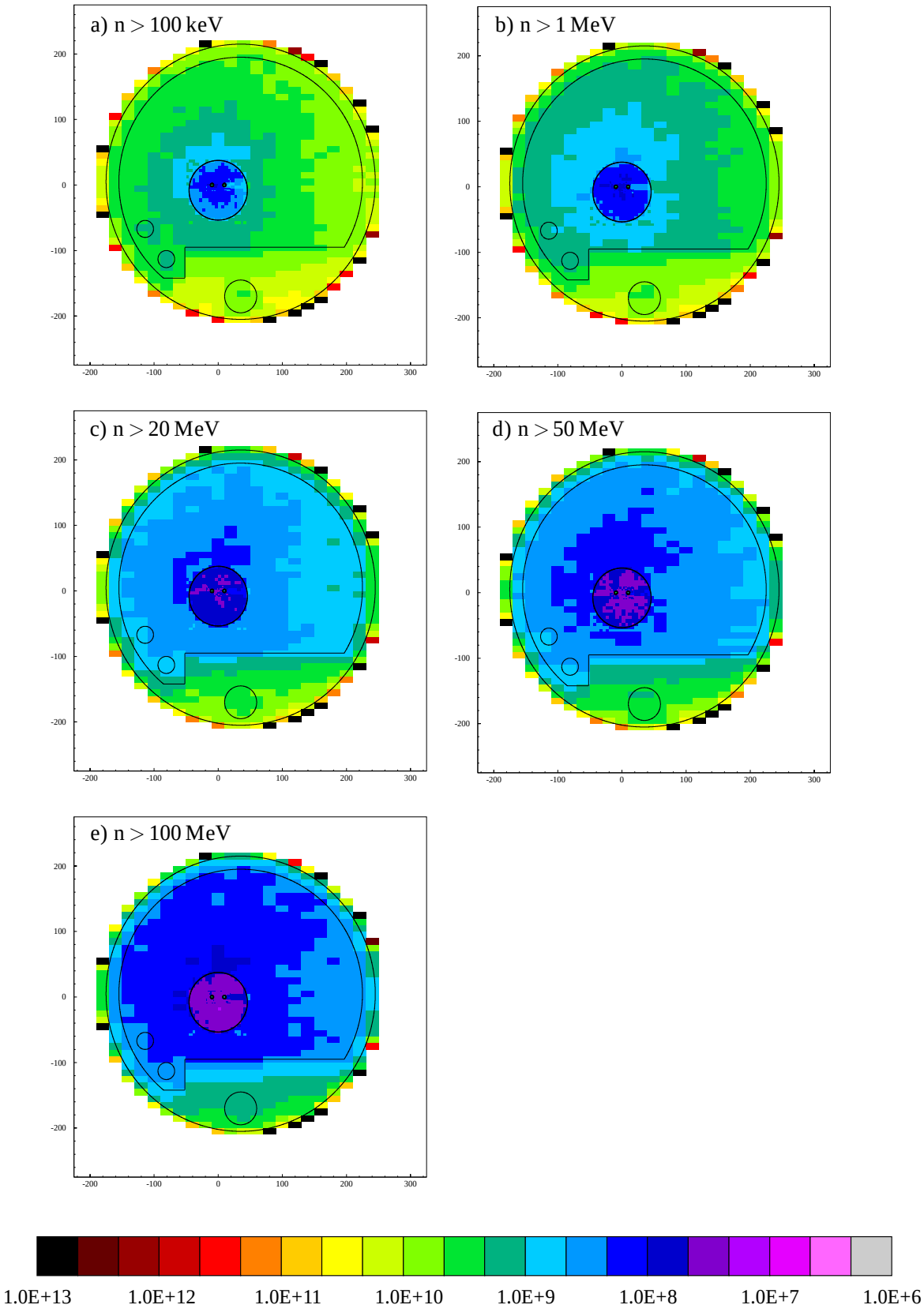

Figure 47: Radial fluence : dose distributions ($cm^{-2}Gy^{-1}$) in the LHC tunnel for neutrons above various energy cuts in the vicinity of the missing magnet for DS1 & DS5.

Hadron Fluence:Dose ratios in LHC tunnel at missing magnet

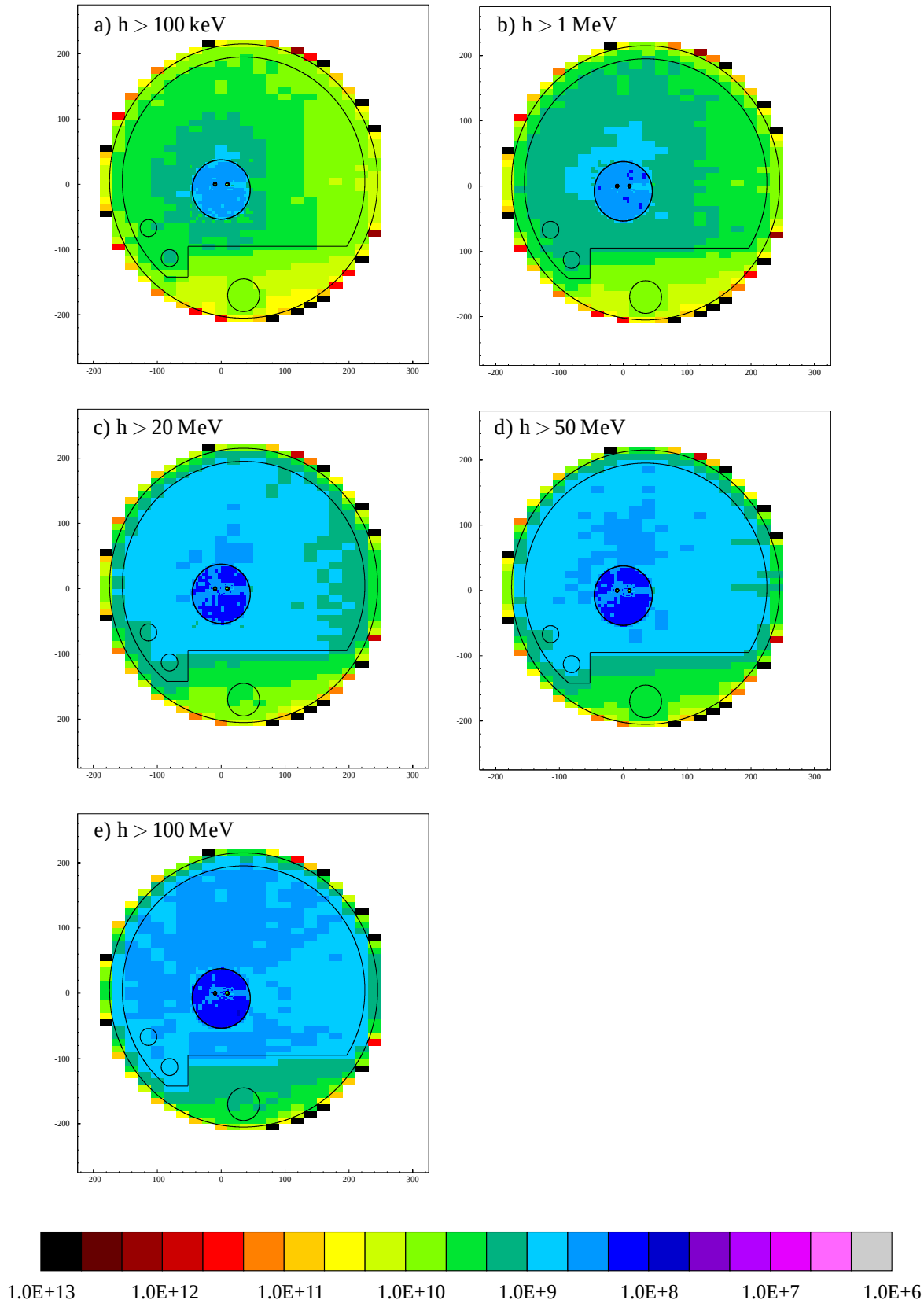

Figure 48: Radial fluence : dose distributions ($cm^{-2}Gy^{-1}$) in the LHC tunnel for total summed hadrons ($n+p+\pi^{\pm}$) above various energy cuts in the vicinity of the missing magnet for DS1 & DS5.

Neutron Fluence:Dose ratios in LHC tunnel at dipole magnet

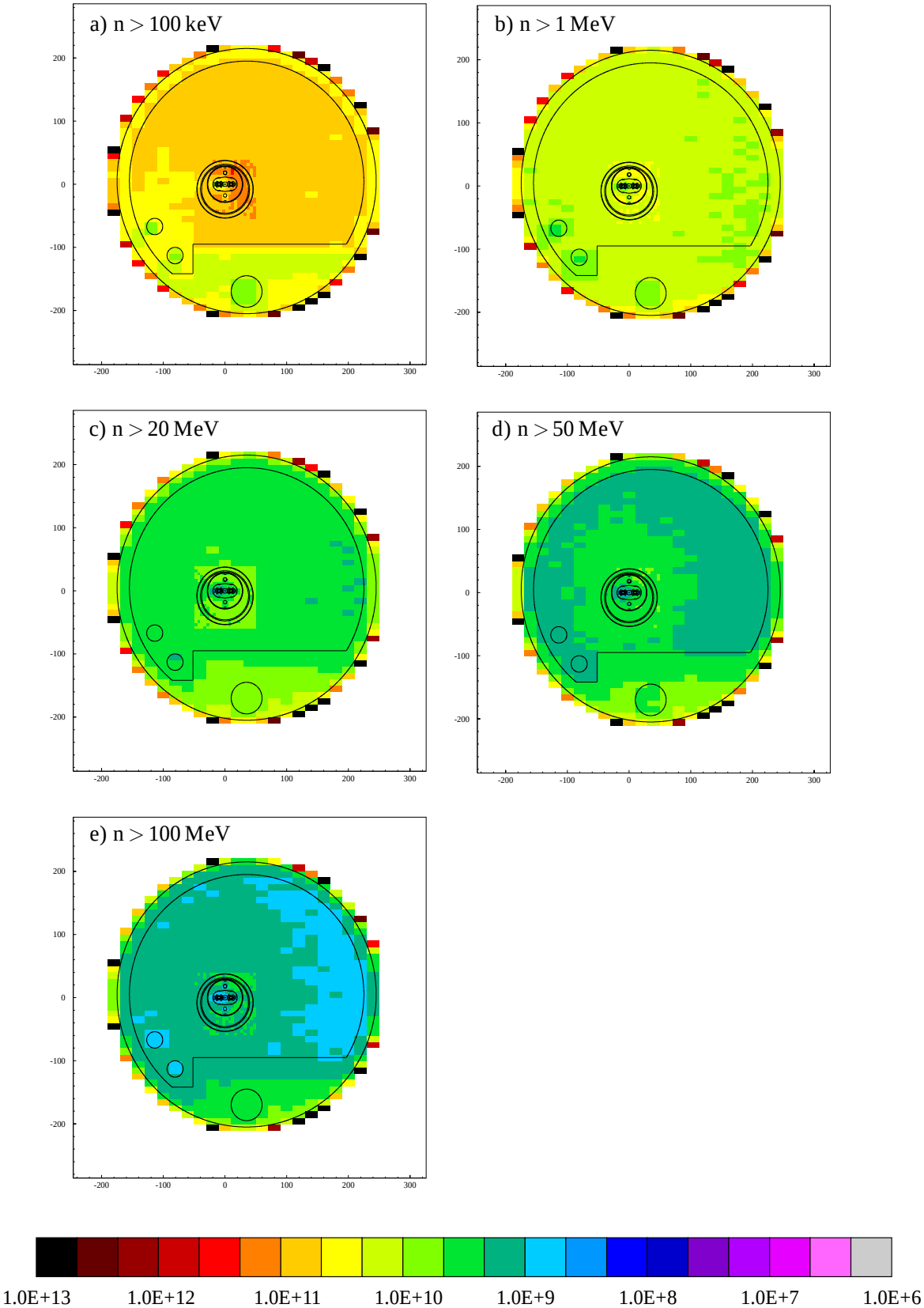

Figure 49: Radial fluence : dose distributions ($cm^{-2}Gy^{-1}$) in the LHC tunnel for neutrons above various energy cuts in the vicinity of a dipole magnet in DS1 & DS5. This cut is specifically of dipole magnet MB9A, but is equally valid for all dipole magnets in the DS region.

Hadron Fluence:Dose ratios in LHC tunnel at dipole magnet

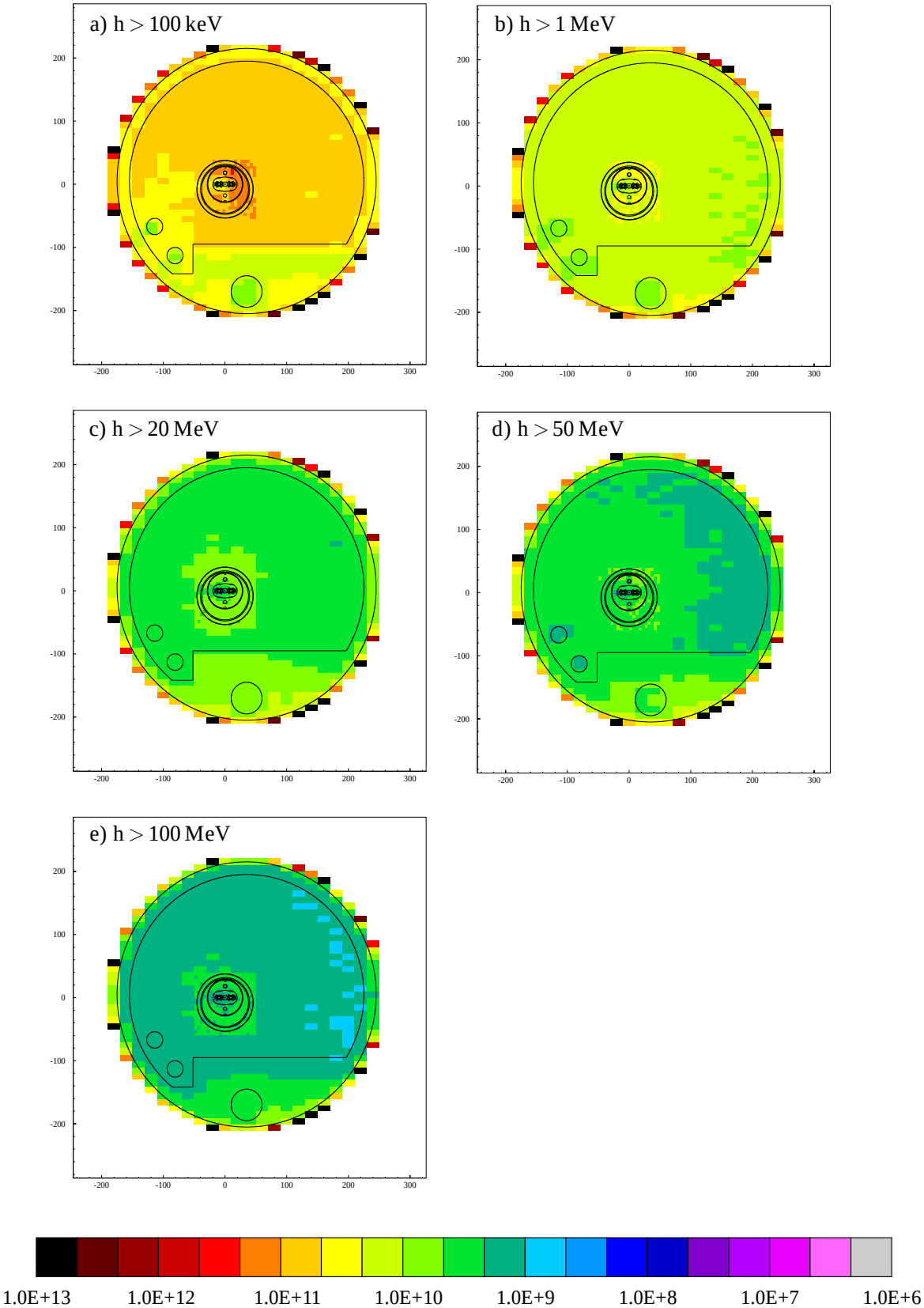

Figure 50: Radial fluence : dose distributions ($cm^{-2}Gy^{-1}$) in the LHC tunnel for total summed hadrons ($n+p+\pi^{\pm}$) above various energy cuts in the vicinity of a dipole magnet in DS1 & DS5. This cut is specifically of dipole magnet MB9A, but is equally valid for all dipole magnets in the DS region.

Neutron Fluence:Dose ratios in LHC tunnel at quadrupole magnet

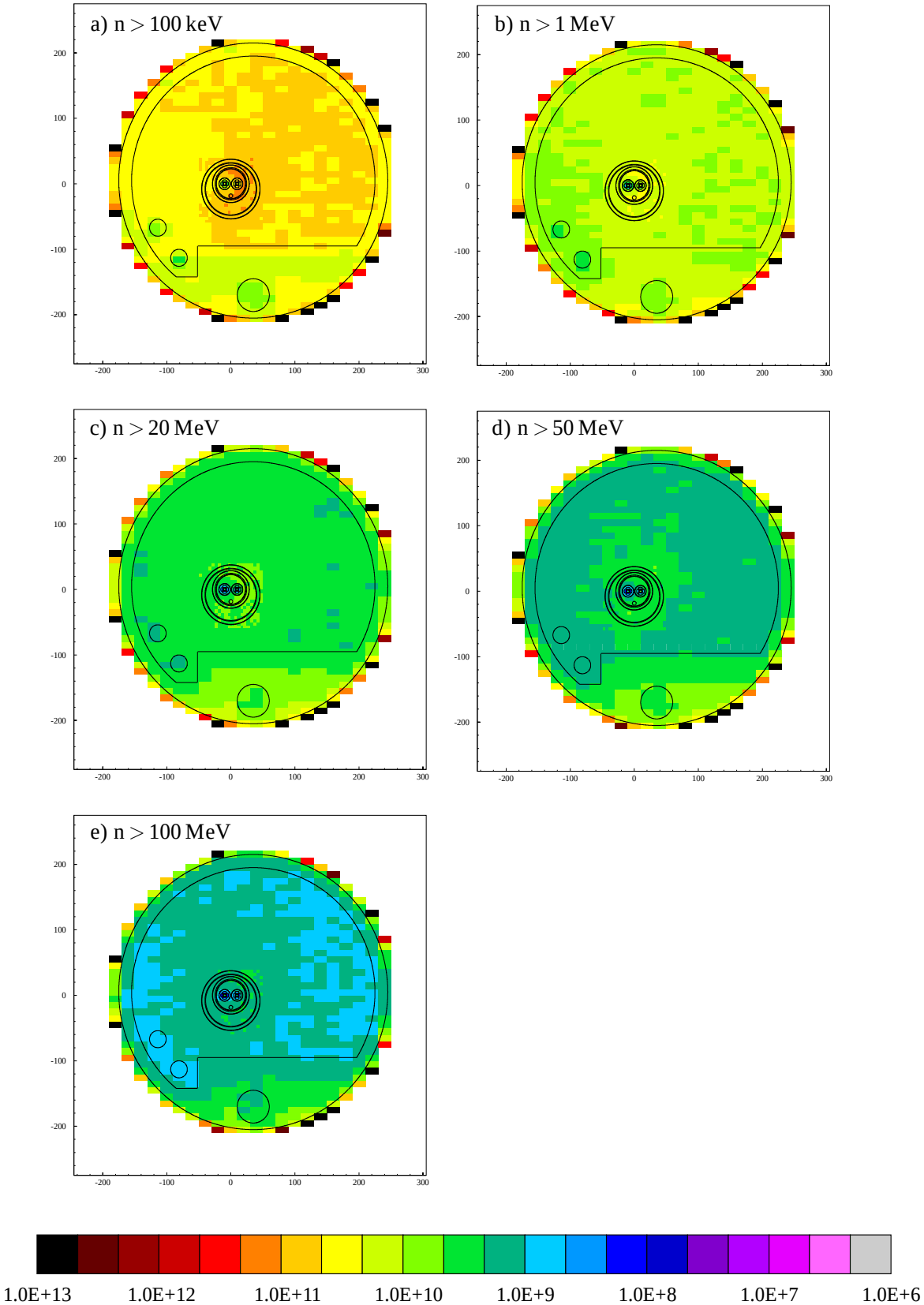

Figure 51: Radial fluence : dose distributions ($cm^{-2}Gy^{-1}$) in the LHC tunnel for neutrons above various energy cuts in the vicinity of a quadrupole magnet (not Q11) in DS1 & DS5. This cut is specifically of quadrupole magnet Q9, but is equally valid for all quadrupole magnets, excepting Q11, in the DS region.

Hadron Fluence:Dose ratios in LHC tunnel at quadrupole magnet

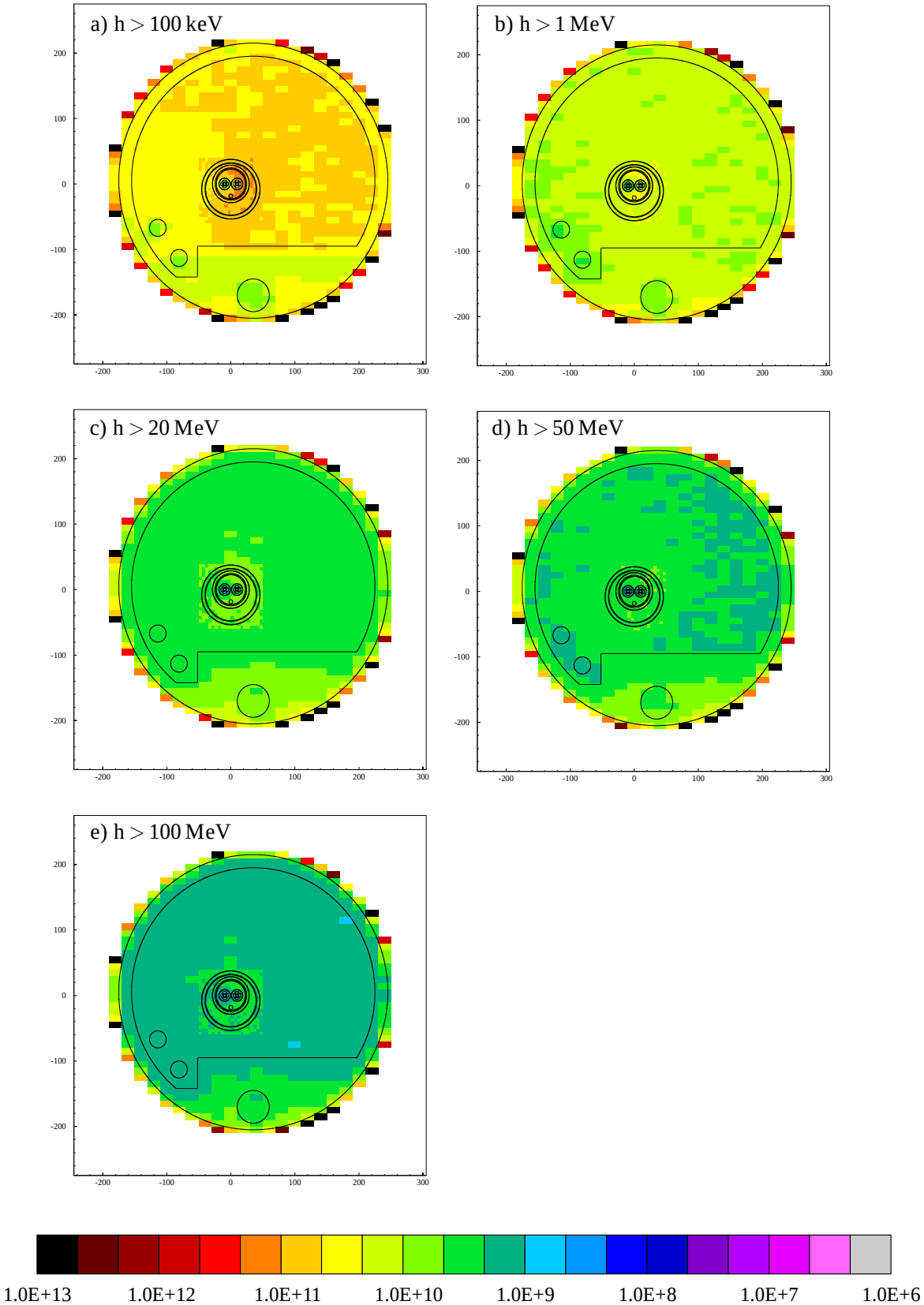

Figure 52: Radial fluence : dose distributions ($cm^{-2}Gy^{-1}$) in the LHC tunnel for total summed hadrons ($n+p+\pi^{\pm}$) above various energy cuts in the vicinity of a quadpole magnet (not Q11) in DS1 & DS5. This cut is specifically of quadrupole magnet Q9, but is equally valid for all quadrupole magnets, excepting Q11, in the DS region.

Neutron Fluence:Dose ratios in LHC tunnel at intermagnet gap

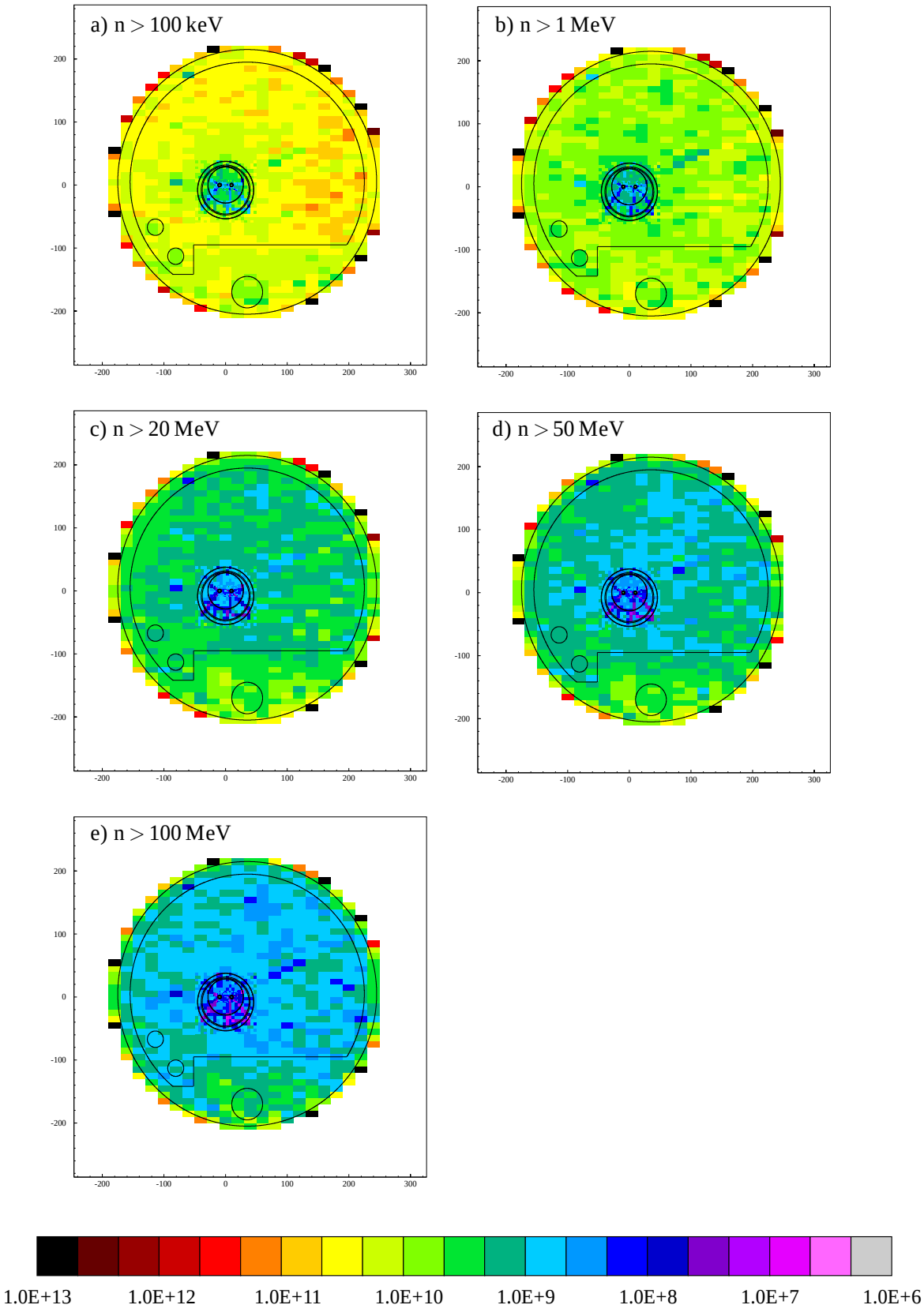

Figure 53: Radial fluence : dose distributions ($cm^{-2}Gy^{-1}$) in the LHC tunnel for neutrons above various energy cuts in the vicinity of an intermagnet gap (in region MB8B-MB11A) in DS1 & DS5.

Hadron Fluence:Dose ratios in LHC tunnel at intermagnet gap

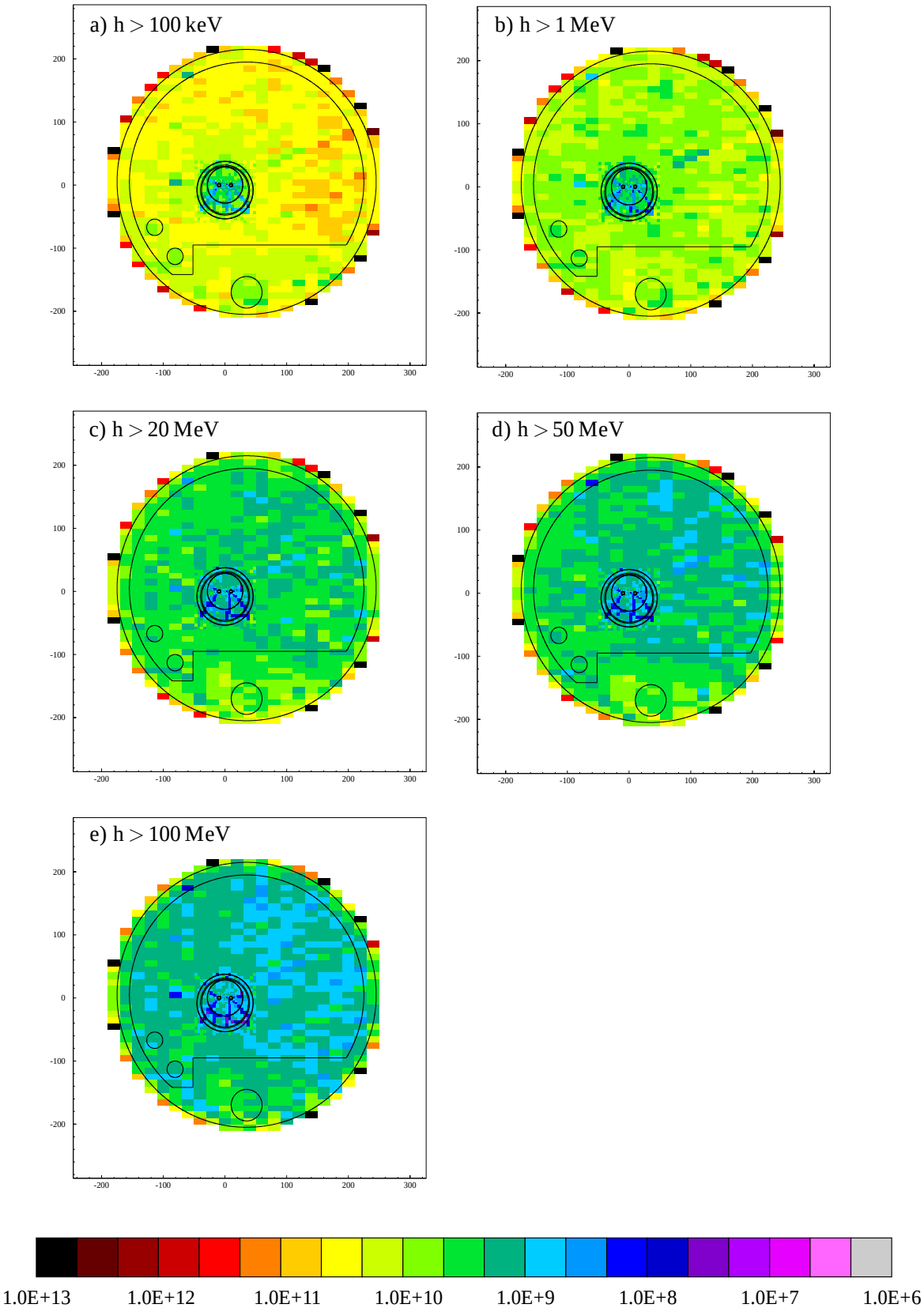

Figure 54: Radial fluence : dose distributions ($cm^{-2}Gy^{-1}$) in the LHC tunnel for total summed hadrons ($n+p+\pi^{\pm}$) above various energy cuts in the vicinity of an intermagnet gap (in region MB8B-MB11A) in DS1 & DS5.

Appendix B.3

Quantitative fluence : dose values
for the dispersion suppressors DS1 & DS5

Ecut = 100 keV

Position	Alongside	neutron	± %	sd %	proton	± %	sd %	pion +-	± %	sd %	hadron	± %	sd %
		cm^{-2} Gy^{-1}											
surface	Q11	1.2E+10	15.6	49.3	1.7E+08	13.1	41.5	4.4E+08	13.7	43.4	1.3E+10	15.3	48.5
cryostat	Missing	2.0E+09	10.8	51.9	1.5E+08	6.3	30.4	4.2E+08	6.3	30.0	2.5E+09	9.2	43.9
inner	Dipole	7.0E+10	7.5	19.8	2.4E+08	3.4	12.4	4.2E+08	6.6	17.4	7.1E+10	7.4	19.5
	Quadrupole	6.8E+10	13.6	24.7	3.0E+08	4.8	25.6	5.5E+08	10.7	23.3	6.9E+10	13.4	24.6
	Int.mag. Gap	2.2E+10	11.8	35.3	2.5E+08	8.8	26.5	4.3E+08	11.3	33.8	2.3E+10	11.6	34.7
surface	Q11	8.2E+09	10.6	33.6	1.7E+08	8.2	25.8	5.2E+08	9.1	28.7	8.9E+09	10.3	32.6
cryostat	Missing	7.7E+08	9.7	46.6	8.9E+07	8.1	38.7	2.9E+08	8.2	39.2	1.2E+09	8.4	40.3
outer	Dipole	5.2E+10	3.9	10.2	2.7E+08	5.4	14.3	7.0E+08	4.1	11.4	5.3E+10	3.8	10.1
	Quadrupole	4.0E+10	8.5	22.0	3.2E+08	9.4	24.6	7.7E+08	11.0	21.0	4.1E+10	8.5	21.8
	Int.mag. Gap	1.2E+10	15.3	45.8	2.1E+08	14.2	42.7	4.9E+08	15.2	45.5	1.3E+10	15.0	45.1
tunnel	Q11	1.2E+10	13.2	41.8	1.7E+08	14.5	45.9	3.1E+08	17.8	56.2	1.3E+10	13.3	41.9
wall	Missing	1.0E+10	15.6	74.9	1.9E+08	12.2	58.3	3.0E+08	11.7	56.1	1.1E+10	15.2	72.8
inner	Dipole	5.4E+10	3.4	9.7	1.4E+08	8.6	22.6	2.0E+08	8.4	22.3	5.4E+10	3.3	9.7
	Quadrupole	5.2E+10	10.7	17.9	1.5E+08	1.0	19.4	2.6E+08	10.0	22.5	5.2E+10	10.7	17.9
	Int.mag. Gap	5.5E+10	2.9	8.6	1.5E+08	9.0	26.9	2.3E+08	19.0	57.1	5.5E+10	2.9	8.7
tunnel	Q11	9.6E+09	10.6	33.4	1.7E+08	10.7	33.8	3.8E+08	12.1	38.4	1.0E+10	10.6	33.4
wall	Missing	2.7E+09	16.1	77.1	9.9E+07	10.8	52.0	1.9E+08	9.8	46.9	3.0E+09	15.2	72.7
outer	Dipole	5.1E+10	3.0	8.7	1.8E+08	5.3	16.0	4.5E+08	7.8	20.7	5.1E+10	2.9	8.7
	Quadrupole	4.2E+10	13.5	19.1	2.4E+08	8.4	25.6	5.4E+08	7.1	18.7	4.2E+10	13.4	18.9
	Int.mag. Gap	3.3E+10	10.2	30.7	2.1E+08	13.5	40.6	4.1E+08	13.6	40.7	3.4E+10	10.2	30.5
under	Q11	9.0E+09	11.0	34.8	1.5E+08	8.9	28.2	4.1E+08	8.9	28.0	9.6E+09	10.9	34.3
magnet	Missing	1.6E+09	11.4	54.8	9.7E+07	6.3	30.2	2.4E+08	7.0	33.3	1.9E+09	9.9	47.3
string	Dipole	5.9E+10	2.4	6.4	1.7E+08	4.8	12.6	2.7E+08	5.7	15.2	5.9E+10	2.4	6.3
	Quadrupole	5.3E+10	4.1	12.7	2.2E+08	4.7	11.7	4.4E+08	5.3	14.8	5.4E+10	4.0	12.6
	Int.mag. Gap	3.5E+10	9.0	26.9	2.2E+08	8.6	25.7	3.7E+08	8.0	24.0	3.6E+10	8.7	26.2
above	Q11	8.8E+09	5.7	17.9	1.4E+08	4.3	13.5	4.3E+08	4.6	14.6	9.4E+09	5.5	17.4
magnet	Missing	1.2E+09	13.9	66.5	7.0E+07	5.4	25.9	1.8E+08	5.4	25.7	1.5E+09	11.9	56.9
string	Dipole	6.6E+10	1.5	5.3	1.8E+08	5.7	15.1	3.0E+08	6.2	16.5	6.6E+10	1.5	5.2
50-100 cm	Quadrupole	5.2E+10	2.4	12.2	2.3E+08	7.1	11.1	4.6E+08	2.9	12.5	5.3E+10	2.4	12.1
	Int.mag. Gap	3.1E+10	10.0	29.9	2.1E+08	7.0	21.0	3.7E+08	7.9	23.6	3.2E+10	9.8	29.3
above	Q11	8.3E+09	3.1	9.7	1.4E+08	3.6	11.4	3.4E+08	4.9	15.6	8.8E+09	3.1	9.7
magnet	Missing	2.6E+09	14.6	70.2	9.5E+07	7.8	37.4	1.8E+08	6.5	31.3	2.8E+09	13.5	64.8
string	Dipole	6.1E+10	1.7	5.4	1.6E+08	7.9	20.8	2.5E+08	8.6	22.8	6.2E+10	1.7	5.4
100-150 cm	Quadrupole	5.0E+10	4.0	7.8	2.0E+08	1.5	9.9	4.0E+08	5.5	12.9	5.0E+10	4.0	7.8
	Int.mag. Gap	4.2E+10	7.2	21.5	1.7E+08	8.4	25.3	2.9E+08	8.1	24.4	4.3E+10	7.1	21.2
above	Q11	7.5E+09	3.7	11.8	1.2E+08	5.9	18.7	2.6E+08	5.7	18.0	7.9E+09	3.7	11.8
magnet	Missing	3.9E+09	14.4	69.2	1.1E+08	7.1	34.0	1.8E+08	6.2	29.9	4.2E+09	13.6	65.1
string	Dipole	6.0E+10	2.3	6.4	1.5E+08	9.2	24.4	2.2E+08	9.0	23.9	6.0E+10	2.2	6.3
150-180 cm	Quadrupole	5.0E+10	3.3	12.2	2.0E+08	2.0	14.0	3.5E+08	2.0	17.1	5.1E+10	3.2	12.2
	Int.mag. Gap	4.4E+10	8.5	25.4	1.7E+08	11.9	35.7	2.4E+08	10.6	31.9	4.4E+10	8.4	25.1
	Q11	9.5E+09			1.5E+08			3.9E+08			1.0E+10		
average	Missing	3.1E+09			1.1E+08			2.5E+08			3.5E+09		
ratio	Dipole	5.9E+10			1.9E+08			3.5E+08			6.0E+10		
	Quadrupole	5.1E+10			2.3E+08			4.7E+08			5.1E+10		
	Int.mag. Gap	3.4E+10			2.0E+08			3.5E+08			3.5E+10		
	max. uncertainty		16.1	77.1		14.5	58.3		19.0	57.1		15.3	72.8
	avg. uncertainty		8.5	29.2		7.6	26.3		8.6	27.8		8.2	27.8

Figure 55: Fluence:dose ratios for neutrons, protons, charged pions and total summed hadrons, above $E_{cut} >$ 100 keV. Values are presented at various positions in the LHC tunnel alongside the different magnet components (*i.e.* averaged over the length of the magnet elements). Since the ratio is relatively uniform in the vicinity of the dipole magnets, the value given for alongside a dipole is the average over all the dipole magnet elements in the dispersion suppressor. Similarly for the quadrupoles (excluding Q11 data) and the inter-magnet gap regions. The percentage error, ±%, is the standard error on the mean of this averaging. To give an idea of the spread in the averaged ratios, the error 'sd%' is the maximum of either the standard deviation obtained from averaging over the various magnet elements, or the combination of the individual standard deviation errors on the values being averaged over. The values 'average ratio' are obtained by averaging over the values at a given position in the LHC tunnel.

Ecut = **1 MeV**

Position	Alongside	neutron	± %	sd %	proton	± %	sd %	pion +-	± %	sd %	hadron	± %	sd %
		cm^{-2} Gy^{-1}											
surface	Q11	3.9E+09	13.5	42.7	1.7E+08	13.1	41.5	4.4E+08	13.7	43.3	4.5E+09	13.3	42.0
cryostat	Missing	1.1E+09	8.5	40.7	1.5E+08	6.4	30.5	4.2E+08	6.3	30.0	1.7E+09	7.1	33.9
inner	Dipole	1.7E+10	4.3	11.4	2.4E+08	3.4	12.4	4.2E+08	6.6	17.4	1.7E+10	4.0	10.7
	Quadrupole	1.6E+10	12.0	23.1	3.0E+08	4.8	25.6	5.5E+08	10.7	23.3	1.7E+10	11.1	22.9
	Int.mag. Gap	7.0E+09	10.5	31.6	2.5E+08	9.0	26.9	4.3E+08	11.3	33.8	7.6E+09	10.1	30.3
surface	Q11	3.2E+09	8.7	27.7	1.7E+08	8.1	25.7	5.2E+08	9.1	28.7	3.9E+09	8.5	26.9
cryostat	Missing	4.9E+08	8.5	40.8	8.9E+07	8.1	38.8	2.9E+08	8.2	39.2	8.8E+08	7.8	37.3
outer	Dipole	1.5E+10	2.9	8.7	2.7E+08	5.4	14.3	7.0E+08	4.1	11.4	1.6E+10	2.9	8.5
	Quadrupole	1.3E+10	7.8	21.0	3.2E+08	9.4	24.6	7.7E+08	11.0	21.0	1.4E+10	8.0	20.3
	Int.mag. Gap	4.4E+09	14.2	42.5	2.1E+08	14.2	42.7	4.9E+08	15.2	45.5	5.1E+09	14.0	42.0
tunnel	Q11	3.9E+09	13.5	42.6	1.7E+08	14.6	46.1	3.1E+08	17.8	56.2	4.3E+09	13.5	42.7
wall	Missing	4.2E+09	13.1	63.0	1.9E+08	12.2	58.3	3.0E+08	11.7	56.1	4.7E+09	12.6	60.2
inner	Dipole	1.1E+10	2.2	9.8	1.4E+08	8.5	22.6	2.0E+08	8.4	22.3	1.1E+10	2.2	9.8
	Quadrupole	1.1E+10	10.9	18.4	1.5E+08	0.9	19.7	2.6E+08	10.0	22.5	1.1E+10	10.6	18.2
	Int.mag. Gap	1.2E+10	4.5	13.4	1.5E+08	9.0	26.9	2.3E+08	19.0	57.1	1.2E+10	4.6	13.8
tunnel	Q11	3.4E+09	10.7	33.7	1.7E+08	10.6	33.5	3.8E+08	12.1	38.4	4.0E+09	10.6	33.6
wall	Missing	1.3E+09	14.0	67.0	9.9E+07	10.9	52.1	1.9E+08	9.8	46.9	1.6E+09	12.9	61.6
outer	Dipole	1.2E+10	1.9	8.8	1.8E+08	5.3	16.0	4.5E+08	7.8	20.7	1.3E+10	1.7	8.7
	Quadrupole	1.1E+10	11.9	16.8	2.4E+08	8.4	25.6	5.4E+08	7.1	18.7	1.2E+10	11.6	16.4
	Int.mag. Gap	9.1E+09	10.0	30.1	2.1E+08	13.5	40.5	4.1E+08	13.6	40.7	9.7E+09	9.9	29.6
under	Q11	3.1E+09	8.7	27.6	1.5E+08	8.9	28.1	4.1E+08	8.9	28.0	3.6E+09	8.6	27.3
magnet	Missing	8.8E+08	9.2	44.0	9.7E+07	6.3	30.2	2.4E+08	7.0	33.3	1.2E+09	7.6	36.6
string	Dipole	1.4E+10	2.4	6.2	1.7E+08	4.8	12.6	2.7E+08	5.7	15.2	1.4E+10	2.3	6.2
	Quadrupole	1.3E+10	2.6	11.4	2.2E+08	4.7	11.7	4.4E+08	5.3	14.9	1.4E+10	2.6	11.0
	Int.mag. Gap	1.0E+10	7.2	21.5	2.2E+08	8.6	25.7	3.7E+08	7.9	23.8	1.1E+10	6.6	19.8
above	Q11	3.0E+09	3.7	11.7	1.4E+08	4.3	13.5	4.3E+08	4.6	14.6	3.6E+09	3.4	10.6
magnet	Missing	6.2E+08	10.8	51.7	7.0E+07	5.4	25.9	1.8E+08	5.4	25.7	8.7E+08	8.5	40.9
string	Dipole	1.5E+10	1.5	5.3	1.8E+08	5.7	15.1	3.0E+08	6.2	16.5	1.5E+10	1.6	5.1
50-100 cm	Quadrupole	1.3E+10	1.5	11.0	2.3E+08	7.1	11.1	4.6E+08	2.9	12.5	1.4E+10	1.6	10.5
	Int.mag. Gap	9.0E+09	8.1	24.3	2.1E+08	7.0	21.0	3.7E+08	7.9	23.6	9.5E+09	7.7	23.1
above	Q11	2.9E+09	3.9	12.2	1.4E+08	3.6	11.4	3.4E+08	4.9	15.6	3.3E+09	3.5	11.2
magnet	Missing	1.2E+09	11.7	56.1	9.5E+07	7.8	37.4	1.8E+08	6.5	31.3	1.4E+09	10.2	49.1
string	Dipole	1.3E+10	1.4	5.2	1.6E+08	7.9	20.8	2.5E+08	8.6	22.8	1.3E+10	1.4	5.0
100-150 cm	Quadrupole	1.2E+10	3.0	7.3	2.0E+08	1.5	9.9	4.0E+08	5.5	12.9	1.3E+10	3.0	7.3
	Int.mag. Gap	1.0E+10	6.3	19.0	1.7E+08	8.4	25.3	2.9E+08	8.1	24.4	1.1E+10	6.1	18.3
above	Q11	2.5E+09	4.0	12.6	1.2E+08	5.9	18.8	2.6E+08	5.7	18.0	2.9E+09	3.9	12.4
magnet	Missing	1.7E+09	11.1	53.2	1.1E+08	7.1	34.0	1.8E+08	6.2	29.9	2.0E+09	9.9	47.5
string	Dipole	1.2E+10	1.9	6.3	1.5E+08	9.3	24.5	2.2E+08	9.0	23.9	1.3E+10	1.9	6.2
150-180 cm	Quadrupole	1.2E+10	1.8	11.7	2.0E+08	2.0	14.0	3.5E+08	2.0	17.1	1.2E+10	1.8	11.8
	Int.mag. Gap	1.0E+10	8.9	26.6	1.7E+08	11.9	35.7	2.4E+08	10.7	32.0	1.1E+10	8.6	25.9
	Q11	3.2E+09			1.5E+08			3.9E+08			3.8E+09		
average	Missing	1.4E+09			1.1E+08			2.5E+08			1.8E+09		
ratio	Dipole	1.4E+10			1.9E+08			3.5E+08			1.4E+10		
	Quadrupole	1.3E+10			2.3E+08			4.7E+08			1.3E+10		
	Int.mag. Gap	9.0E+09			2.0E+08			3.5E+08			9.6E+09		
	max. uncertainty		14.2	67.0		14.6	58.3		19.0	57.1		14.0	61.6
	avg. uncertainty		7.3	25.5		7.6	26.3		8.6	27.8		7.1	23.9

Figure 56: Fluence:dose ratios for neutrons, protons, charged pions and total summed hadrons, above $E_{cut} > 1$ MeV. Values are presented at various positions in the LHC tunnel alongside the different magnet components (*i.e.* averaged over the length of the magnet elements). Since the ratio is relatively uniform in the vicinity of the dipole magnets, the value given for alongside a dipole is the average over all the dipole magnet elements in the dispersion suppressor. Similarly for the quadrupoles (excluding Q11 data) and the inter-magnet gap regions. The percentage error, ±%, is the standard error on the mean of this averaging. To give an idea of the spread in the averaged ratios, the error 'sd%' is the maximum of either the standard deviation obtained from averaging over the various magnet elements, or the combination of the individual standard deviation errors on the values being averaged over. The values 'average ratio' are obtained by averaging over the values at a given position in the LHC tunnel.

Ecut = **20 MeV**

Position	Alongside	neutron	± %	sd %	proton	± %	sd %	pion +-	± %	sd %	hadron	± %	sd %
		cm^{-2} Gy^{-1}											
surface	Q11	1.2E+09	13.1	41.4	1.6E+08	13.3	41.9	4.4E+08	13.7	43.2	1.8E+09	12.8	40.5
cryostat	Missing	4.1E+08	8.7	41.6	1.5E+08	6.5	31.4	4.2E+08	6.3	30.0	9.8E+08	6.2	29.9
inner	Dipole	4.8E+09	5.2	13.8	2.3E+08	3.6	12.5	4.1E+08	6.6	17.4	5.4E+09	4.2	11.2
	Quadrupole	4.5E+09	12.1	24.7	2.8E+08	5.7	26.5	5.5E+08	10.7	23.3	5.4E+09	9.2	23.9
	Int.mag. Gap	1.8E+09	10.0	30.0	2.4E+08	8.8	26.3	4.2E+08	11.3	33.8	2.4E+09	8.9	26.5
surface	Q11	9.7E+08	7.8	24.8	1.7E+08	8.2	25.8	5.2E+08	9.1	28.7	1.7E+09	7.8	24.5
cryostat	Missing	2.0E+08	8.0	38.2	8.8E+07	8.1	38.8	2.9E+08	8.2	39.1	5.8E+08	7.6	36.6
outer	Dipole	4.3E+09	3.1	8.9	2.6E+08	5.3	14.1	6.9E+08	4.1	11.5	5.2E+09	3.1	8.5
	Quadrupole	3.5E+09	5.9	20.4	3.1E+08	9.3	24.4	7.7E+08	11.0	21.1	4.5E+09	7.0	18.9
	Int.mag. Gap	1.2E+09	13.4	40.2	2.0E+08	14.2	42.6	4.8E+08	15.2	45.5	1.9E+09	13.6	40.8
tunnel	Q11	1.0E+09	13.5	42.7	1.6E+08	14.5	45.9	3.1E+08	17.8	56.3	1.5E+09	14.1	44.4
wall	Missing	1.0E+09	12.3	58.8	1.9E+08	12.4	59.4	3.0E+08	11.7	56.2	1.5E+09	11.1	53.1
inner	Dipole	2.4E+09	2.7	10.3	1.3E+08	8.9	23.5	2.0E+08	8.5	22.6	2.7E+09	3.0	10.2
	Quadrupole	2.3E+09	6.8	21.0	1.5E+08	1.7	19.9	2.5E+08	10.2	22.7	2.7E+09	5.8	19.3
	Int.mag. Gap	2.4E+09	4.2	12.7	1.4E+08	8.9	26.7	2.2E+08	19.4	58.3	2.8E+09	4.7	14.0
tunnel	Q11	9.4E+08	11.4	36.0	1.6E+08	10.7	33.7	3.8E+08	12.1	38.4	1.5E+09	11.3	35.6
wall	Missing	4.0E+08	12.3	59.2	9.7E+07	10.9	52.2	1.9E+08	9.8	47.2	6.9E+08	10.9	52.3
outer	Dipole	3.0E+09	2.6	9.1	1.7E+08	5.5	16.1	4.5E+08	7.9	20.8	3.6E+09	2.7	9.0
	Quadrupole	2.6E+09	7.9	16.4	2.4E+08	8.9	26.3	5.3E+08	7.1	18.9	3.4E+09	7.8	16.2
	Int.mag. Gap	2.3E+09	8.3	25.0	2.0E+08	12.7	38.1	4.1E+08	13.7	41.0	2.9E+09	8.6	25.8
under	Q11	9.4E+08	9.2	28.9	1.4E+08	9.0	28.4	4.1E+08	8.9	28.0	1.5E+09	8.9	28.2
magnet	Missing	3.0E+08	8.5	40.9	9.4E+07	6.3	30.1	2.3E+08	6.9	33.3	6.3E+08	6.6	31.5
string	Dipole	3.8E+09	2.6	6.9	1.6E+08	5.0	13.2	2.7E+08	5.7	15.1	4.3E+09	2.7	7.2
	Quadrupole	3.3E+09	0.7	11.1	2.1E+08	4.7	11.4	4.4E+08	5.2	15.1	4.0E+09	1.1	10.2
	Int.mag. Gap	2.4E+09	7.4	22.1	2.1E+08	8.5	25.4	3.6E+08	8.2	24.5	3.0E+09	5.6	16.8
above	Q11	9.3E+08	3.5	11.1	1.4E+08	4.3	13.7	4.3E+08	4.7	14.8	1.5E+09	3.1	9.9
magnet	Missing	2.2E+08	10.3	49.6	6.8E+07	5.4	25.8	1.8E+08	5.4	25.7	4.6E+08	6.7	32.3
string	Dipole	4.1E+09	1.8	5.4	1.8E+08	5.8	15.2	2.9E+08	6.3	16.7	4.6E+09	2.1	5.6
50-100 cm	Quadrupole	3.5E+09	0.5	9.9	2.2E+08	7.1	11.7	4.5E+08	3.0	12.6	4.2E+09	0.8	8.7
	Int.mag. Gap	2.3E+09	8.0	24.0	2.1E+08	7.1	21.4	3.6E+08	7.8	23.3	2.8E+09	6.7	20.2
above	Q11	8.4E+08	2.9	9.3	1.3E+08	3.6	11.4	3.4E+08	4.9	15.6	1.3E+09	3.1	9.8
magnet	Missing	3.5E+08	11.7	55.9	9.2E+07	7.8	37.4	1.8E+08	6.5	31.2	6.2E+08	8.6	41.1
string	Dipole	3.2E+09	1.7	5.4	1.6E+08	8.3	22.0	2.5E+08	8.7	23.0	3.6E+09	2.3	6.0
100-150 cm	Quadrupole	2.9E+09	3.0	7.5	2.0E+08	1.8	9.9	4.0E+08	5.8	12.9	3.5E+09	3.1	7.5
	Int.mag. Gap	2.4E+09	6.5	19.4	1.7E+08	8.8	26.4	2.8E+08	8.3	25.0	2.9E+09	5.9	17.6
above	Q11	7.1E+08	4.8	15.3	1.1E+08	6.0	18.9	2.6E+08	5.8	18.2	1.1E+09	5.0	15.8
magnet	Missing	4.9E+08	10.4	49.7	1.1E+08	7.1	33.9	1.8E+08	6.3	30.0	7.7E+08	8.0	38.2
string	Dipole	2.9E+09	2.3	6.3	1.4E+08	9.8	25.8	2.2E+08	9.1	24.1	3.2E+09	2.8	7.4
150-180cm	Quadrupole	2.7E+09	3.0	12.0	1.9E+08	2.4	14.0	3.4E+08	2.2	17.1	3.2E+09	2.9	12.2
	Int.mag. Gap	2.3E+09	7.9	23.8	1.6E+08	12.5	37.6	2.4E+08	10.6	31.8	2.7E+09	7.5	22.6
	Q11	9.5E+08			1.5E+08			3.8E+08			1.5E+09		
average	Missing	4.2E+08			1.1E+08			2.5E+08			7.8E+08		
ratio	Dipole	3.6E+09			1.8E+08			3.5E+08			4.1E+09		
	Quadrupole	3.2E+09			2.2E+08			4.7E+08			3.9E+09		
	Int.mag. Gap	2.1E+09			1.9E+08			3.5E+08			2.8E+09		
	max. uncertainty		13.5	59.2		14.5	59.4		19.4	58.3		14.1	53.1
	avg. uncertainty		6.9	24.8		7.7	26.5		8.6	27.9		6.4	22.2

Figure 57: Fluence:dose ratios for neutrons, protons, charged pions and total summed hadrons, above $E_{cut} > 20$ MeV. Values are presented at various positions in the LHC tunnel alongside the different magnet components (*i.e.* averaged over the length of the magnet elements). Since the ratio is relatively uniform in the vicinity of the dipole magnets, the value given for alongside a dipole is the average over all the dipole magnet elements in the dispersion suppressor. Similarly for the quadrupoles (excluding Q11 data) and the inter-magnet gap regions. The percentage error, ±%, is the standard error on the mean of this averaging. To give an idea of the spread in the averaged ratios, the error 'sd%' is the maximum of either the standard deviation obtained from averaging over the various magnet elements, or the combination of the individual standard deviation errors on the values being averaged over. The values 'average ratio' are obtained by averaging over the values at a given position in the LHC tunnel.

Ecut = **50 MeV**

Position	Alongside	neutron	± %	sd %	proton	± %	sd %	pion +-	± %	sd %	hadron	± %	sd %
		cm^{-2} Gy^{-1}											
surface	Q11	8.4E+08	13.0	40.9	1.4E+08	13.6	43.1	4.3E+08	13.8	43.5	1.4E+09	12.6	39.8
cryostat	Missing	3.2E+08	8.4	40.4	1.4E+08	6.6	31.7	4.1E+08	6.3	30.1	8.7E+08	6.1	29.0
inner	Dipole	3.3E+09	5.4	14.2	2.1E+08	4.1	12.8	3.9E+08	6.7	17.8	3.8E+09	4.0	10.5
	Quadrupole	3.1E+09	10.9	25.5	2.5E+08	5.4	28.2	5.3E+08	11.7	22.6	3.9E+09	7.4	24.1
	Int.mag. Gap	1.2E+09	9.7	29.1	2.1E+08	8.2	24.5	3.9E+08	11.2	33.6	1.8E+09	8.7	26.0
surface	Q11	6.8E+08	8.0	25.3	1.6E+08	8.3	26.3	5.1E+08	9.2	29.1	1.3E+09	8.0	25.2
cryostat	Missing	1.5E+08	7.8	37.6	8.2E+07	8.0	38.5	2.9E+08	8.2	39.2	5.3E+08	7.7	36.7
outer	Dipole	2.9E+09	3.1	8.9	2.3E+08	5.1	14.0	6.7E+08	4.2	11.5	3.8E+09	3.0	8.5
	Quadrupole	2.3E+09	5.5	20.1	2.9E+08	10.7	24.7	7.4E+08	11.2	21.2	3.4E+09	7.1	18.8
	Int.mag. Gap	8.4E+08	13.9	41.7	1.8E+08	14.5	43.4	4.6E+08	15.2	45.5	1.5E+09	14.0	42.1
tunnel	Q11	7.0E+08	12.8	40.5	1.5E+08	14.6	46.1	3.0E+08	18.1	57.3	1.1E+09	13.9	43.8
wall	Missing	6.5E+08	12.8	61.4	1.7E+08	13.3	63.6	2.8E+08	11.9	56.9	1.1E+09	11.3	54.2
inner	Dipole	1.5E+09	2.5	10.5	1.1E+08	9.8	25.8	1.9E+08	8.5	22.5	1.8E+09	3.1	10.3
	Quadrupole	1.4E+09	7.3	19.1	1.3E+08	2.9	18.8	2.4E+08	9.1	21.4	1.8E+09	5.2	17.4
	Int.mag. Gap	1.5E+09	5.5	16.4	1.3E+08	9.5	28.4	2.1E+08	20.1	60.2	1.8E+09	5.6	16.7
tunnel	Q11	6.1E+08	11.5	36.3	1.5E+08	10.5	33.3	3.7E+08	12.2	38.6	1.1E+09	11.3	35.7
wall	Missing	2.7E+08	12.5	59.7	8.7E+07	10.8	51.9	1.8E+08	9.7	46.7	5.5E+08	10.7	51.1
outer	Dipole	1.9E+09	3.0	9.4	1.5E+08	6.0	16.3	4.3E+08	7.9	20.9	2.5E+09	3.2	9.2
	Quadrupole	1.6E+09	5.7	17.9	2.1E+08	11.0	27.5	5.2E+08	7.1	19.2	2.4E+09	6.3	17.0
	Int.mag. Gap	1.4E+09	9.6	28.8	1.6E+08	14.1	42.3	3.9E+08	14.1	42.2	2.0E+09	9.5	28.6
under	Q11	6.5E+08	9.2	29.0	1.3E+08	8.8	28.0	4.0E+08	8.9	28.2	1.2E+09	8.9	28.3
magnet	Missing	2.2E+08	8.2	39.5	8.7E+07	6.3	30.3	2.3E+08	7.0	33.6	5.3E+08	6.4	30.5
string	Dipole	2.6E+09	2.4	6.3	1.4E+08	4.9	12.9	2.5E+08	5.8	15.4	2.9E+09	2.6	7.0
	Quadrupole	2.2E+09	0.5	10.8	1.9E+08	7.1	10.0	4.2E+08	4.9	15.5	2.8E+09	0.3	9.6
	Int.mag. Gap	1.6E+09	7.1	21.2	1.9E+08	8.1	24.2	3.3E+08	8.4	25.1	2.1E+09	5.0	15.1
above	Q11	6.6E+08	3.3	10.4	1.3E+08	4.3	13.6	4.2E+08	4.8	15.0	1.2E+09	3.2	10.3
magnet	Missing	1.6E+08	10.4	50.0	6.3E+07	5.2	25.0	1.7E+08	5.4	25.7	3.9E+08	6.4	30.6
string	Dipole	2.8E+09	2.0	5.4	1.5E+08	6.3	16.6	2.8E+08	6.6	17.5	3.2E+09	2.5	6.5
50-100 cm	Quadrupole	2.4E+09	0.3	10.5	2.0E+08	7.2	12.7	4.4E+08	3.3	13.1	3.0E+09	1.0	8.9
	Int.mag. Gap	1.5E+09	7.7	23.2	1.8E+08	6.7	20.2	3.4E+08	7.9	23.8	2.0E+09	6.4	19.1
above	Q11	5.9E+08	3.1	9.8	1.2E+08	3.7	11.8	3.3E+08	5.0	15.8	1.0E+09	3.5	11.1
magnet	Missing	2.4E+08	11.3	54.4	8.3E+07	7.8	37.5	1.7E+08	6.5	31.2	5.0E+08	7.9	37.8
string	Dipole	2.1E+09	1.9	5.4	1.4E+08	8.9	23.5	2.4E+08	9.1	24.0	2.5E+09	2.8	7.3
100-150 cm	Quadrupole	1.9E+09	3.4	7.9	1.7E+08	2.1	11.7	3.9E+08	6.6	13.2	2.5E+09	3.4	8.2
	Int.mag. Gap	1.6E+09	6.6	19.8	1.4E+08	8.9	26.7	2.7E+08	8.8	26.3	2.0E+09	6.0	17.9
above	Q11	4.9E+08	5.7	18.0	1.0E+08	6.4	20.3	2.5E+08	5.8	18.3	8.4E+08	5.7	17.9
magnet	Missing	3.2E+08	10.7	51.5	9.5E+07	7.2	34.7	1.7E+08	6.3	30.0	5.8E+08	7.7	36.7
string	Dipole	1.9E+09	2.3	6.5	1.2E+08	10.0	26.6	2.1E+08	9.3	24.7	2.2E+09	3.1	8.1
150-180 cm	Quadrupole	1.7E+09	3.2	12.9	1.7E+08	2.5	15.4	3.3E+08	2.5	17.5	2.2E+09	2.9	13.0
	Int.mag. Gap	1.5E+09	8.1	24.2	1.4E+08	13.1	39.4	2.3E+08	10.8	32.5	1.8E+09	7.5	22.4
	Q11	6.5E+08			1.4E+08			3.8E+08			1.2E+09		
average	Missing	2.9E+08			1.0E+08			2.4E+08			6.3E+08		
ratio	Dipole	2.4E+09			1.6E+08			3.3E+08			2.9E+09		
	Quadrupole	2.1E+09			2.0E+08			4.5E+08			2.7E+09		
	Int.mag. Gap	1.4E+09			1.7E+08			3.3E+08			1.9E+09		
	max. uncertainty		13.9	61.4		14.6	63.6		20.1	60.2		14.0	54.2
	avg. uncertainty		6.9	25.0		8.1	26.3		8.8	28.2		6.3	22.3

Figure 58: Fluence:dose ratios for neutrons, protons, charged pions and total summed hadrons, above $E_{cut} > 50$ MeV. Values are presented at various positions in the LHC tunnel alongside the different magnet components (*i.e.* averaged over the length of the magnet elements). Since the ratio is relatively uniform in the vicinity of the dipole magnets, the value given for alongside a dipole is the average over all the dipole magnet elements in the dispersion suppressor. Similarly for the quadrupoles (excluding Q11 data) and the inter-magnet gap regions. The percentage error, ±%, is the standard error on the mean of this averaging. To give an idea of the spread in the averaged ratios, the error 'sd%' is the maximum of either the standard deviation obtained from averaging over the various magnet elements, or the combination of the individual standard deviation errors on the values being averaged over. The values 'average ratio' are obtained by averaging over the values at a given position in the LHC tunnel.

Ecut = 100 MeV

Position	Alongside	neutron	± %	sd %	proton	± %	sd %	pion +-	± %	sd %	hadron	± %	sd %
		cm^{-2} Gy^{-1}											
surface	Q11	5.2E+08	12.9	40.7	1.2E+08	13.3	42.2	4.1E+08	13.8	43.8	1.1E+09	11.9	37.7
cryostat	Missing	2.3E+08	8.2	39.4	1.2E+08	6.9	33.0	4.0E+08	6.3	30.0	7.5E+08	6.0	28.6
inner	Dipole	1.9E+09	5.5	14.5	1.6E+08	4.1	13.6	3.6E+08	7.1	18.9	2.4E+09	3.4	9.0
	Quadrupole	1.9E+09	6.9	26.0	2.0E+08	4.5	30.6	4.8E+08	12.0	23.4	2.6E+09	3.6	23.7
	Int.mag. Gap	7.2E+08	10.1	30.4	1.6E+08	8.4	25.2	3.6E+08	12.0	36.1	1.2E+09	8.6	25.7
surface	Q11	4.2E+08	7.7	24.3	1.4E+08	9.0	28.6	4.9E+08	9.1	28.8	1.1E+09	8.0	25.4
cryostat	Missing	1.1E+08	7.6	36.3	7.1E+07	8.4	40.2	2.8E+08	8.2	39.1	4.7E+08	7.7	36.7
outer	Dipole	1.7E+09	2.9	7.6	1.9E+08	5.8	15.4	6.3E+08	4.3	11.5	2.5E+09	3.0	8.5
	Quadrupole	1.4E+09	4.2	21.1	2.4E+08	10.9	26.1	6.9E+08	11.2	20.5	2.3E+09	6.9	19.1
	Int.mag. Gap	5.1E+08	14.4	43.2	1.4E+08	14.8	44.5	4.3E+08	15.0	45.0	1.1E+09	14.1	42.2
tunnel	Q11	4.2E+08	13.8	43.6	1.2E+08	16.2	51.2	2.8E+08	17.7	55.9	8.2E+08	14.8	46.8
wall	Missing	3.4E+08	13.1	63.0	1.3E+08	13.6	65.3	2.5E+08	12.3	59.2	7.2E+08	11.3	54.0
inner	Dipole	8.3E+08	2.9	11.3	8.7E+07	10.0	26.6	1.7E+08	9.0	23.8	1.1E+09	3.6	11.0
	Quadrupole	8.2E+08	5.8	19.0	9.8E+07	7.6	20.6	2.1E+08	9.0	23.4	1.1E+09	2.6	17.1
	Int.mag. Gap	8.7E+08	7.8	23.5	1.1E+08	10.5	31.5	1.9E+08	21.4	64.2	1.2E+09	7.4	22.2
tunnel	Q11	3.6E+08	12.6	39.8	1.3E+08	10.9	34.6	3.6E+08	12.4	39.2	8.4E+08	11.8	37.5
wall	Missing	1.7E+08	13.0	62.2	6.9E+07	10.6	50.9	1.7E+08	10.0	47.9	4.1E+08	10.5	50.4
outer	Dipole	1.1E+09	4.4	11.7	1.2E+08	6.6	17.6	4.0E+08	8.3	21.9	1.6E+09	4.6	12.2
	Quadrupole	8.8E+08	3.5	18.5	1.7E+08	10.9	34.1	4.9E+08	7.1	18.8	1.5E+09	4.6	17.4
	Int.mag. Gap	8.3E+08	10.3	30.9	1.2E+08	13.2	39.5	3.5E+08	15.3	45.9	1.3E+09	10.2	30.6
under	Q11	4.1E+08	8.9	28.2	1.1E+08	8.7	27.6	3.9E+08	9.0	28.5	9.1E+08	8.8	27.8
magnet	Missing	1.4E+08	8.3	39.7	7.2E+07	6.4	30.5	2.2E+08	7.1	34.1	4.3E+08	6.4	30.6
string	Dipole	1.4E+09	2.4	6.3	1.1E+08	5.7	15.2	2.3E+08	6.3	16.6	1.8E+09	2.9	7.7
	Quadrupole	1.3E+09	1.5	11.3	1.5E+08	10.2	14.5	3.8E+08	4.6	17.1	1.8E+09	0.6	10.4
	Int.mag. Gap	9.1E+08	7.9	23.7	1.4E+08	8.3	25.0	2.9E+08	9.5	28.4	1.3E+09	5.4	16.3
above	Q11	4.2E+08	3.2	10.0	1.1E+08	4.6	14.7	4.1E+08	4.9	15.6	9.4E+08	3.6	11.5
magnet	Missing	1.1E+08	9.8	47.2	5.3E+07	4.8	23.0	1.7E+08	5.4	25.7	3.3E+08	5.7	27.4
string	Dipole	1.6E+09	2.4	6.4	1.2E+08	6.4	16.8	2.5E+08	6.9	18.3	1.9E+09	3.1	8.1
50-100 cm	Quadrupole	1.4E+09	0.9	11.0	1.6E+08	6.4	13.9	4.0E+08	3.2	13.8	1.9E+09	0.9	9.3
	Int.mag. Gap	8.7E+08	7.5	22.6	1.3E+08	8.3	25.0	3.0E+08	7.9	23.7	1.3E+09	6.3	19.0
above	Q11	3.7E+08	4.3	13.7	1.1E+08	4.3	13.6	3.2E+08	5.2	16.4	7.9E+08	4.5	14.3
magnet	Missing	1.5E+08	10.3	49.4	6.6E+07	7.8	37.4	1.6E+08	6.6	31.5	3.8E+08	7.0	33.4
string	Dipole	1.2E+09	2.7	7.1	1.0E+08	9.4	24.9	2.2E+08	9.6	25.5	1.5E+09	3.9	10.4
100-150 cm	Quadrupole	1.1E+09	4.6	9.4	1.4E+08	2.8	12.9	3.6E+08	6.4	13.5	1.6E+09	4.3	9.6
	Int.mag. Gap	9.0E+08	6.4	19.3	1.0E+08	10.2	30.7	2.3E+08	8.2	24.5	1.2E+09	5.9	17.8
above	Q11	2.9E+08	6.7	21.1	8.7E+07	6.9	21.7	2.4E+08	6.0	18.9	6.2E+08	6.3	19.9
magnet	Missing	1.9E+08	9.8	47.1	7.4E+07	7.5	35.8	1.6E+08	6.5	30.9	4.2E+08	6.5	31.4
string	Dipole	1.0E+09	3.3	8.7	8.8E+07	9.4	24.9	1.9E+08	10.0	26.5	1.3E+09	4.4	11.7
150-180cm	Quadrupole	9.7E+08	4.8	14.5	1.4E+08	1.9	17.7	3.0E+08	2.3	18.6	1.4E+09	3.9	14.6
	Int.mag. Gap	8.3E+08	8.2	24.7	1.1E+08	17.3	51.8	1.9E+08	11.0	33.0	1.1E+09	8.4	25.1
	Q11	4.0E+08			1.2E+08			3.6E+08			8.8E+08		
average	Missing	1.8E+08			8.1E+07			2.3E+08			4.9E+08		
ratio	Dipole	1.3E+09			1.2E+08			3.1E+08			1.8E+09		
	Quadrupole	1.2E+09			1.6E+08			4.1E+08			1.8E+09		
	Int.mag. Gap	8.0E+08			1.3E+08			2.9E+08			1.2E+09		
	max. uncertainty		14.4	63.0		17.3	65.3		21.4	64.2		14.8	54.0
	avg. uncertainty		7.0	25.7		8.6	28.7		9.0	29.0		8.7	36.6

Figure 59: Fluence:dose ratios for neutrons, protons, charged pions and total summed hadrons, above $E_{cut} >$ 100 MeV. Values are presented at various positions in the LHC tunnel alongside the different magnet components (*i.e.* averaged over the length of the magnet elements). Since the ratio is relatively uniform in the vicinity of the dipole magnets, the value given for alongside a dipole is the average over all the dipole magnet elements in the dispersion suppressor. Similarly for the quadrupoles (excluding Q11 data) and the inter-magnet gap regions. The percentage error, ±%, is the standard error on the mean of this averaging. To give an idea of the spread in the averaged ratios, the error 'sd%' is the maximum of either the standard deviation obtained from averaging over the various magnet elements, or the combination of the individual standard deviation errors on the values being averaged over. The values 'average ratio' are obtained by averaging over the values at a given position in the LHC tunnel.